SCHOOL OF MECHANICAL ENGINEERING

TORSIONAL PROPERTIES OF SPUR GEARS IN MESH USING NONLINEAR FINITE ELEMENT ANALYSIS

BY

SENEY SIRICHAI

This thesis is presented as part of the requirements for the award of the Degree of Doctor of Philosophy of the Curtin University of Technology

JUNE 1999

To my loving wife, **Tao** and daughters **Pearl** and **Please**

CANDIDATE'S STATEMENT

To the best of my knowledge this thesis does not contain any material which has been accepted for the award of any other degree or qualification at any educational institution. Material previously written or published by any other person is acknowledged by due reference.

The particular software used and mentioned predominantly in some parts of this thesis was because of its availability during the course of this research. There has been no intention to endorse, recommend or rank any software against any other.

Seney Sirichai
June 1999

ABSTRACT

This thesis investigates the characteristics of static torsional mesh stiffness, load sharing ratio, and transmission errors of gears in mesh with and without a localised tooth crack.

Gearing is perhaps one of the most critical components in power transmission systems. The transmission error of gears in mesh is considered to be one of the main causes of gear noise and vibration. Numerous papers have been published on gear transmission error measurement and many investigations have been devoted to gear vibration analysis. There still, however, remains to be developed a general non-linear Finite Element Model capable of predicting the effect of variations of gear torsional mesh stiffness, transmission error, transmitted load and load sharing ratio. The primary purpose of this study was to develop such a model and to study the behaviour of the static torsional mesh stiffness, load sharing ratio, and transmission error over one completed cycle of the tooth mesh.

The research outlined in this thesis considers the variations of the whole gear body stiffness arising from the gear body rotation due to tooth bending deflection, shearing displacement, and contact deformation. Many different positions within the

meshing cycle were investigated and then compared with the results of a gear mesh having a single cracked tooth.

In order to handle contact problems with the finite element method, the stiffness relationship between the two contact areas must be established. Existing Finite Element codes rely on the use of the variational approach to formulate contact problems. This can be achieved by insertion of a contact element placed in between the two contacting areas where contact occurs. For modelling of gear teeth in mesh, the penalty parameter of the contact element is user-defined and it varies through the cyclic mesh. A simple strategy of how to overcome these difficulties is also presented. Most of the previously published finite element analysis with gears has involved only partial teeth models. In an investigation of gear transmission errors using contact elements, the whole body of the gears in mesh must be modelled, because the penalty parameter of the contact elements must account for the flexibility of the entire body of the gear not just the local stiffness at the contact point.

ACKNOWLEDGMENTS

I would like to offer my sincere gratitude to Dr. I. Howard for his technical guidance throughout the course of my research. I also wish to thank all the members of the Mechanical Engineering School/Laboratory for their help during my research. I am grateful also to the Australian Agency for International Development (AusAID) for providing the Scholarship for my doctoral study. Finally, I would especially like to thank my wife, Tao, and my daughters, Pearl and Please for their continuing support and encouragement.

CONTENTS

APPENDIX F

MEASUREMENT OF THE COMBINED TORSIONAL MESH STIFFNESS

LIST OF FIGURES

LIST OF PUBLICATIONS

Sirichai, S., Morgan, L., Howard, I., and Teh, K. (1996). "The Measurement of Static Torsional Stiffness of Gears in Mesh." *Third International Symposium on Measurement Technology and Intelligent Instruments*, Japan, pp 251-258.

Sirichai, S., Howard, I., Morgan, L., and Teh, K. (1997). "A Synthetic Verification of 2D Contact Stiffness." *Second International Conference on the Application of Numerical Methods in Engineering*, Malaysia (June 1997), pp 261-271.

Sirichai, S., Howard, I., Morgan, L., and Teh, K. (1997). "Finite Element Analysis of Gears in Mesh." *Fifth International Congress on Sound and Vibration*, Australia (December 1997), pp 869-876.

Sirichai, S., Howard, I., Morgan, L., and Teh, K. (1998). "A Finite Element Model of Spur Gears in Mesh with a Single Tooth Crack." *Third International Symposium on Advanced & Aerospace Science and Technology in Indonesia*, Jakarta, Indonesia (August 31-September 3), pp 233-241.

Sirichai, S., Howard, I., Morgan, L., and Teh, K. (1998). "The Static Transmission Error of Cracked Spur Gear Teeth Using FEA." *1998 ASME Design Engineering Technical Conference*, Atlanta, GA, USA (September 1998), pp DETC98/CIE-5510.

Howard, I., Sirichai, S., and Morgan, L. (1998). "A Simplified Model of the Effect of a Crack in a Spur Gear on the Resultant Gear Vibration." *Condition Monitoring and Diagnostic Engineering Management*, Tasmania, Australia (December 1998), pp 397- 406.

NOTATION

The notation defined below is a partial list of the principal notation used throughout this thesis. Due to the wide variety of topics covered in this thesis, some exceptions will exist. Less frequently used symbols, and symbols that have different meanings in different contexts, are defined where they are used. Matrices and vectors are denoted by boldface type.

General Symbols

Symbol	Meaning
Δt	Time increment
a	Element acceleration vector, addendum of the involute tooth (mm)
a	Acceleration vector
A	Global acceleration vector
b	Dedendum of the involute tooth, mm
b	Body force vector
B_p^A, B_p^D, B_g^A, B_g^D	The tooth displacement vector caused by bending and shearing for the tooth pair A and D of the pinion and gear

	respectively, m.
C	Constitutive matrix
e	Linear strain tensor, offset of the rack cutter (mm)
E	Young's modulus
$\mathbf{E_t}$,	Hardening modulus
f	Concentrated force vector
F_p^A, F_p^D, F_g^A, F_g^D	The component of the total applied force vector $F_{tot,p}^{A,D}$, $F_{tot,g}^{A,D}$, at the contact A and D of the pinion and gear respectively, N.
$F_{tot,p}^{A,D}$, $F_{tot,g}^{A,D}$	The total applied force vectors of the pinion and gear respectively, N.
F_{sp}^A, F_{sp}^D, F_{sg}^A, F_{sg}^D	The friction force contributions along the path of contact of each meshing tooth pair at the contact A and D of the pinion and gear respectively, N.
F_{np}^A, F_{np}^D, F_{ng}^A, F_{ng}^D	The normal force contributions along the path of contact of each meshing tooth pair at the contact A and D of the pinion and gear respectively, N.
$F_{tot,np}^{A,D}$, $F_{tot,ng}^{A,D}$	The total normal forces along the path of contact of the pinion and gear respectively, N.
H_p^A, H_p^D, H_g^A, H_g^D	The contact deformation vector of the tooth pair A and D of the pinion and gear respectively, m.
k	Element stiffness matrix
K	Global stiffness matrix
$K_{g,p}$	The single tooth torsional mesh stiffness of the output and input gear, N.m/rad.
KN_c	The combined normal contact stiffness of the pinion and gear, N.m/rad.

KN_p, KN_g	The single tooth normal contact stiffness of the pinion and gear respectively, N.m/rad.
K_p, K_g	The single tooth torsional mesh stiffness at particular meshing positions of the pinion and gear respectively, N.m/rad
KT_c	The combined tangential contact stiffness of the pinion and gear, N.m/rad.
L_{np}^A, L_{np}^D, L_{ng}^A, L_{ng}^D	The corresponding normal load sharing ratios of each meshing tooth pair at the contact A and D of the pinion and gear respectively
m	Metric module, mm
m	Element mass matrix
M	Global mass matrix
m_g	Speed ratio.
N	Number of gear teeth
N_p, N_g	Number of gear teeth of the input gear and output gear respectively
$\mathbf{N_1}$, $\mathbf{N_2}$, $\mathbf{N_3}$,	Boundary unit vectors
q	Boundary traction vector
R_p^A, R_p^D, R_g^A, R_g^D	The transverse plane contact radius vector on the pinion and gear tooth pair A and D respectively, m.
t,	Time, thickness
$T_{g,p}$	The torsional load vector of the output and input gear, N.m.
T_p^A, T_p^D, T_g^A, T_g^D	The vectorial contribution to the total applied torque of the tooth pair A and D of the pinion and gear respectively, N.m.
$T_{tot,p}^{A,D}$, $T_{tot,g}^{A,D}$	The total applied torque vector of the pinion and gear

	respectively, N.m.
T_p , T_g	The total applied torque vectors at particular meshing positions of the pinion and gear respectively, N.m.
u	Displacement vector with component u_1 , u_2 , and u_3
U	Global displacement vector
u	Element displacement vector
v	Velocity vector with components υ_1 , υ_2 , and υ_3
V	Global velocity vector
x	Spatial coordinates
X	Material coordinates
Z	The gear ratio
[B]	Strain-displacement matrix
[C]	Damping matrix
[D]	Elasticity matrix
{F}	Force vector
f_n	The normal force
f_s	The tangential force
[I]	Identity matrix
[K]	Stiffness matrix
[M]	Mass matrix
[0]	Null matrix
[S]	Stress stiffness matrix
u, v, w, {u}	Displacement, displacement vector
δ U	Virtual internal work
δ V	Virtual external work

x, y, z	Element coordinate
X, Y, Z	Nodal coordinates (usually global cartesian)

Greek Symbols

Symbol	Meaning
θ_p^A, θ_p^D, θ_g^A, θ_g^D	The transverse plane angular rotation of the gear body caused by bending deflection, shearing displacement and contact deformation of the single tooth pair A and D of the pinion and gear respectively, rad.
$\theta_p^{A,D}$, $\theta_g^{A,D}$	The transverse plane angular rotation of the gear body caused by bending deflection, shearing displacement and contact deformation of the double tooth pair A and D of the pinion and gear respectively, rad.
$\theta_{g,p}$	Angular rotation of the output and input gear, rad.
Δ	Increment
σ	Cauchy stress tensor, stress
ρ	Mass density of the material
υ	Element velocity vector
μ	Coefficient of friction
ν	Poisson's ratio
ε	Green-Lagrange strain tensor, strain
η	Non-linear strain tensor
Γ	Material particle set on a boundary, boundary of Ω
${}^t\Gamma$	Space occupied by a boundary Γ

$\overline{\Omega}$	Material particle set of a body
Ω	Material particle set within the interior of a body, Any domain
${}^{t}\overline{\Omega}$	Space occupied by a body
${}^{t}\Omega$	Space taken by the interior particle Ω of a body
δw	Virtual work in an element
δW	Virtual work in a system
ϕ	Shape function
σ_y	Yield stress
α	Penalty parameter, coefficient of thermal expansion

Superscripts and Subscripts Symbols

Symbol	Meaning
subscripts p and g	Represent the pinion (input gear) and gear (output gear) respectively.
subscript s	Denotes single tooth pair in contact.
Subscript m	Denotes double tooth pair in contact.
Subscript c	Denotes combined normal or tangential contact stiffness.
superscripts A and D	Represents the contact point along the path of contact of the double tooth pair contact zone.
superscript i	Indicates the contact point along the path of contact of single tooth pair contact zone., equilibrium iteration number

CHAPTER 1

INTRODUCTION AND JUSTIFICATION

1.1 General Introduction

Out of all the types of gearbox noise, one of the most difficult to control is gear noise generated at the tooth mesh frequency. Transmission error is considered to be one of the main contributors to noise and vibration in a gear set and is defined as the difference between the theoretical and actual angular positions of a gear in relation to the pinion. According to most authors, gear noise is closely related to transmission error. A pinion and gear having ideal involute profiles running with no loading torque should theoretically run with zero transmission error. However, when these same gears transmit torque, the combined torsional mesh stiffness of each gear changes throughout the mesh cycle as the teeth deflect, causing variations in angular rotation of the gear body. The difference in angular rotation position between where the gear is in relation to the pinion, as opposed to where it should theoretically be, is what is termed transmission error. Even though the transmission error is relatively small, it is these slight variations which can cause noise and vibration in rotating gears in mesh. If the tooth mesh excitation occurs at a frequency which matches a resonance of the shafts or gear housing, the noise is enhanced. This phenomenon is actively being researched in order to try to minimize the amount of transmission error in gears, and thereby reduce the amount of noise generated.

1.2 TORSIONAL MESH STIFFNESS

The torsional mesh stiffness of gears in mesh is defined by Sirichai (Sirichai et al. 1997; Sirichai et al. 1998; Sirichai et al. 1998), as the ratio between the torsional load and the total elastic angular rotation of the gear body. Total angular rotation is defined as the angle through which a gear turns due to bending, shearing and contact of the gear teeth when in loaded mesh with the fixed mating gear. The torsional mesh stiffness varies as the gear teeth rotate through the mesh cycle. In spur gears, where contact alternates between the single-tooth-pair contact and the double-tooth-pair contact, each tooth pair may be thought of as a spring. The torsional mesh stiffness alternates between the stiffness of a single spring and the stiffness of two springs in parallel, that is, the torsional mesh stiffness varies throughout the meshing position as it decreases and increases dramatically as the meshing of the teeth change from the double pair to single pair of teeth in contact and vice-versa. The development of a torsional mesh stiffness model of gears in mesh can be used to determine the transmission error throughout the mesh cycle.

1.3 GEAR TRANSMISSION ERROR

The transmission error of gears in mesh (TE) is the single most important factor in the generation of gear noise and vibration. It has been defined by Welbourn (Welbourn 1972; Welbourn 1979) as the difference between the actual position of the output gear and the position it would occupy if the gear drive were perfectly conjugate. The equation for transmission error may be expressed in angular units as given below,

$$\text{TE} = \theta_g - (Z)\theta_p, \quad \text{rad,} \qquad (1.3.1)$$

where Z is the gear ratio and $\theta_{p,g}$ denotes the angular rotation of the input and output gear in radians respectively. The definition above is appropriate for both loaded and unloaded gears, and can be applied statically or dynamically. Harris (Harris 1958) was the first to identify transmission error as a significant contributor to gear dynamics and the measurement of transmission error was first performed in

the 1960's by the National Engineering Laboratory and by Gregory, Harris and Munro (Gregory et al. 1963; Gregory et al. 1963; Gregory et al. 1963). Many others have performed measurements of transmission errors since that time.

When gears are unloaded, a pinion and gear with the involute profiles should theoretically run with zero transmission error, except for manufacturing inaccuracies such as profile errors, spacing errors, and runout. Transmission errors can also result from imperfect mounting such as geometrical errors of alignment, and static and dynamic elastic deflections in the supporting bearing shafts and structure. However, when gears with the ideal involute profiles are loaded, the torsional mesh stiffness of each gear changes throughout the mesh cycle, causing variations in angular rotation of the gear body and subsequent transmission error.

1.4 General Remarks on Contact Analysis

In almost all mechanical and structural engineering systems, interactions occur between two mechanical components or two parts of a single component when they come into contact with each other. Contact problems are highly nonlinear and require significant computer resources to solve. Contact nonlinearities occur when two or more components come into or out of contact with each other. One may argue that the subject of contact mechanics started in 1882 with the publication of the classical work by Hertz (Hertz 1881). The Hertz theory is however restricted to frictionless contact and perfectly elastic solids, (see: Refaat 1995). Progress in contact mechanics in the second half of this century has been associated largely with the removal of these restrictions. A proper treatment of friction at the interface of bodies in contact has enabled the elastic theory to be extended to both slipping and rolling contact in a realistic way.

The contact between two components or bodies is a static phenomenon if the two bodies are in static equilibrium, (Zhong 1993). Otherwise the contact is a dynamic phenomenon. A dynamic contact is often much more complicated than a static one. In engineering applications, most contact processes are dynamic in a restrictive sense. Many of them can, however, be regarded as static for simplicity. By nature, contact phenomena always involve friction phenomena. However, friction effects

may be neglected for simplicity in situations where frictional forces are sufficiently small. Therefore, we may have a frictionless contact, which is a special case of general contact.

Despite the importance of contacts in the mechanics of solids and its engineering applications, contact effects are rarely taken into account seriously in conventional engineering analysis, because of the extreme complexity involved. Mechanical problems involving contacts are inherently non-linear. In contrast to other mechanical problems, contact problems involve unknown boundary conditions. Specifically, the actual contacting surface and the stresses and displacements on the contact surface are all unknown prior to the solution of the problem. Consequently, a mathematical model of contact problems involves systems of inequalities or non-linear equations. Furthermore, rigorous modelling of friction is quite difficult as the friction depends on, among other factors, the surface smoothness, the physical and chemical properties of the material, the motion, and the temperature of the contacting surface.

A rigorous analysis of the contact problem that takes all these complex aspects into account remains extremely difficult. With the rapid development of computational mechanics, however, great progress has been made in numerical studies of the problem. By use of the finite element method, many contact problems, ranging from relatively simple ones to quite complicated ones, can be solved with high accuracy.

1.5 Objectives of the Research

Despite a lot of investigations devoted to gear research and analysis (Gregory et al. 1963; Hayashi and Hayashi 1981; Milenkovic and Shmuter 1982; Kohler and Regan 1985; Mark 1987; Smith 1987; Smith 1987; Baron et al. 1988; Houser and Blankenship 1989; Vinayak and Houser 1992; Bard et al. 1994; Barnett and Yildrim 1994; Kurokawa et al. 1994; Munro and Yildirim 1994; Sundaresan et al. 1994; Umeyama 1994; Gosselin et al. 1995; Litvin and Lu 1995; Toshinari 1995; Velex et al. 1995; Houser et al. 1996; Sweeney and Randall 1996; Litvin and Kim 1997; Regalado and Houser 1998; Sirichai et al. 1998) there still remains to be developed a general numerical approach capable of predicting the effects of variations in gear

geometry, torsional mesh stiffness, transmission error, and transmitted load. The objectives of this thesis are to use a numerical approach to develop theoretical models of the behaviour of spur gears in mesh, to help predict the effect of gear tooth damage on transmission error. The main focus of the current research as developed here is,

- to devise efficient and reliable CAD solution techniques (AUTODESK 1995; AUTODESK 1995; AUTODESK 1997) to generate the profile of spur gear teeth for transfer to subsequent analysis using the finite element method,

- to develop a strategy to determine an appropriate value of the penalty parameter of generalised contact elements and to compare with Hertzian theory.

- to devise efficient and reliable solution techniques and programs necessary to define the penalty parameter of the contact elements at each contact position throughout the gear mesh cycle,

- to develop the theoretical changes in the torsional mesh stiffness of ideal involute spur gears throughout the mesh cycle using finite element analysis,

- to develop a program for determining the static transmission error of ideal involute spur gears in mesh at each position of the mesh cycle,

- to use Finite Element Analysis to determine the load sharing ratio of ideal involute spur gears in mesh at each position of the mesh cycle,

- to use Finite Element Analysis to predict the effect of localised gear tooth damage on the torsional mesh stiffness, transmission error, and the load sharing ratio of the ideal involute spur gears in mesh, at each position of the mesh cycle, where the tooth damage occurs outside of the contact region.

1.6 LAYOUT OF THESIS

This thesis comprises a total of eight chapters. Chapter 1 presents a general introduction, the significance of the research work and objectives to be achieved. The definition of torsional mesh stiffness for gears in mesh and gear transmission error and the reasons for their occurrences are also given. A general statement of contact analysis is given, along with the specific characteristics of the research work. Finally the layout of the study is described.

Chapter 2 provides a critical review of the state of the literature relating to the research. It contains a significant presentation of relevant and pertinent publications on the subject of contact analysis and documents a vast amount of literature on gear mathematical models and measurements for vibration analysis and noise control.

Chapter 3 provides a concise representation of the variational inequalities and variation equality formulations of contact problems for elastic media, suitable for implementation in engineering applications. It also describes an analytical model of the gear body rotation compatibility condition, the static torsional mesh stiffness and the gear transmission error.

Chapter 4 describes a contact problem classification, capability and kinematics, as well as advantages and disadvantages of contact elements and how to overcome some of the disadvantages. In order to model a contact problem with the finite element method, the stiffness relationship between the two contact surfaces must be established. This relationship can be established through a contact element that is inserted between the two contacting areas. The accuracy of contact problems depends on the choice of the penalty parameter which is not known at the start of any analysis. A high value of the penalty parameter can lead to ill-conditioning of the global stiffness matrix as well as convergence difficulties, giving a very slow convergence rate and a large number of equilibrium iterations or a very small time step to generate a solution in each substep. A low value of the penalty parameter can lead to over-penetration of the surfaces. In this chapter, a case study of how to select an appropriate value of the penalty parameter is presented using finite element analysis and the results of an approach deflection study are compared to analytical

formulations based upon Hertzian stress theory, Boresi and Sidebottom (1985) and Young (1989).

In Chapter 5, the involute and fillet tooth profile equations used in the finite element model have been introduced. A customised CAD program was used to generate the profile of the teeth and the profile was then transferred to an FEA program to generate the finite element model of gears in mesh. The accuracy of finite element modelling of contact problems depends on the choice of the penalty parameter for the contact element. For modelling of gear teeth in mesh, the penalty parameter also varies as the gear teeth rotate through the cyclic mesh. This chapter provides a Finite Element Model which is used to predict the torsional mesh stiffness of a pair of spur gears in mesh. The model involves the use of 2D plain strain elements, coupled with contact elements at the area of contact between the meshing teeth. A simple strategy of how to determine an appropriate value of the penalty parameter of the contact elements is also presented. The theoretical changes in the torsional mesh stiffness throughout the mesh cycle are developed using finite element analysis. A 5mm through thickness tooth crack is also modelled, and the comparison of the torsional mesh stiffness with and without the tooth crack is discussed.

In Chapter 6, a spur gear mesh consisting of a pinion with a single cracked tooth in a gear is considered and a comparison of results of static transmission error between gears with and without the cracked tooth is made. The theoretical changes in the torsional mesh stiffness throughout the mesh cycle, presented in chapter 5 using finite element analysis, are related to the static transmission error in this chapter. At each particular meshing position, the angular rotation of the pinion due to tooth bending, shearing and contact displacement is calculated in the gear reference frame by restraining the gear from rotating, with the pinion having a torque input load. In relation to the pinion reference frame, the pinion is restrained from rotating, with the gear having the torque input load and the resulting angular rotation of the gear is also computed. The angular rotations obtained by these two models provide the static transmission error of the ideal involute profile gears under load. In this chapter, a detailed analysis of the variation of the transmission error throughout the mesh cycle is presented and discussed. Many different positions within the meshing cycle were investigated and then compared with a pinion with a single cracked

tooth. Variations of applied torque that affect the transmission error were also investigated.

Chapter 7 presents the development of an FEA program used to determine the load sharing ratio of spur gears in mesh. The development of the torsional mesh stiffness model of gears in mesh is used to determine the load sharing ratio throughout the mesh cycle and a comparison of results of load sharing ratio between gears with and without the cracked tooth is made. In this chapter, a detailed variation of the load sharing ratio throughout the mesh cycle is presented. Different values of input torque that might affect the load sharing ratio were investigated and then compared with results from a pinion with a single cracked tooth.

Finally, Chapter 8 summarises the general conclusions of the thesis and its contribution to the area of contact mechanics, torsional mesh stiffness, transmission load sharing ratio, and gear transmission error, together with some recommendations for future work.

Appendix F describes the static torsional mesh stiffness measurement set-up and method. This Appendix presents data measured from a static gear test rig, which was designed to create a pure torque transmitted to a spur gear pair in mesh. Once the gears were pre-loaded, the known torque load was increased while the angular deflection of the spur gears was measured by a pair of optical auto-collimators. The same procedure was followed for a variety of different loads allowing a graph of torque versus angular displacement to be obtained. The relationship between torque and angular displacement was linear within the elastic range as expected. From the measurements, the static torsional mesh stiffness of the gear mesh at particular positions was obtained by calculating the gradient from the corresponding torque versus angular displacement relationship. By changing the meshing positions, the mesh stiffness of the gear during the entire meshing cycle was obtained. Attention is devoted to the strategy adopted in treating the elastic torsional mesh stiffness, together with discussions, comparison of results with the finite element model and conclusions.

CHAPTER 2

LITERATURE REVIEW

2.1 OVERVIEW

Gears are one of the most critical components in industrial rotating machinery. There is a vast amount of literature on gear modelling. The objectives in dynamic modelling of gears has varied from vibration analysis and noise control, to transmission errors and stability analysis over at least the past five decades. The ultimate goals in gear modelling may be summarised as the study of the following,

stress analysis such as bending and contact stresses,
surface pitting and scoring,
transmission efficiency,
radiated noise,
loads on the other machine elements of the system especially on bearings, stability regions,
natural frequencies of the system,
vibratory motion of the system,
whirling of rotors,
condition monitoring, fault detection, diagnosis, prognosis, reliability,
and fatigue life.

The models proposed by several investigators show considerable variations not only in the effects included, but also in the basic assumptions made. Although it is quite difficult to group the mathematical models developed in gear dynamics, Ozguven and Houser (Ozguven and Houser 1988; Ozguven and Houser 1988) have presented a thorough classification of gear dynamic mathematical models. In 1990, Houser (Houser 1990) and Zakrajsek et al. (Zakrajsek and al. 1990) outlined the past and current research projects of gear dynamics and gear noise at Ohio State University's Research Laboratory and NASA Lewis Research Centre respectively. Du (Du 1997) also classified various gear dynamic models into groups.

The current literature review also attempts to classify gear dynamic models into groupings with particular relevance to the research presented in this thesis. It is possible for some models to be considered in more than one grouping, and so the following classification seems appropriate.

- Models with Tooth Compliance. There is a very large number of studies which include the tooth stiffness as the only potential energy storing element in the system. This group includes single tooth models and tooth pair models. For single tooth models, the objectives usually are tooth stress analysis. For the models with a pair of teeth, the focuses mostly are contact stress and mesh stiffness analysis. That is, the flexibility (torsional and/or transverse) of the shafts, bearings, etc., are all neglected. In such studies the system is usually modelled as a single degree of freedom spring-mass system. Some of the models have also been analysed using the Finite Element Method.

- Models for Gear Dynamics. Such models include the flexibility of the other elements as well as the tooth compliance. Of particular interest have been the torsional flexibility of shafts and the lateral flexibility of the bearings and shafts along the line of action. In some studies, the transverse vibrations of a gear-carrying shaft are considered in two mutually perpendicular directions, thus allowing the shaft to whirl. In such models, the torsional vibration of the system is usually considered.

- Models With A Whole Gearbox. The studies in this group may be viewed as current and advanced studies and all elements in the system including the gear casing, are considered in the models. The gearbox may be single stage or multi-stage.

In the solution of the system equations, numerical techniques have usually been employed. Although most of the models for which numerical techniques are used are lumped parameter models, some investigators have introduced continuous system or finite element models. While closed form solutions are given for some simple mathematical models, analog computer solutions have sometimes been preferred for non-linear and more complicated models, particularly in the earlier studies.

In some studies the main objective has been to find the system natural frequencies and mode shapes and, therefore, only free vibration analyses are made. However, usually the dynamic response of the system is analysed for a defined excitation. In most of the studies the response of the system to forcing due to gear errors and to parametric excitation due to tooth stiffness variation during the tooth contact cycle is determined. The models constructed to study the excitations due to gear errors and/or tooth stiffness variation provide either a transient vibration analysis or a harmonic vibration analysis by first determining the Fourier series coefficients of the excitation. Some studies also include the non-linear effect caused by loss of tooth contact or by the friction between meshing teeth. The excitation is then taken as an impact load and a transient vibration analysis is made.

2.2 GEAR MODELLING

Numerous mathematical models have been developed for different purposes, the basic characteristics of each class of dynamic models along with the objectives and different parameters considered in modelling has been discussed in section 2.1. This section presents a review of papers published in the areas outlined above, including brief information about the model and the approximations and assumption made.

2.2.1 Models with Tooth Compliance

The basic characteristic of the models in this group is that the only compliance considered is due to the gear tooth and that all other elements have been assumed to be perfectly rigid. The model is either a single tooth model or a tooth pair model. For single tooth models, the objectives usually are tooth stress analysis. For models with a pair of teeth, the focus is mostly contact stress and meshing stiffness analysis. The resulting models are either translational or torsional. With torsional models one can study the torsional vibrations of gears in mesh, whereas with translational models the tooth of a gear is considered as a cantilever beam and one can study the forced vibrations of the teeth. In either of these models, the transmission error excitation is simulated by a displacement excitation at the gear mesh.

In 1956, Nakada and Utagawa (Nakada and Utagawa 1956) considered varying elasticity of the mating teeth in their vibratory model. The torsional vibrations of two mating gears were simulated by introducing an equivalent translational vibratory system. The time variation of stiffness was approximated as a rectangular wave and closed form solutions of piecewise linear equations were obtained for different damping cases for accurately manufactured gear tooth profiles. Another mass and equivalent spring model was introduced in 1957 by Zeman (Zeman 1957). He neglected the variation of stiffness and analysed the transient effects of periodic profile errors. Harris's work (Harris 1958) was an important contribution in which the importance of transmission error in gear trains was discussed and photo-elastic gear models were used. In his single degree of freedom model, he considered three internal sources of vibration: manufacturing errors, variation in the tooth stiffness and non-linearity in tooth stiffness due to the loss of contact. He treated the excitation as periodic and employed a graphical phase-plane technique for the solution. Harris seems to have been the first to point out the importance of transmission error by showing that the behavior of spur gears at low speeds can be summarised in a set of static transmission error curves. He also appears to have been the first to predict the dynamic instability due to parametric excitation of the gear mesh.

In 1963, Gregory, et al. (Gregory et al. 1963; Gregory et al. 1963) extended the theoretical analysis of Harris (Harris 1958) and made comparisons with experimental observations. The torsional vibratory model of Gregory, et al., included a sinusoidal-type stiffness variation as an approximation. They treated the excitation as periodic, and solved the equations of motion analytically for zero damping and on an analog computer for non-zero damping. The experimental data (Gregory et al. 1963) and the computational results (Gregory et al. 1963) generally confirmed Harris's contention that non-linear effects are insignificant when damping is more than about 0.07 of critical. It was claimed that when damping is heavy the simple theory of damped linear motion could be used. Aida, et al. (Aida et al. 1967; Aida 1968; Aida 1969) presented examples of other studies in this area. He modelled the vibration characteristics of gears by considering the excitation terms due to tooth profile errors and pitch errors, and by including the variation of teeth mesh stiffness. In the model of Aida, et al., time varying mesh stiffness and periodic tooth errors were considered, and the model was used for determining stability regions and steady state gear vibrations. A comparison with experimental measurements was also made.

Bollinger and Harker (Bollinger and Harker 1967) investigated the dynamic instability that may arise due to varying mesh stiffness. They used a simple single degree of freedom model with an equivalent mass representing the inertia of the gear and pinion. Mesh stiffness variation was assumed to be harmonic. The solution of the resulting equation of motion was obtained by using an analog computer, and it was shown that the dynamic load may be reduced by increasing the damping between the gear teeth or by reducing the amount of stiffness variation.

In 1967, Tordion and Gerardin (Tordion and Gerardin 1967) used an equivalent single degree of freedom dynamic model to determine transmission error from experimental measurements of angular vibrations. They first constructed a torsional multi-degree of freedom model for a general rotational system with a gear mesh. Then, only the equations of the gears were considered for obtaining an equivalent single degree of freedom model with constant mesh stiffness and a displacement excitation representing the transmission error. An analog computer solution was used to obtain the transmission error from the measured angular accelerations. The

transmission error was proposed to be used as a new concept for determining the gear quality, rather than individual errors.

In 1973, Wallace and Seireg (Wallace and Seireg 1973) used a finite element model of a single tooth to analyze the stress, deformation and fracture in gear teeth when subjected to dynamic loading. Impulsive loads applied at different points on the tooth surface and moving loads normal to the tooth profile were studied. In the same year, Wilcox and Coleman (Wilcox and Coleman 1973) also analysed gear tooth stresses. They developed a new accurate stress formula for gear teeth based entirely on the finite element method and presented a comparison between the new formula and the previous one.

In 1978, Remmers (Remmers 1978) presented a damped vibratory model in which the transmission error of a spur gear was expressed as a Fourier series. He used viscous damping and constant tooth pair stiffness, and considered the effects of spacing errors, load, and design contact ratio and profile modifications.

Rebbechi and Crisp (Rebbechi and Crisp 1981; Rebbechi and Crisp 1983) considered the material damping of the gear-wheel shafts, while the compliance of the shafts was neglected. The three-degree of freedom model was reduced to a two degree of freedom model for the study of the torsional vibrations of a gear pair, and an uncoupled equation, which gave the tooth deflection. The other effects included in the model were material damping inherent to the tooth, perturbations of input and output torque, arbitrary tooth profile errors, time variation of that error due to deformation, and perturbations of the base circle due to profile errors. The effects of kinetic sliding friction at the contact point and the sliding velocity on the dynamics of continuous meshing were also studied (Rebbechi and Crisp 1983) and in 1996, Rebbechi, et al. (Rebbechi et al. 1996), obtained measurements of the gear tooth dynamic friction under various speed and load situations.

In 1985, Wang (Wang 1985) studied the effect of torsional vibration in his model. The research was focused on the analytical evaluation of gear dynamic factors based on rigid body dynamics and discussed different cases in which the transmission errors have different effects on the dynamic load. He commented that the

transmission errors have a system wide effect and could be used to analyse rigid-body vibrating gear systems in which the gear deflection is not considered.

In the late 1980s, Ramamurti and Rao (Ramamurti and Rao 1988) presented a new approach to the stress analysis of spur gear teeth using FEM. Their new approach, with a cyclic system of gear teeth and with asymmetry of the load on the teeth, allowed computation of the stress distribution in the adjacent teeth from the analysis of one tooth only. The boundary conditions imposed between the two adjacent teeth in the conventional FEM were avoided in their approach.

In 1988, Vijayakar, Busby, and Houser (Vijayakar et al. 1988) used a simplex type algorithm to impose frictional contact conditions on finite element models. They established the contact equations with the frictional factor and solved them for known output moment load on the output gear. In their finite element model, they analysed their problem in two dimensions and in order to model the involute profile as closely as possible, a special five node linear transition element was used. In the same year, Ozguven and Houser (Ozguven and Houser 1988) presented a non-linear model of a single degree of freedom system for the dynamic analysis of a gear pair. In their studies, they developed two methods for calculating the dynamic mesh and tooth forces, dynamic factors based on stresses, and dynamic transmission error from measured or calculated loaded static transmission errors. The first method was an accurate method, which included the time variation of both mesh stiffness and damping. The second approach was a more approximate method in which the time average of the mesh stiffness was used.

In 1990, Sundarajan and Young (Sundarajan and Young 1990) developed a three dimensional finite element substructure method to improve the accuracy of calculation of the gear tooth contact and fillet stress in large spur and helical gear systems. The finite element analysis and pre-processing software they developed simplified the data input and reduced the manual effort involved in the analysis. When some parameters (misalignment for example) were changed, most of the stiffness matrices were not recalculated. They considered the contact problem by using contact boundary conditions, which meant that the contact or area was defined in the analysis. One year later, Sundarajan and Amin (Sundarajan and Amin 1991)

investigated the finite element analysis of a ring gear and the casing and presented another finite element computer program to solve this problem.

The contact conditions of gear teeth are very sensitive to the geometry of the contacting surfaces, which means that the finite element mesh near the contact zone needs to be very highly refined. However it is not recommended to have a fine mesh everywhere in the model, in order to reduce the computational requirements. Vijayakar and Houser (Vijayakar and Houser 1993) studied the contact analysis of gears using a combined finite element and surface integral method. They developed a Contact Analysis Program Package which supports stress contours, transmission errors, contact pressure distribution and load distribution calculation. Their approach was based on the assumption that beyond a certain distance from the contact zone, the finite element method predicted deformations well and the elastic half space method was accurate in predicting relative displacements of points near the contact zone. Under these assumptions, it was possible to make predictions of surface displacements that make use of the advantages of both the finite element method as well as the surface integral approach.

In 1994, a review of the current contact stress and deformation formulations compared to finite element analysis was given by Gosselin, et al. (Gosselin et al. 1994). They presented an original approach to meshing line contact for spur gears and point contact for spiral bevel gear pairs for finite element analysis using contact elements and they then compared the contact deformation results with recognised analytical formulations. Their results showed that the contact deformations differ from 20% to 150% between the analytical approaches and FEM. In the same year, Chen, Litvin, and Shabana (Chen et al. 1994) proposed an approach for the computerised simulation of mesh and contact of loaded gear drives that enables determination of the instantaneous contact ellipse, the contact force distributed over the contact ellipse and the real contact ratio. They also established a finite element model for the maximum bending stress calculation on a tooth. The friction forces between gear teeth, the elastic deflection of the body of the gear, the shaft and the bearings were neglected in their approach and their model.

2.2.2 Models for Gear Dynamics

Some of the early mathematical models, in which the stiffness and mass contribution of the shafts carrying the gears in mesh were ignored, showed good agreement with the experimental measurements. However, it was realized in the late 1960s and early 1970s that dynamic models in which the shaft and bearing flexibility were considered would be necessary for more general models. Unless the stiffness of these elements were relatively high or low compared to the effective mesh stiffness, the vibration coupling of different elements cannot be neglected. In general, a high degree of correlation was obtained between the experimental results and the predictions provided by many of the early single degree of freedom models. This can be explained by the fact that the experimental rigs used in such studies satisfied most of the basic assumptions made in the mathematical model. For example, a very short shaft might be assumed to be rigidly mounted in the transverse direction. In practical applications however, these assumptions may not always be satisfied and so one then needs more general models in which the flexibility and mass of the other elements are considered as well.

The models that could be considered in this group are either torsional models, in which only the torsional stiffness of the gear-carrying shafts is included, or torsional and translational models, in which both the torsional and transverse flexibility of the gear-carrying shafts are considered.

In the early 1960s, Johnson (Johnson 1962) used a receptance coupling technique to calculate the natural frequencies from the receptance equation obtained by first separately finding the receptances at the meshing point of each of a pair of general shafts. In the model, the varying mesh stiffness was replaced by a constant stiffness equal to the mean value of the varying stiffness and thus a linear system was obtained. His work was one of the first attempts to use mesh stiffness in coupling the torsional vibration of gear shafts. Mahalingam (Mahalingam 1968) presented a similar model in 1968, where the formulae for support receptance at a gear-wheel bearing was developed and then used to study the effects of gearbox and frame flexibility on the torsional vibration.

An important contribution in this area came in 1970 from Kobler, Pratt and Thomson (Kobler et al. 1970) who concluded from their experimental results that dynamic loads and noise result primarily from the steady state vibration of the gear system when forced by transmission errors. They developed a six-degree of freedom dynamic model with four torsional degrees of freedom and one lateral degree of freedom in the direction of the tooth force on each shaft. They assumed the tooth mesh stiffness to be constant in their model and the spectrum analysis of the static transmission error for the single-stage reduction gear unit used was also given. In 1971, Kasuba (Kasuba 1971) used one and two degree of freedom models based on his previous work (Kasuba 1961), to determine dynamic load factors for gears which were heavily loaded. He used a torsional vibratory model, which considered the torsional stiffness of the shaft. He also argued that the rigidity of the connection shafts is much lower than the rigidity of the gear teeth in meshing, and then decoupled the meshing system. The tooth error in mesh was represented by a pure sine function having the frequency of tooth meshing. In his model the tooth meshing stiffness was time varying.

In 1972, Wang and Morse (Wang and Morse 1972) constructed a torsional model including shaft and gear web stiffness as well as a constant mesh stiffness. The model was represented by a spring mass system having many degrees of freedom. The transfer matrix technique was applied to give the static and dynamic torsional response of a general gear train system. It was found that the torsional natural frequencies and mode shapes determined from a free vibration analysis correlated with experimental results at low frequencies. Later, Wang (Wang 1974) extended this work to the linear and non-linear transient analysis of complex torsional gear train systems. In this later model he considered the variation of tooth stiffness, and included gear tooth backlash, linear and non-linear damping elements and multi-shock loading. Three different numerical methods that can be used in the solution of non-linear systems that cannot be approximated piecewise linearly were also briefly discussed in his work.

In the 1980s more and more complicated models were developed in order to include several other effects and to obtain more accurate predictions, while some simple models were still developed for the purpose of simplifying dynamic load prediction

for gear standards. In 1980, Iida, et al. (Iida et al. 1980) investigated the coupled torsional-flexural vibration of a shaft in spur geared systems in which they assumed that the output shaft was flexible in bending and the input shaft was rigid in bending. They derived equations of motion for a 6-degree-of-freedom (DOF) system where the driving gear had a torsional DOF while the driven gear had x, y and torsional DOF is due to mass imbalance and geometrical eccentricity. They assumed that the tooth contact was maintained during the rotation and that the mesh was rigid. Four years later, Iida and Tamura (Iida and Tamura 1984) continued to study coupled torsional flexural vibration of geared shaft systems. In that study, their model consists of three shafts, rather than two shafts, one of them being a counter shaft.

Neriya, et al. in 1985 (Neriya et al. 1985) also investigated the coupled torsional flexural vibration of a geared shaft system due to imbalance and geometrical eccentricity. The difference in the work with respect to Iida, et al. (Iida et al. 1980) was that they used the finite element method to solve their problem. In their model, there were 6 beam elements for each of the driving and driven shafts which were coupled at the contact to account for the tooth flexibility. Their model had 41 degrees of freedom. They solved the free vibration problem to obtain the natural frequencies and mode shapes. The normal mode analysis was then employed to obtain the dynamic response of the system under the excitations arising from the mass imbalance and geometrical eccentricity in gears.

In early studies, the mesh stiffness of teeth was considered to be constant. Iwatsubo and Kawai (Iwatsubo et al. 1984), studied the coupled lateral and torsional vibrations of geared rotors, considering mainly the effect of the periodic variation of mesh stiffness and a tooth profile correction. Their model had two simply supported rotors with a spur gear at the centre of each rotor. The stability condition of the system was analysed in their study. In the same year, Iwatsubo, Arii and Kawai (Iwatsubo et al. 1984) analysed the coupled lateral and torsional vibration of the geared system constructed from a pair of spur gears using the transfer matrix method. In their research, they considered three cases in the analysis of the free vibration of the system: 1. The mesh force acting on the contact line was a function of the rotation of each gear, 2. The mesh force acting on the contact line was a function of the rotation and flexure at each gear, and 3. The system was not coupled

by the gears. The forced vibration caused by the mass imbalance of the gears was also calculated.

A new topic, the computer simulation of the torsional and flexural vibration in drive systems, was studied by Laschet and Troeder (Laschet and Troeder 1984). They developed computer programs and applied simulation techniques to predict and analyse the performance of gears trains. The distinctive feature of their research was that the backlash of the gears was considered in their programs and CAD data of the gear geometry could be used in their programs.

In 1985, Wang (Wang 1985) developed a torsional only vibration model. He focused on an analytical evaluation of gear dynamic factors based on rigid body dynamics and discussed different cases in which the transmission errors have different effects upon the dynamic load. He commented that the transmission error had a system wide effect and could be used to analyse rigid-body vibrating gear systems in which the gear deflection was not considered.

Tavares and Prodonoff (Tavares and Prodonoff 1986) proposed a new approach for torsional vibration analysis of gear-branched propulsion systems in 1986. Idle gears in a gear-branched system were modelled as part of the inertia of the master gear and the finite element method was used in their approach. In the same year, Umezawa, et al. (Umezawa et al. 1986) set up a test gearing unit which consisted of an input shaft, countershaft and output shaft. The gears were placed at arbitrary positions on the shafts in their unit so that the effect of the countershaft on the bending vibration and on the sound radiation became clear. At almost the same time, Iida, et al. (Iida et al. 1986) studied a three axis gear system but with some differences from Umezawa, et al., firstly, because the countershaft was on soft supports and secondly, the model was a coupled torsional-lateral vibration analytical model.

In 1992, a finite element model of a geared rotor system on flexible bearings was developed by Kahraman, et al. (Kahraman et al. 1992). The coupling between the torsional and transverse vibrations of the gears were considered in the model. They applied the transmission error as excitation at the mesh point to simulate the variable mesh stiffness. They presented three different geared systems as numerical examples

and discussed the effect of bearing compliance on gear dynamics. The assumptions they used were that the gear mesh was modelled by a pair of rigid disks connected by a spring and a damper with constant value which represented the average mesh values and tooth separation was not considered.

Another model presented by Kahraman (Kahraman 1993) was a linear dynamic model of a helical gear pair. The model considered the shaft and bearing flexibility and the dynamic coupling among the transverse, torsional, axial, and rocking motions due to the gear mesh. The natural frequencies and mode shapes were predicted and the forced response due to the static transmission error was predicted. After the parametric study of the effect of the helix angle on the free and forced vibrational characteristics of a gear pair, the conclusion was reached that the axial vibrations of a helical gear system could be neglected in predicting the natural frequencies and the dynamic mesh forces. The assumption for their model was that the gears were modelled as rigid disks, the clearances and stiffness changes of the bearings were neglected, and the system was assumed to be symmetrical about the transverse plane of the gears.

2.2.3 Models with a Whole Gearbox

The research models reviewed in this section are seen as being advanced because traditional analysis approaches mentioned previously in the gear dynamic area have concentrated on the internal rotating system and have excluded dynamic effects of the casing and flexible mounts. The focus of this group is on the dynamic analysis of the geared rotor system, which includes the gear pair, shafts, rolling element bearings, a motor, a load, a casing and flexible or rigid mounts.

In 1991, Lim and Singh (Lim and Singh 1991) presented a detailed study of the vibration analysis of complete gear boxes. Their research was based on previous studies including the bearing stiffness formulation (Lim and Singh 1990) and system studies (Lim and Singh 1990). They developed linear time-invariant, discrete dynamic models of an overall box by using lumped parameter and dynamic finite element techniques. They studied three example cases: case I, a single-stage rotor system with rigid casing and flexible mounts; case II, a spur gear drive system with

rigid casing and flexible mounts; and case III, a high-precision spur gear drive system with flexible casing and rigid mounts. They used the gear mesh coupling stiffness matrix to couple the two gears and used the bearing stiffness matrix to link the shafts and casing. In their finite element model, the gear, pinion, motor and load were simulated as generalised mass and inertia elements and the gear mesh stiffness matrix and bearing stiffness matrix were modelled as six-dimensional generalised stiffness matrices. They used the FEM software ANSYS to analyse their models. They made a parametric study of the effect of casing mass and mount stiffness on the system natural frequencies. A comparison of the casing flexural vibrations between the simulation and the experiment was presented.

Choy, et al. (Choy et al. 1991) presented a vibration analysis with the effect of casing motion and mass imbalance for a multi-stage gear transmission in 1991. In order to investigate the effect of the casing motion and mass imbalance, four major cases of external excitations were examined in their study. They employed the modal method to transform the equations of motion into modal coordinates to solve the uncoupled system. They concluded that the influence of the casing motion on system vibration is more pronounced in a stiffer rotor system. In the same year, El-Saeidy Fawzi (El-Saeidy Fawzi 1991) presented an analytical model for simulating the effect of tooth backlash and ball bearing deadband clearance on the vibration spectrum in a spur gearbox. The contact between meshing teeth using the time-varying mesh stiffness and mesh-damping factor was discussed. From their study, they concluded that the backlash and bearing deadband clearance had a pronounced effect on the vibration spectrum of a gearbox. In this model, the gearbox casing was assumed to be rigid, therefore, both ends of each shaft had the same displacements. There was no experimental result to verify the analytical result of this research.

One year later, Choy, et al. (Choy et al. 1992) continued their study on the multi-stage gear system. The work presented in that study was the development and application of a combined approach of using the modal synthesis and finite element methods in analysing the dynamics of multi-stage gear systems coupled with the gearbox structure or casing. In their solution procedure, modal equations of motion were developed for each rotor-bearing-gear stage using the transfer matrix method to evaluate the modal parameters, and the modal characteristics of the gearbox

structure were evaluated using a finite element model in NASTRAN. The modal equations for each rotor stage and the gearbox structure were coupled through the bearing supports and gear mesh.

After this study, they used their analytical model to predict the dynamic characteristics of a gear noise rig at the NASA Lewis Research Centre and then used experimental results from the test rig to verify the analytical model (Choy et al. 1993). Their conclusions were that the dynamics of the casing can be accurately modelled with a limited amount of analytically predicted vibration modes, and that the characteristics and trends of the casing vibration spectra predicted by the analytical model were very similar to those found in the experimental data.

In 1992, Ong (Ong 1992) described the application of the eigenvalue economisation method coupled with the frontal solution technique to a vehicle transmission system comprising an integral bell-housing gearbox, extension housing, drive shaft and rear-axle assembly. In this study, super-elements were applied using the structural dynamic substructuring technique for the finite element analysis. The pinion shafts were represented by beam elements and the gears and bearings were represented by lumped mass elements in the analytical model. Finally, a comparison was made between experimental results and the finite element method, which showed good agreement.

Most analyses of gearboxes appear to be concerned with the dynamic response and vibration characteristics. In 1994, Sabot and Peret-Liaudet (Sabot and Perret-Liaudet 1994) presented another phase of study, noise analysis of gearboxes. They pointed out that a troublesome part of the noise within the car or truck cab could be attributed to the gearbox and that this noise was associated with the vibrations induced by the transmission error which gives rise to dynamic loads on the teeth, shafts, bearings and casing. They computed the noise radiated by the gearbox casing using the Rayleigh Integral Formulation in which the acceleration response of the casing associated with the finite element method calculation was considered. Their results showed that although the test model was a simplified gearbox, their numerical analysis provided a better understanding of the sound radiation characteristics of geared transmission systems.

At the same time, Kato, et al. (Kato et al. 1994) developed a simulation method by integrating finite element vibration analysis and boundary element acoustic analysis for the purpose of evaluating the sound power radiated from the gearbox and achieved good agreement with the experimental results. In their model, each shaft was modelled using beam elements and the mass and rotating inertia of the gear was modelled as lumped masses and added to the shaft. Each of the rolling element bearings was represented as a spring and damper and the casing of the gearbox was modelled by a thin shell element in the finite element package program ISAP-6. Their acoustic analysis in the frequency domain showed that the sound power at the mesh frequency was greater than the sound power at other frequencies.

There have also been various studies aimed at modelling a single mechanical element, a complex system containing several gears as well as other mechanical or electrical elements and other special topics, such as,

Load Sharing Ratio (Remmers 1978; Drago et al. 1979; Walford and Stone 1980; Bahgat et al. 1983; Ozguven and Houser 1988; Kuang and Yang 1992; Liou et al. 1992; Liou et al. 1996; Litvin et al. 1996; Zhang and Fang 1998, Chabert, 1974 #35)
Mesh Stiffness (Gargiulo 1980; Kahraman and Singh 1991; Kuang and Yang 1992; Brousseau et al. 1994; Daniewicz et al. 1994; Sirichai et al. 1996; Velinsky 1996; Du et al., Elkholdy et al. 1998; Gosselin et al. 1998; Nadolski and Pielorz 1998)
Bearing Stiffness (Childs 1980; Gargiulo 1980; Bahgat et al. 1981; Smith 1987; Lim and Singh 1990; Lim and Singh 1990; Kahraman and Singh 1991; Lim and Singh 1991; Lim and Singh 1992)
Shaft In A Gear System (Johnson 1962; Iida et al. 1980; Iida and Tamura 1984; Neriya et al. 1985; Iida et al. 1986; Lin et al. 1988; Prasad et al. 1992; Zhong-Sheng et al. 1993; Okamoto et al. 1994)
Casing Analysis Of A Gearbox (Drago et al. 1979; Randall 1980; Randall 1984; Mcfadden 1985; Tavares and Prodonoff 1986; Houser 1990; Randall and Kelly 1990; Zakrajsek and al. 1990; Sundarajan and Amin 1991; Choy et al. 1992; Inoue et al. 1992; Maruyama et al. 1992; Oswald et al. 1992; Oswald et al. 1992; Perret-Liaudet and Sabot 1992; Kato et al. 1994; Kissling 1994; Oswald et al. 1994; Sabot

and Perret-Liaudet 1994; Sabot and Perret-Liaudet 1994; Zhang and Kohler 1994; Zhang et al. 1994; Du 1997)

Gear Transmission Error Measurement (Gregory et al. 1963; Tordian and Geraldin 1967; Tordion and Gerardin 1967; Hayashi and Hayashi 1981; Houser and Blankenship 1989; Rebbechi et al. 1992; Vinayak and Houser 1992; Bard et al. 1994; Barnett and Yildrim 1994; Munro and Yildirim 1994; Velex et al. 1995; Houser et al. 1996; Sweeney and Randall 1996)

Transmission System (Drago et al. 1979; Ong 1992; Choy and Polyshchuk 1995; Choy et al. 1996; Choy et al. 1996; Forrester 1996; Regalado and Houser 1998)

Computerized Design And Generation Of Gears (Litvin and Hsiao 1993; Litvin and Lu 1993; Blazakis and Houser 1994; Zhang et al. 1994; Litvin et al. 1995; Litvin et al. 1995; Litvin and Lu 1995; Litvin and Feng 1996; Litvin and Seol 1996; Seol and Litvin 1996; Seol and Litvin 1996; Litvin and Kim 1997; Litvin et al. 1998; Litvin et al. 1998)

Gear Geometry (Chen et al. 1992; Fujio et al. 1992; Kin 1992; Kubo et al. 1992; Tsai and Chang 1992; Donno and Litvin 1998; Dooner and Seireg 1998; Feng et al. 1998; Su and Houser 1998)

Gear Noise Design (Aida et al. 1967; Aida 1968; Aida 1969; Kobler et al. 1970; Daly and Smith 1979; Drago et al. 1979; Welbourn 1979; Smith 1987; Baron et al. 1988; Houser 1990; Randall and Deyang 1990; Randall and Kelly 1990; Zakrajsek and al. 1990; Mark 1992; Maruyama et al. 1992; Oswald et al. 1992; Oswald et al. 1992; Alattass et al. 1994; Lewicki et al. 1994; Oswald et al. 1994; Sabot and Perret-Liaudet 1994; Sabot and Perret-Liaudet 1994; Tuma et al. 1994; Zhang and Kohler 1994; Zhang et al. 1994; Litvin et al. 1995; Roosmalen 1995; Wang and Tong 1996; Cheng and Lim 1998; Stadtfeld 1998)

Stress Analysis (Arikan and Kaftanoglu 1989; Arikan 1991; Arikan and Tamar 1992; Moriwaki et al. 1993; Rao and Muthuveerappan 1993; Baret et al. 1994; Daniewicz et al. 1994; Vijayarangan and Ganesan 1994; Lu et al. 1995; Refaat and Meguid 1995; Litvin et al. 1996; Kalluri and Houser 1998; Kim et al. 1998; Richard E. Dippery et al. 1998)

2.3 CONTACT ANALYSIS

Studies on contact problems began hundreds of years ago and their history may be divided into various stages, as briefly described in the following sections.

In the first stage, contact bodies were restricted to rigid bodies or simple elastic bodies and only global phenomena such as the total contact forces were observed. Newton's third law and Coulomb's friction law may be considered as the two greatest results in this stage. The basic ideas developed are still used today in some analyses. As an example, the problem depicted in Figure 2.3.1 (a) can be considered. A stiff elastic block A lies on another stiff elastic block B which lies on a rigid ground C. A force P is applied on block A as shown in the figure.

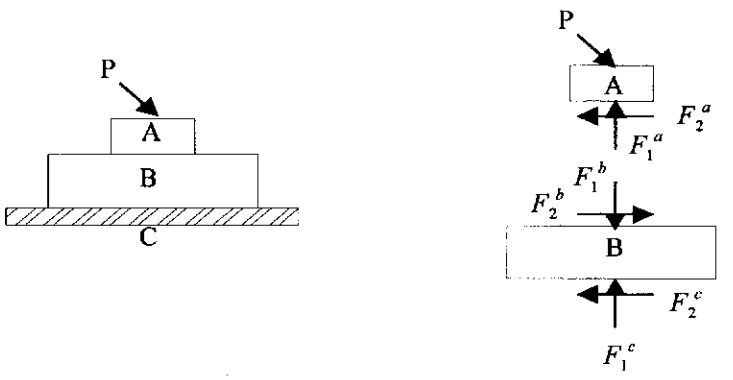

(a) (b)

Figure 2.3.1. (a) A contact system consisting of two elastic blocks and a rigid ground. (b) Decomposition of the contact system into free bodies.

To study its global behavior, this simple contact system may be decomposed by making free bodies as shown in Figure 2.3.1 (b), where the contact forces and frictional forces are subjected to the following contact conditions:

$$F_1^b = F_1^a, \qquad F_2^b = F_2^a \quad \text{(Newton's third law)} \qquad (2.3.1)$$

$$F_2^a \le \mu_1 F_1^a$$

$$F_2^c \le \mu_2 F_1^c \qquad \text{(Coulomb's friction law)} \qquad (2.3.2)$$

where μ_1 and μ_2 are friction coefficients between A and B and between B and C, respectively.

In this example, only the total contact force and the total frictional force are considered, without bothering about how these forces are actually distributed on the contact surface. While this procedure can be used to analyse the global behaviour of the block for some purposes, it is not sufficient for other purposes, such as studying the damage of the block due to wear, which demands the knowledge of contact stress distributions on the contacting surface.

The development of Mechanical Science and the advances in engineering activities made it of interest to study increasingly complex contact problems. Local phenomena, like stress distributions on contacting surfaces, began to be observed. Among others, Hertz was a leading scientist in this area. His successful treatment of a static contact problem in elasticity in the 1880s (Hertz 1881; Hertz 1882), has been regarded as a milestone in the field. In his study, Hertz assumed that contact bodies can be regarded as elastic half-spaces with small deformations and that contacting areas are small and, in general, elliptical. He also assumed that the contacting boundaries are frictionless. An example of the classical Hertzian contact problem is presented here for clarification.

Two elastic spheres in contact are shown in Figure 2.3.2(a). In the Hertzian contact theory, the displacements of the contacting boundaries are assumed to satisfy the following condition (Johnson 1985),

$$u_3^1 + u_3^2 \approx g - (1/2R)(r)^2 \quad , \qquad (2.3.3)$$

where u_3^1 and u_3^2 are the displacement components in the x_3 direction of the contacting boundaries from the two spheres, respectively. The initial separation of

the two contacting boundaries is given by g, and $\frac{1}{R} = \frac{1}{R_1} + \frac{1}{R_2}$ in which R_1 and R_2 are the radii of the two spheres, respectively, and r is the distance between a given contacting point and the centre of the contacting area, which is a circle in this case.

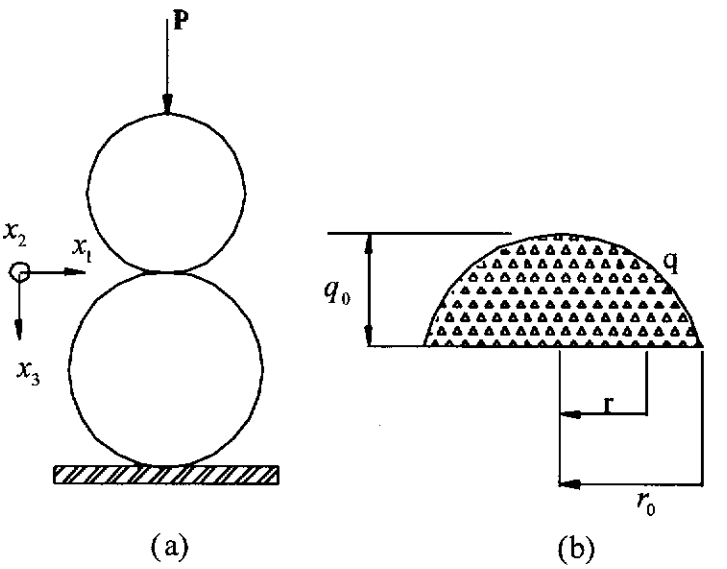

Figure 2.3.2. (a) Two spheres in contact. (b) Contact pressure distribution between the two spheres according to Hertzian contact theory.

On the basis of equation (2.3.3), the contact pressure distribution on the contacting area can be found as,

$$q = q_0[1-(\frac{r}{r_0})^2]^{\frac{1}{2}} \quad , \tag{2.3.4}$$

where r_0 is the radius of the contacting area and q_0 is the maximum pressure at the centre. The pressure distribution in equation (2.3.4) is plotted in Figure 2.3.2(b).

In spite of the fact that the Hertz theory of contact has stood the test of time and has been a landmark in applied mechanics for many decades, it suffers from major restrictions. These limitations are that the bodies have smooth continuous surfaces, the stress and displacements can be deduced from the small strain theory of elasticity applied to a linear elastic half-space, and that the surfaces are frictionless. Following

Hertz's work, many researchers and scientists studied contact problems between elastic bodies of different shapes and under different circumstances with or without friction. Examples can be found in Goodman, Gladwell, and Johnson (Goodman 1954; Goodman and Keer 1965; Gladwell 1980; Johnson 1985). In the work by Goldsmith (Goldsmith 1960), impact problems were studied via analytical and experimental approaches. A common feature in these studies is that the geometry and deformation of a contact body was assumed in such a way that available mathematical and mechanical tools can be used to obtain a close-form solution of the problem. We may classify such studies as the second stage. The approaches used in this stage are obviously very restrictive and can only be applied to very special problems.

With the rapid development in the capabilities of digital computers, numerical methods became the prime interest of researchers, especially in engineering disciplines where the aim was to obtain more realistic solutions. Therefore, the third stage may be viewed as the numerical study stage, in which numerical methods have been used for the solution of contact problems. Among other possible methods, the finite element method has been most widely used. With the finite element method, the references included in this area include (Zienkiewicz 1967; Zienkiewicz 1971; Oden 1972; Hinton and Owen 1977; Zienkiewicz 1977; Bathe 1982; Pittman et al. 1984; Cook et al. 1989; Kleiber 1989; Zienkiewicz and Taylor 1994; Zienkiewicz and Taylor 1994; Cook 1995). Contact bodies are approximated by collections of finite elements and contact boundaries are approximated by collections of polygons. The contact bodies may have complicated geometry and material properties and may deform in an arbitrary way. The solution of the contact problem finally involves solving algebraic equation systems instead of obtaining a close-form solution.

CHAPTER 3

ANALYTICAL MODELS

3.1 NUMERICAL METHOD OF CONTACT ANALYSIS

Contact problems present many significant difficulties. Firstly, the actual region of contact between deformable bodies in contact is not known until the solution has been obtained. Depending on the loads, material, boundary conditions, and other factors, surface can come into and go out of contact with each other in a largely unpredictable and abrupt manner. Secondly, most contact problems need to account for friction. There are several friction laws and models to choose from, and all are nonlinear. Frictional response can be chaotic, making solution convergence difficult (ANSYS 1997). In addition to those difficulties, many contact problems must also address multi-field effects, such as the conductance of heat and electrical currents in the areas of contact.

Bodies in contact may have complicated geometries and material properties and may deform in an arbitrary way. The solution of the contact problem involves solving algebraic equation systems instead of obtaining a closed-form solution. To demonstrate the basic ideas in the solution procedure of contact problems using the finite element method, a simple contact problem can be demonstrated (Zhong 1993). A simply connected body consisting of an elastic material is subjected to the load

and boundary conditions as shown in Figure 3.1.1(a). The body occupies a space domain Ω in a coordinate system $0x_1x_2x_3$ as shown in the figure. Let t denote time, **x** a position vector, **u**(**x**,t) the displacement field, and **a**(**x**,t) the acceleration field within the body, respectively. The motion of block is then governed by the following equation,

$$\frac{\partial \sigma_{ji}(\mathbf{x},t)}{\partial x_j} + b_i(\mathbf{x},t) = \rho a_i(\mathbf{x},t), \qquad \text{i = 1 to 3 and j = 1 to 3} \qquad (3.1.1)$$

where σ_{ji} (**x**,t) is the Cauchy stress component, b_i (**x**,t) is the ith component of the body force vector **b** (**x**,t), ρ is the mass density of the material which is assumed constant within Ω, and a_i (**x**,t) is the ith component of the acceleration vector of a material particle within the body.

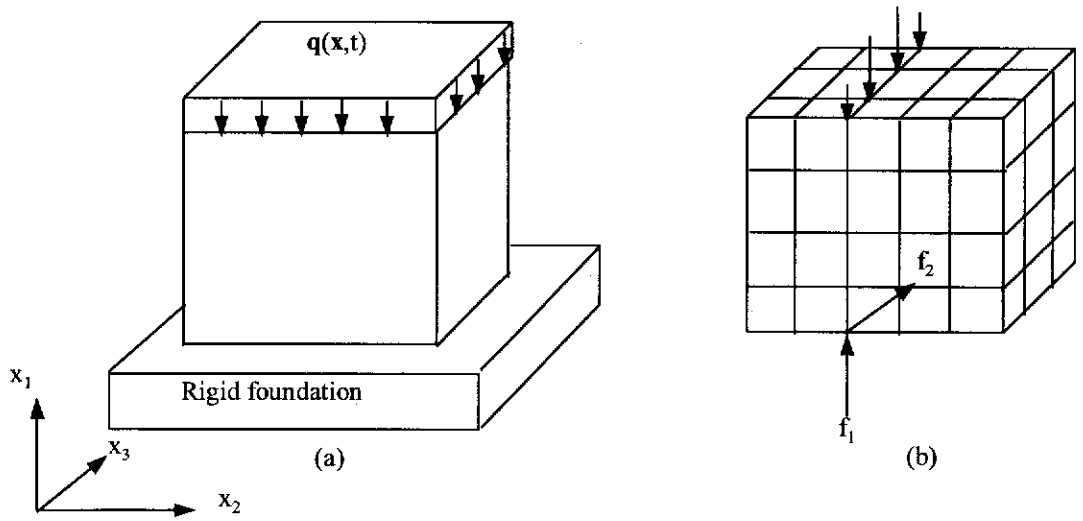

Figure 3.1.1. (a) An elastic body in contact (b) A finite element model of the body.

For elastic materials, the stress-strain relation is given by the generalized Hook's law as,

$$\sigma_{ji}(\mathbf{x},t) = c_{ijkl} e_{kl}(\mathbf{x},t), \qquad \text{k = 1 to 3 and l = 1 to 3} \qquad (3.1.2)$$

where c_{ijkl} are material parameters and $e_{kl}(\mathbf{x},t)$ are the strain components, which are related to the displacement $\mathbf{u}(\mathbf{x},t)$ as follows,

$$e_{kl}(\mathbf{x},t) = \frac{1}{2}\left[\frac{\partial u_k(\mathbf{x},t)}{\partial x_i} + \frac{\partial u_i(\mathbf{x},t)}{\partial x_k}\right] . \tag{3.1.3}$$

The boundary of Ω is denoted by Γ and consists of three distinct parts,

$$\Gamma = \Gamma_d \cup \Gamma_f \cup \Gamma_c , \tag{3.1.4}$$

where Γ_d denotes the part of the boundary where displacements are prescribed, Γ_f denotes the part where boundary traction are prescribed, and Γ_c denotes the part where contacts may occur. The prescribed boundary conditions are expressed as,

$$u_i(\mathbf{x},t) = \bar{u}_i(\mathbf{x},t), \qquad \mathbf{x} \in \Gamma_d , \tag{3.1.5}$$

and

$$\sigma_{ij}(\mathbf{x},t)N_j = \bar{q}_i(\mathbf{x},t), \qquad \mathbf{x} \in \Gamma_f , \tag{3.1.6}$$

where $\bar{u}_i(\mathbf{x},t)$ and $\bar{q}_i(\mathbf{x},t)$ are prescribed displacement components and boundary traction components, respectively, and N_j are the components of an outward unit normal vector on the boundary Γ_f, which can be considered as constants.

The initial conditions which are to be satisfied by the displacement field $\mathbf{u}(\mathbf{x},t)$ can be simply expressed as,

$$\mathbf{u}(\mathbf{x},0) = \bar{\mathbf{u}}(\mathbf{x}), \qquad \mathbf{x} \in \Omega , \tag{3.1.7}$$

and

$$\mathbf{v}(\mathbf{x},0) = \bar{\mathbf{v}}(\mathbf{x}), \qquad \mathbf{x} \in \Omega , \tag{3.1.8}$$

where $\bar{\mathbf{u}}(\mathbf{x})$ and $\bar{\mathbf{v}}(\mathbf{x})$ are the prescribed values for $\mathbf{u}(\mathbf{x},0)$ and $\mathbf{v}(\mathbf{x},0)$, respectively.

On the boundary Γ_c, the condition which must be satisfied is that the normal contact stress should be compressive and that the boundary should not penetrate into the rigid ground. These condition are expressed as,

$$g(\mathbf{x},t) = g(\mathbf{x}) - \mathbf{u}(\mathbf{x},t)\times\mathbf{N} \geq 0, \qquad \mathbf{x} \in \Gamma_c , \tag{3.1.9}$$

and

$$q_1(\mathbf{x},t) = \mathbf{q}_c(\mathbf{x},t)\times\mathbf{N} \leq 0, \qquad \mathbf{x} \in \Gamma_c , \tag{3.1.10}$$

where $g(\mathbf{x},t)$ defines the gap between the contact surface and the rigid ground, $g(\mathbf{x})$ denotes the initial value of $g(\mathbf{x},t)$, $\mathbf{q}_c(\mathbf{x},t)$ is the contact traction, and $q_1(\mathbf{x},t)$ is the normal component of $\mathbf{q}_c(\mathbf{x},t)$ in the outward normal direction of the surface. Furthermore, the condition must be satisfied that,

$$g(\mathbf{x},t)\times q_1(\mathbf{x},t) = 0 , \tag{3.1.11}$$

which means that if $g(\mathbf{x},t)$ is non-zero, $q_1(\mathbf{x},t)$ must be zero and if $q_1(\mathbf{x},t)$ is non-zero, $g(\mathbf{x},t)$ must be zero.

Assuming Coulomb's friction law on the surface, the tangential component, denoted by $q_1(\mathbf{x},t)$, of the contact traction must satisfy the condition that,

$$q_1(\mathbf{x},t) \leq \nu\, q_1(\mathbf{x},t), \qquad \mathbf{x} \in \Gamma_c , \tag{3.1.12}$$

and the tangential velocity of the contacting boundary, denoted by $\mathbf{v}_t(\mathbf{x},t)$, must satisfy the condition that,

$$\mathbf{v}_t(\mathbf{x},t) = 0, \quad \text{if } q_t(\mathbf{x},t) < \nu\, q_1(\mathbf{x},t), \qquad \mathbf{x} \in \Gamma_c , \tag{3.1.13}$$

and

$$\mathbf{v}_t(\mathbf{x},t) = \lambda\, \mathbf{q}_t(\mathbf{x},t), \quad \text{if } q_t(\mathbf{x},t) = \nu\, q_1(\mathbf{x},t), \qquad \mathbf{x} \in \Gamma_c , \tag{3.1.14}$$

where ν is the friction coefficient, λ is a non-negative scalar, and

$$\mathbf{q}_t(\mathbf{x},t) = \mathbf{q}_c(\mathbf{x},t) - q_1(\mathbf{x},t)\mathbf{N} \quad . \tag{3.1.15}$$

Equations (3.1.9) to (3.1.14) are the governing conditions which characterise the contact problem. It is convenient to drop the arguments **x** and t in the parentheses for all quantities for simplicity. It must be remembered though, that all the kinematic and mechanical quantities are functions of both position **x** and time t for general dynamic problems, but are functions only of position **x** for static problems.

3.1.1 Variation Inequalities

Let us consider now, the classic Signorini problem (Kikuchi and Oden 1988) of the static equilibrium of the elastic body in frictionless contact with the rigid ground. The acceleration of the body is zero and no friction forces are assumed to act on the body. Furthermore, all prescribed displacements are assumed to be zero. The equation of motion and boundary conditions for the body reduce to the following equations.

Static equilibrium condition,

$$\frac{\partial \sigma_{ji}}{\partial x_j} + b_i = 0, \qquad \text{i = 1 to 3 and j = 1 to 3.} \tag{3.1.16}$$

Prescribed boundary conditions,

$$u_i = \bar{u}_i, \qquad \text{on } \Gamma_d \quad , \tag{3.1.17}$$

and

$$\sigma_{ij} N_j = \bar{q}_i, \qquad \text{on } \Gamma_f \quad . \tag{3.1.18}$$

Contact conditions,

$$g = g_0 - \mathbf{u}\,\mathbf{N} \geq 0, \qquad \text{on } \Gamma_c \quad , \tag{3.1.19}$$

and

$$q_1 = \mathbf{q}_c \mathbf{N} \le 0, \qquad \text{on } \Gamma_c \ , \tag{3.1.20}$$

and

$$q_1 g = 0, \qquad \text{on } \Gamma_c \ . \tag{3.1.21}$$

The Signorini problem can be formulated in an alternative way by using the principle of virtual work. Let **V** denote a set of admissible displacement fields for the body. It is assumed that any member **v** of **V** is sufficiently smooth that all necessary mathematical operations are well defined. By an admissible displacement field, it is also meant that the contact condition is satisfied by the displacement field, which gives,

$$g = g_0 - \mathbf{v}\,\mathbf{N} \ge 0, \qquad \text{on } \Gamma_c \ . \tag{3.1.22}$$

Suppose now that **u** is the true solution of the Signorini problem. This also means that **u** is a member of **V**, i.e. $\mathbf{u} \in \mathbf{V}$. The actual stress produced by **u** is denoted by σ (**u**). Let $\delta\mathbf{u}$ be an admissible virtual displacement given by $\delta\mathbf{u} = \mathbf{v}\text{-}\mathbf{u}$ and $\delta\mathbf{e}$ be the virtual strain produced by $\delta\mathbf{u}$. Then, the principle of virtual work can be stated as,

$$\int_\Omega \sigma_{ij}\delta e_{ij} d\Omega = \int_\Omega \bar{b}_i\, \delta u_i d\Omega + \int_{\Gamma_f} \bar{q}_i\, \delta u_i dS + \int_{\Gamma_c} q_i\, \delta u_i dS \ , \tag{3.1.23}$$

where summations on i and j are assumed with i and j ranging from 1 to 3, and δu_1 denoting the virtual displacement in the normal direction on the potential contacting boundary Γ_c.

Now it holds that,

$$\begin{aligned} q_1\, \delta u_1 &= q_1\, (\mathbf{v}\,\mathbf{N} - \mathbf{u}\,\mathbf{N}), \\ &= q_1\, (\mathbf{v}\,\mathbf{N} - \mathbf{u}\,\mathbf{N} + g_0 - g_0), \\ &= q_1\, (\mathbf{v}\,\mathbf{N} - g_0) \ge 0 \ . \end{aligned} \tag{3.1.24}$$

Thus, it can be obtained from equation (3.1.23) and (3.1.24) that,

$$\int_{\Omega} \sigma_{ij} \delta e_{ij} d\Omega \quad \geq \quad \int_{\Omega} \bar{b}_i \, \delta u_i d\Omega + \int_{\Gamma_f} \bar{q}_i \, \delta u_i dS \quad . \tag{3.1.25}$$

Equation (3.1.25) is a variation inequality. An advantage of the formulation is that all the boundary conditions, including the contact conditions, are incorporated into a single variation inequality. Furthermore, with the variation inequality formulation, the existence and/or uniqueness of solution can be proved and error estimates can be obtained for some contact problems.

3.1.2 Variation Equalities

Although the methods of solution of such an inequality are now well established, a comprehensive mathematical background is required to work with such a formulation, as shown by (Panagiotopoulos 1975; Panagiotopoulos 1977; Kikuchi and Song 1980; Compos et al. 1982; Talaslidis and Panagiotopoulos 1982; Martins and Oden 1983; Pires and Oden 1983; May 1986; Sayegh and Tso 1986; Klarbring 1986a; Klarbring 1986b; Panagiotopoulos and Lazaridis 1987; Klarbring et al. 1988; Zhong and Sun 1988; Johnson and Quigley 1989; Lee and Kwak 1989; Refaat and Meguid 1994a; Refaat and Meguid 1994b; Refaat 1995; Refaat and Meguid 1995; Refaat and Meguid 1996; Refaat and Refaat 1997).

While many prefer to work with a variational inequality, many others prefer to work straightforwardly with a variational equality as can be seen for example in (Wilson and Parsons 1970; Chan and Tuba 1971a; Chan and Tuba 1971b; Hughes et al. 1976; Fredriksson 1976a; Fredriksson 1976b; Sachdeva et al. 1981; Tseng and Olsen 1981; Arya and Hegemier 1982; Goudreau and Hallquist 1982; Mahmoud et al. 1982; Haber and Abel 1983; Fredriksson 1984; Padovan et al. 1984; Rahman et al. 1984; Bathe and Chaudhary 1985; Hallquist et al. 1985; Rothert et al. 1985; Chaudhary and Bathe 1986; Chen and Pwu 1986; Nour-Omid and Wriggers 1986; Tzou and Schiff 1987; Heyliger and Reddy 1987a; Heyliger and Reddy 1987b; Doudoumis and Mitsopoulou 1988; Noor and Kim 1989; Lee 1989a; Lee 1989b).

For engineering researchers, it is perhaps more straightforward to consider the following variation equality formulation.

In applying the principle of virtual work, we recognize the fact that contact traction exists only on contacting boundaries, i.e. the boundaries that actually are in contact. Let the contacting boundary be denoted by Γ_c. Then, we can write, instead of equation (3.1.23), the following equation,

$$\int_{\Omega} \sigma_{ij} \delta e_{ij} d\Omega - \int_{\Omega} \bar{b}_i \, \delta u_i d\Omega - \int_{\Gamma_f} \bar{q}_i \, \delta u_i dS - \int_{\Gamma_c} q_i \, \delta u_i dS \quad = \quad 0 \quad . \tag{3.1.26}$$

Our problem is now to find the displacement field **u** and the contact traction **q** such that equation (3.1.26) and all the boundary conditions, including contact conditions, are satisfied. One problem associated with the variation equalities formulation is that the actual contacting boundary is in general unknown a priori in implicit analysis, bringing difficulties in carrying out the surface integral on Γ_c in equation (3.1.26). To solve equation (3.1.26), an incremental trial-error procedure with iteration is thus required.

Dynamic effects have not been included in equation (3.1.26). For dynamic contact problems, the virtual work done by inertia forces also needs to be considered and the following equation is obtained in place of equation (3.1.26),

$$\int_{\Omega} \sigma_{ij} \delta e_{ij} d\Omega + \int_{\Omega} \rho a_i \delta u_i d\Omega - \int_{\Omega} \bar{b}_i \, \delta u_i d\Omega - \int_{\Gamma_f} \bar{q}_i \, \delta u_i dS - \int_{\Gamma_c} q_i \, \delta u_i dS = \quad 0 \quad . \tag{3.1.27}$$

3.2 THE FINITE ELEMENT METHOD OF CONTACT ANALYSIS

This section reviews the basic steps and ingredients in the solution of equation (3.1.27) using finite element analysis. To carry out the integrations in equation (3.1.27), the domain Ω is divided into subdomains, called finite elements, for example as shown in Figure 3.1.1(b). Integrations in equation (3.1.27) are carried

out on element level and assembled to obtain an equation system for the whole domain. If contact does not occur, i.e. $q_1 = 0$, the finite element discretization of equation (3.1.27) leads to,

$$[M]\{A\} + [K]\{U\} = \{F\}, \tag{3.2.1}$$

where [M] is the mass matrix, [K] is the stiffness, {U} is the displacement vector, {A} is the acceleration vector, and {F} is the external load vector as in the standard finite element procedure.

If contact does occur, q_1 will be non-zero and will contribute to equation (3.2.1). In the finite element method, q_1 can be obtained from its nodal values, denoted by q_1^m at node m, at discrete finite element nodes by interpolations. Then q_1^m can be taken as the primary unknowns to be solved for. Denoting the contribution of contact forces to the load vector by $\{F_c\}$, we can write,

$$[M]\{A\} + [K]\{U\} = \{F\} + \{F_c\} \quad . \tag{3.2.2a}$$

In equation (3.2.2a), $\{F_c\}$ is unknown and is to be calculated under the constraint given in equation (3.2.2b). With the finite element discretization, the kinematic constraint on contacting nodes can be put into the form,

$$[Q]\{U\} + \{G\} = 0 \quad , \tag{3.2.2b}$$

where {G} is calculated from initial gaps of contacting nodes and [Q] is a coefficient matrix resulting from the finite element discretization.

In order to solve equation (3.2.2), we must first determine the total number of contacting nodes, which are unknown until the solution is found. Thus, trial contacting nodes need to be used and iterations need to be carried out to find the true contacting nodes. At the same time, the contact condition must be enforced to solve the unknown contact force, which necessitates a constraint method. If frictional effects are to be considered, a friction law governing the tangential contact force is

required. Furthermore, we have both displacements and accelerations as unknowns in equation (3.2.2). Therefore, a time integration method is also required for the solution.

The above discussion on the finite element solution procedure for contact problems is neither general nor complete, rather, it can help to show some of the ingredients in solving contact problems with the finite element method. These basic ingredients may be classified as follows.

- Variational formulation, which provides a basis for the finite element discretisation.
- Element formulation, which calculates the element contribution to the coefficient matrix and the load vector in equation (3.1.2).
- Material modelling, which determines the stress-strain relationships and plays an important role in the element formulation.
- Friction law, which governs the frictional forces if frictional effects are to be included.
- Contact constraint method, which provides a means of calculating the unknown contact forces under contact constraints.
- Contact searching algorithm, which searches potential contacting nodes and determines the locations of contacting nodes accurately and efficiently.
- Time integration method, which integrates in the time domain.
- Linearisation and iterative procedure, which transforms a geometrical non-linear problem into a series of geometrical linear problems. In general contact problems with geometrical non-linearities, a linearisation procedure will be required to treat the geometrical non-linearity.

With the use of advanced finite element techniques, no restriction is in principle necessary on the geometry, material properties, and deformation patterns of contacting bodies. The versatility of the finite element method makes it possible to attack extremely complicated problems. Over the last few decades, great efforts have been devoted to the finite element study of contact problems. Remarkable progress has been made in both theoretical studies and engineering applications.

3.3 GEAR BODY ROTATION COMPATIBILITY

Evaluating load share between meshing teeth gears is a complex process when more than one-tooth pair are simultaneously in contact and an iterative numerical solution must be used. This section presents a general approach to calculate how load is shared between meshing teeth in spur gear pairs, taking into account the composite tooth deflection due to bending, shearing and contact deformation.

When the gears are put into mesh as shown in Figure 3.3.1, the line tangent to both base circles is defined as the line of action for involute gears. In one complete tooth mesh cycle, the contact starts at point A, as shown in Figure 3.3.1(a), where the outside diameter circle, the addendum circle, of the gear intersects the line of action. The mesh cycle ends at point E, as shown in Figure 3.3.1(e), where the outside diameter of the pinion intersects the line of action. Consider the two identical spur gears in mesh, as shown in Figure 3.3.1. When the first tooth pair contacts at point A, between the tooth tip of the output gear and the root of the input gear (pinion), a second tooth pair is already in contact at point D. As the gear rotates, the point of contact will move along the line of action APE. When the first tooth pair reaches point B, as shown in Figure 3.3.1(b), the second tooth pair disengages at point E leaving only the first tooth pair in the single contact zone. When this first tooth pair rotates to point D, as shown in Figure 3.3.1(d), the next tooth pair begins engagement at point A which starts another mesh cycle. Finally, one complete tooth meshing cycle is completed when this first tooth pair rotates to point E, as shown in Figure 3.3.1(e).

In order to simplify the complexity of the problem, the load sharing compatibility condition is based on the assumption that the sum of the torque contributions of each meshing tooth pair must equal the total applied torque.

In considering the single pair contact zone between points B to D, as shown in Figure 3.3.1(b) to Figure 3.3.1(d), for example at contact point B of Figure 3.3.2, the torque vectors are defined by the following cross product,

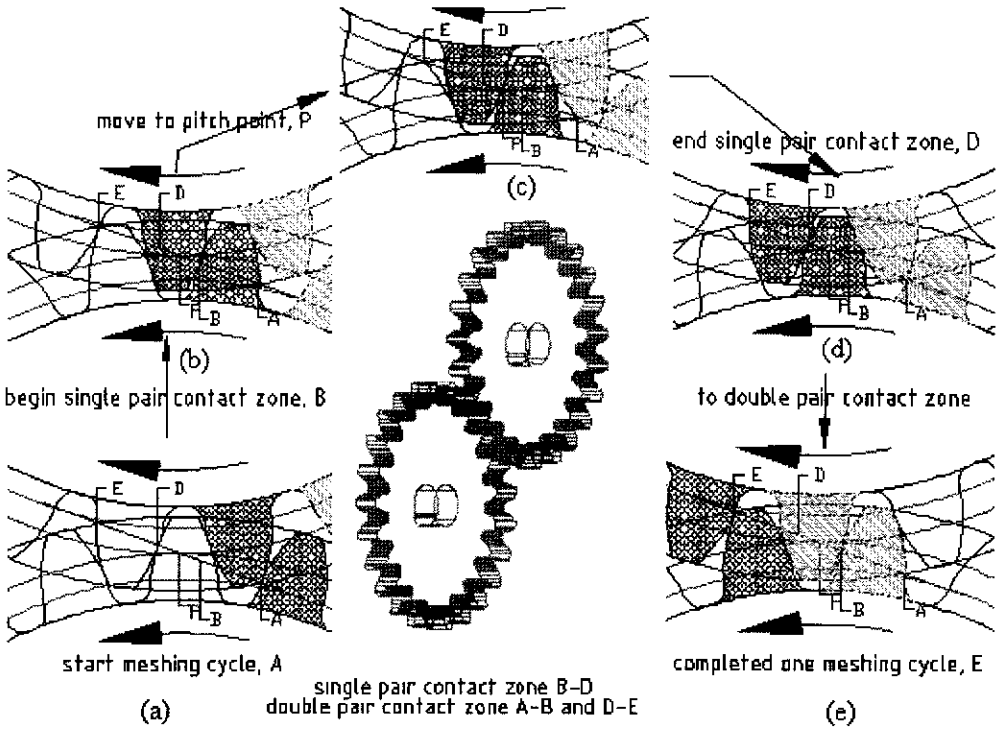

Figure 3.3.1. Illustration of one complete tooth meshing cycle.

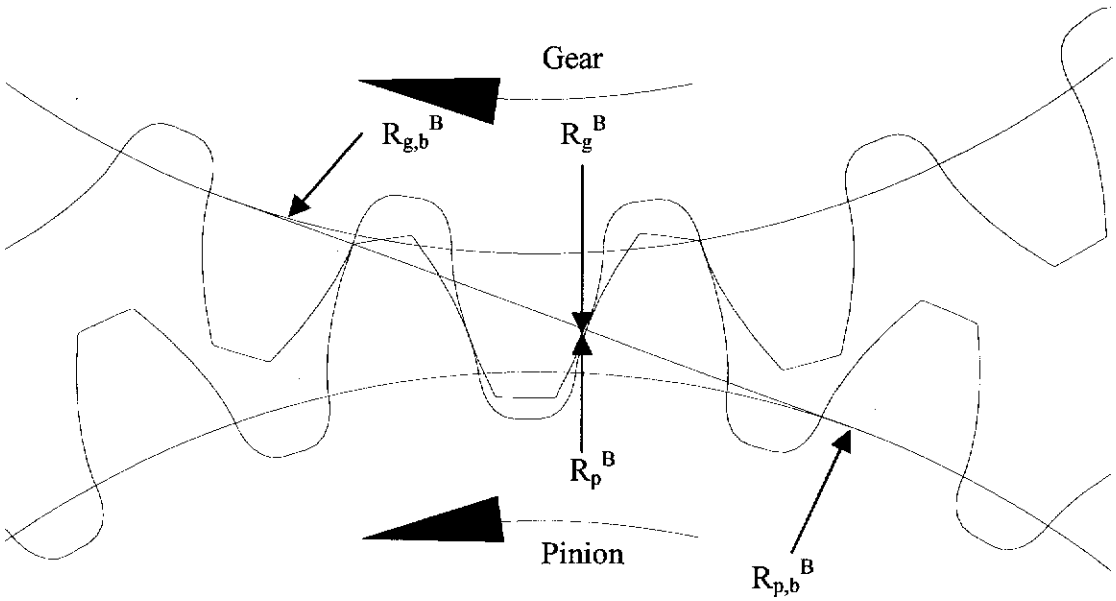

Figure 3.3.2. Illustration of the single pair contact zone at point B.

for the pinion,

$$T_p^B = R_p^B \times F_p^B \quad , \tag{3.3.1}$$

and for the gear,

$$T_g^B = R_g^B \times F_g^B \quad , \tag{3.3.2}$$

where T_p^B and T_g^B, are the torque vectors of the single pair contact zone at point B of the pinion and gear respectively. The transverse plane contact radius vectors on the pinion and gear tooth at point B are given by R_p^B and R_g^B, and the applied force vectors of the pinion and gear are given by F_p^B and F_g^B, at the contact points B of the pinion and gear respectively.

Next, considering the double pair contact zone of the two contact pairs at A and D as shown in Figure 3.3.3, where the sum of the torque contributions of each meshing tooth pair A and D must equal the total applied torque, the torques will be given by,

for the pinion,

$$\begin{aligned} T_{tot,p}^{A,D} &= T_p^A + T_p^D \quad , \\ &= \left(R_p^A \times F_p^A\right) + \left(R_p^D \times F_p^D\right) \quad , \end{aligned} \tag{3.3.3}$$

and for the gear,

$$\begin{aligned} T_{tot,g}^{A,D} &= T_g^A + T_g^D \quad , \\ &= \left(R_g^A \times F_g^A\right) + \left(R_g^D \times F_g^D\right) \quad , \end{aligned} \tag{3.3.4}$$

where T_p^A, T_p^D, T_g^A, T_g^D are the torque vectorial contributions to the total applied torque of tooth pairs at A and D of the pinion and gear respectively and $T_{tot,p}^{A,D}$, and $T_{tot,g}^{A,D}$ are the total applied torque vectors of the pinion and gear respectively. The transverse plane contact radius vectors on the pinion and gear tooth pair A and D are given by R_p^A, R_p^D, R_g^A, R_g^D and the load share vectors F_p^A, F_p^D, F_g^A, F_g^D are part of the total applied force vectors $F_{tot,p}^{A,D}$ and $F_{tot,g}^{A,D}$, at the contact points A and D of the pinion and gear respectively.

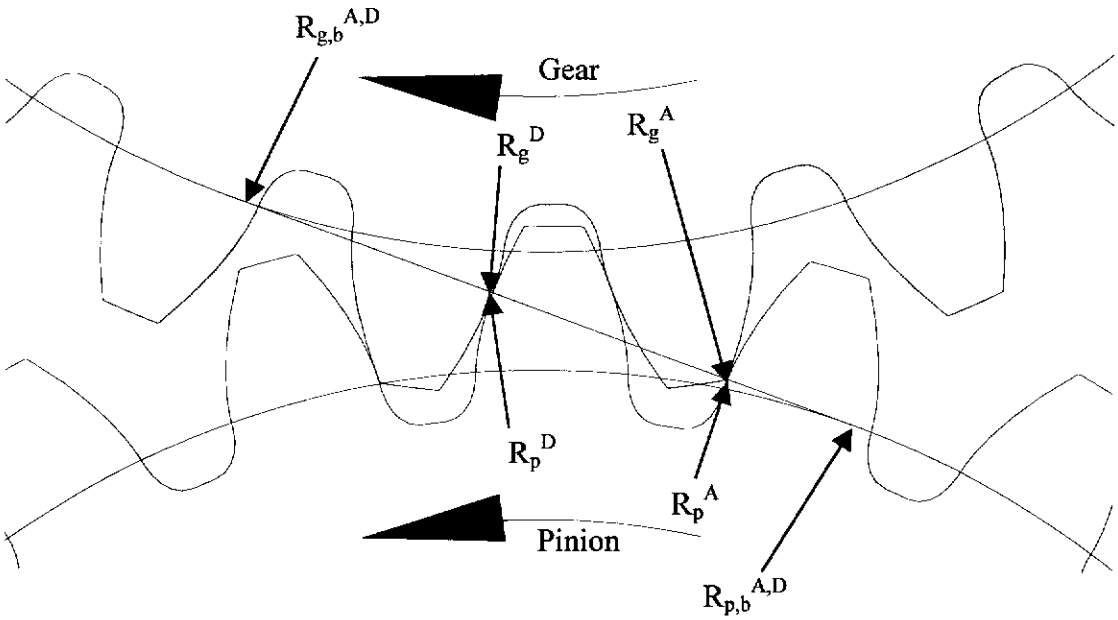

Figure 3.3.3. Illustration of the double pair contact zone, points A and D.

Analytical equations can also be developed for the rotation of the gear and pinion hubs, including the effects of tooth bending deflection and shearing displacement and contact deformation. In the pinion reference frame, it is assumed that the pinion hub remains stationary, (infinitely stiff for rotation), while the gear rotates due to an applied torque. All rotation formulae will therefore relate to the pinion, although this approach can easily be reversed to consider pinion rotation instead of the gear rotation.

Considering the single pair contact zone at point B as shown in Figure 3.3.2, the condition of angular rotation of the gear body will then be given by,

for the pinion,

$$\theta_p^B = \frac{B_p^B + H_p^B}{R_p^B}, \tag{3.3.5}$$

and for the gear,

$$\theta_g^B = \frac{B_g^B + H_g^B}{R_g^B}, \qquad (3.3.6)$$

where B_p^B and B_g^B are the tooth displacement vectors caused by bending and shearing for tooth pairs B of the pinion and gear respectively, H_p^B and H_g^B are the contact deformation vectors of tooth pairs B of the pinion and gear respectively. θ_p^B denotes the transverse plane angular rotation of the pinion body caused by bending deflection, shearing displacement and contact deformation of the tooth pair B while the gear is stationary. Conversely, for the gear rotation while the pinion is stationary, θ_g^B gives the transverse plane angular rotation of the gear body.

3.4 THE COMBINED SINGLE PAIR TORSIONAL MESH STIFFNESS

The combined torsional mesh stiffness is defined as the ratio between the torsional load and the angular rotation of the gear body. The torsional mesh stiffness varies throughout the meshing position as it decreases and increases dramatically as the meshing of the teeth change from the double pair to single pair of teeth in contact and vice-versa. The development of a torsional mesh stiffness model of gears in mesh can be used to determine the transmission error throughout the mesh cycle.

Considering the combined torsional mesh stiffness of a single tooth pair contact zone as shown in Figure 3.3.2, the single tooth torsional mesh stiffness of a single tooth pair in contact is defined as the ratio between the torsional load (T) and the elastic angular rotation (θ) of the gear body as shown in Figure 3.4.1. In the single tooth pair contact zone, as the pinion rotates, the single tooth torsional mesh stiffness of the pinion, K_p, is decreasing while the single tooth torsional stiffness of the gear, K_g, is increasing. When the pinion rotates to the pitch point P as shown in Figure 3.3.1(c), the single tooth torsional stiffness of both gears are equal because both of them are assumed to be identical spur gears with ratio 1:1.

The single tooth torsional mesh stiffness of the pinion is given by,

$$K_p^B = \frac{T_p^B}{\theta_p^B} \quad . \tag{3.4.1}$$

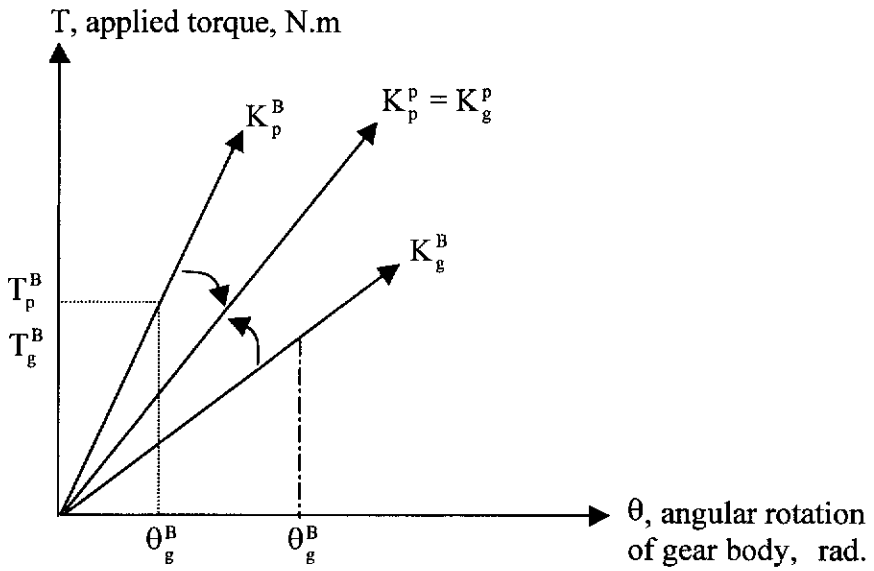

Figure 3.4.1. The single tooth torsional mesh stiffness of a single tooth pair in contact with identical spur gears.

and the single tooth torsional mesh stiffness of the gear is given by,

$$K_g^B = \frac{T_g^B}{\theta_g^B}, \tag{3.4.2}$$

where K_p^B and K_g^B denote the single tooth torsional mesh stiffness's of the single tooth pairs at B of the pinion and gear respectively.

The combined single pair torsional mesh stiffness at contact point B of Figure 3.3.2, K_m^B, is calculated by combining the single tooth torsional mesh stiffness K_p^B and K_g^B, as springs connected in series as shown in Figure 3.4.2, and is given by,

$$K_m^B = \frac{K_p^B \times K_g^B}{K_p^B + K_g^B}, \tag{3.4.3}$$

where the superscript ^{B} denotes the point along the path of contact of the single tooth pair contact zone. The single tooth torsional mesh stiffness's K_p^B and K_g^B are obtained by equation (3.4.1) and (3.4.2) respectively.

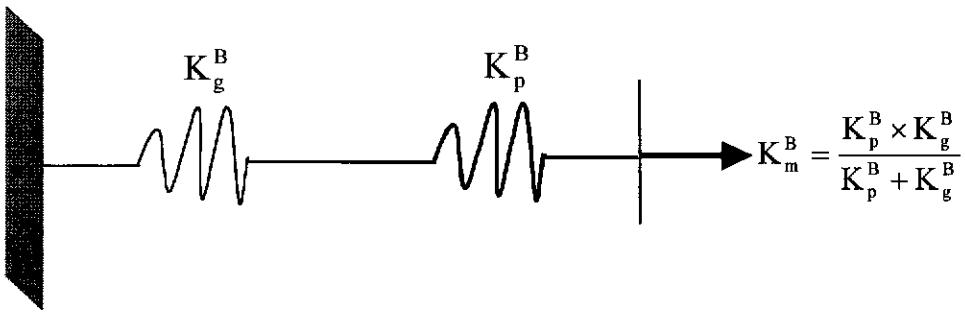

Figure 3.4.2. Two springs connected in series.

3.5 THE COMBINED DOUBLE PAIRTORSIONAL MESH STIFFNESS

For the double tooth pair in contact, the combined double pair torsional mesh stiffness $K_m^{A,D}$ is calculated by combining the combined single pair torsional mesh stiffness's K_m^A and K_m^D as springs connected in parallel, as shown in Figure 3.5.1, and is given by,

$$K_m^{A,D} = K_m^A + K_m^D, \tag{3.5.1}$$

with the combined single pair torsional mesh stiffness's given by,

$$K_m^A = \frac{K_p^A \times K_g^A}{K_p^A + K_g^A},$$

$$K_m^D = \frac{K_p^D \times K_g^D}{K_p^D + K_g^D}, \tag{3.5.2}$$

where the superscripts ^{A,D} denote the contact points of each tooth pair along the path of contact of the double tooth pair contact zone respectively.

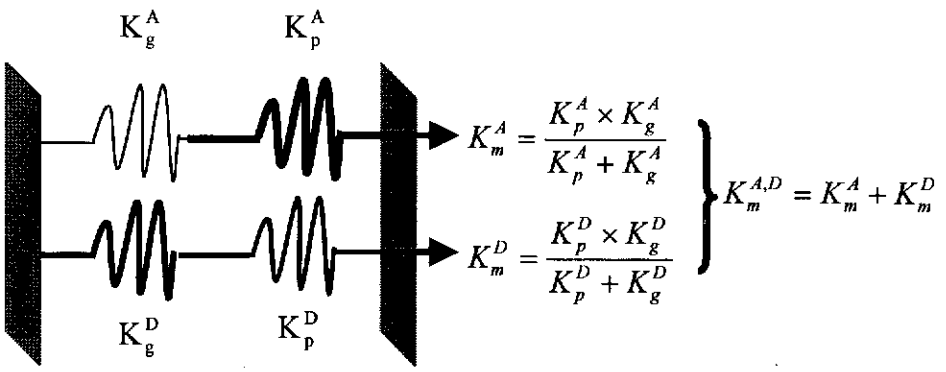

Figure 3.5.1. A double spring connected in parallel.

3.6 THE TRANSMISSION ERROR

The term transmission error is used to describe the difference between the theoretical and actual relative angular rotation between a pinion and a gear. Two types of transmission error are commonly referred to in the literature (Townsend 1991; Dudley et al. 1995). The first is the manufactured transmission error such as profile inaccuracies, spacing errors, and gear tooth runout. When gears are unloaded, a pinion and gear with perfect involute profiles and no spacing or runout errors should theoretically run with zero transmission error. The second is loaded transmission error, which is similar in principle to the manufactured transmission error but takes into account tooth bending deflection, shearing displacement and contact deformation due to load. When gears with perfect involute profiles are loaded, the combined torsional mesh stiffness of each gear changes, causing variations in angular rotation of the gear body. The gear transmission error is related directly to the deviation of the angular rotation of the two gear bodies and the relative angular rotation of the two gears is inversely proportional to the combined torsional mesh stiffness. The combined torsional mesh stiffness varies throughout the meshing position as it decreases and increases dramatically as the meshing of the teeth change from the double pair to single pair of teeth in contact and vice-versa.

The transmission error of gears in mesh at particular positions throughout the mesh cycle was generated in this research by rotating both solid gears then creating a finite element model in that particular position. In order to develop representative results, a large number of finite element models at different meshing positions were undertaken for this investigation. One of the most important criteria for each model was that the first potential contact nodes of both surfaces would be created exactly on the intersection point between the pressure line and the involute curve for that particular tooth. The additional problem of determining the penalty parameter at each contact position was overcome, so that it could be user-defined in the finite element model. At each particular meshing position, the angular rotation of the pinion due to tooth bending, shearing and contact displacement was calculated in the gear reference frame by restraining the gear from rotating, $\theta_g = 0$, with the pinion having a torque input load. In this case, $\theta_g = 0$, and θ_p is in the opposite direction to that resulting from forward motion of θ_g, changing the TE result to positive as seen by equation (3.6.1),

$$\text{TE} = \theta_g - (Z)\theta_p, \quad \text{rad}, \tag{3.6.1}$$

where Z is the gear ratio and $\theta_{p,g}$ is the angular rotation of the input and output gears in radians respectively.

In relation to the pinion reference frame, the pinion was restrained from rotating, $\theta_p = 0$, with the gear having the torque input load and the resulting angular rotation of the gear was computed. In this second case, $\theta_p = 0$, and the TE will be positive for forward motion of θ_g. After compensating torque and angular rotation for the gear ratio, the result from these two models should be the same, and so the mean of these two angular rotations would give the best estimate of the true static transmission error of the involute profile gears under load.

CHAPTER 4

MODELLING WITH CONTACT ELEMENTS

4.1 Overview of Contact Analysis

Contact problems are highly nonlinear and require significant computer resources to solve. Contact nonlinearities occur when two or more components come into or out of contact with each other or when two components slide relative to each another. The computational difficulties occur because one or both of the following are unknown,

- The contacting areas. In general, the exact regions of contact are unknown as they are dependant on the loads, materials, and the boundary conditions of the problem being considered. The contact surface can come into and go out of contact with the other surface in a largely unpredictable and erratic manner.
- The forces transmitted, both normal and tangential (frictional forces). Most contact problems need to account for friction. Several friction laws are available, and all are nonlinear, making the frictional response solution convergence difficult.

In addition to these difficulties, the conductance of heat and electrical currents in the areas of contact must also be addressed in many contact problems.

4.2 Contact Problem Classification

There are many types of contact problems that may be encountered, including gear transmissions, dynamic impacts, metal forming, bolted joints, crash dynamics, assemblies of components, interference fits, etc. All of these contact problems, as well as others types of contact analysis, can be split into two general classes (ANSYS 1997),

- rigid–to–flexible bodies in contact,

and

- flexible–to–flexible bodies in contact.

In rigid–to–flexible contact problems, one or more of the contacting surfaces are treated as rigid, which has a much higher stiffness relative to the deformable body it contacts. Many metal forming problems fall into this category.

The other class, flexible–to–flexible, is where both or all contacting bodies are deformable. Examples of a flexible–to–flexible analysis include gears in mesh, bolted joints, interference fits, etc.

4.3 Contact Element Capability

In general, there are three basic types of contact model applications (ANSYS 1995),

- Point-to-point contact, where the exact location of contact should be known beforehand. These types of contact problems usually only allow small amounts of relative sliding deformation between contact surfaces,
- Point-to-surface contact, where the exact location of the contacting area may not be known beforehand. These types of contact problems allow large

amounts of deformation and large relative sliding. Also, the opposing meshes do not have to have the same discretisation or compatible mesh,

and

- Surface-to-surface contact, typically used to model surface–to–surfcae contact applications of rigid-to-flexible classification.

To use the contact capability, the possible interaction areas where contact might occur needs to be identified. This identification is achieved through contact elements, which can then be used to track the kinetics of the deformation process. These contact elements are then overlaid on the parts of the model that are being analyzed for interaction.

4.4 CONTACT ELEMENT KINEMATICS

With the rapid development in the capabilities of digital computers, numerical methods became the prime interest of many researchers, especially, in engineering disciplines (See for example: Bathe 1982; Cook et al. 1989; Zienkiewicz and Taylor 1994; Zienkiewicz and Taylor 1994; Cook 1995). The Finite Element Method (FEM) can now be considered the favourite method to treat frictional contact problems, because of its proven success in treating a wide range of engineering problems in areas of solid mechanics, fluid flow, heat transfer, electromagnetic field and coupled field problems.

The FEM treats contact problems by extending the variational formulation upon which the FE method is based. The stiffness matrix associated with contact elements and other element stiffness matrices of the body are formulated and assembled into the original FE code. The solution is then obtained by solving the resulting set of nonlinear equations.

Figure 4.4.1 shows a typical example of such contact elements. This particular element, 2D contact element for point to surface contact problem, is adopted in several FE packages including ANSYS (ANSYS 1995). It is applicable to 2-D geometry, plane strain, plain stress, or axisymmetry situations. The area of contact

between two or more bodies is generally not known in advance. It may be applied to the contact of solid bodies for static or dynamic analyses, to problems with or without friction, and to flexible-to-flexible or rigid-to-flexible body contact. In this case, the element is based on two stiffness values. They are the combined normal contact stiffness KN_c and the combined tangential contact stiffness KT_c. The combined normal contact stiffness KN_c is used to penalise interpenetration between the two bodies, while the combined tangential contact stiffness KT_c is used to approximate the sudden jump in the tangential force, as represented by Coulomb's friction law when sliding is detected between the two contacting nodes.

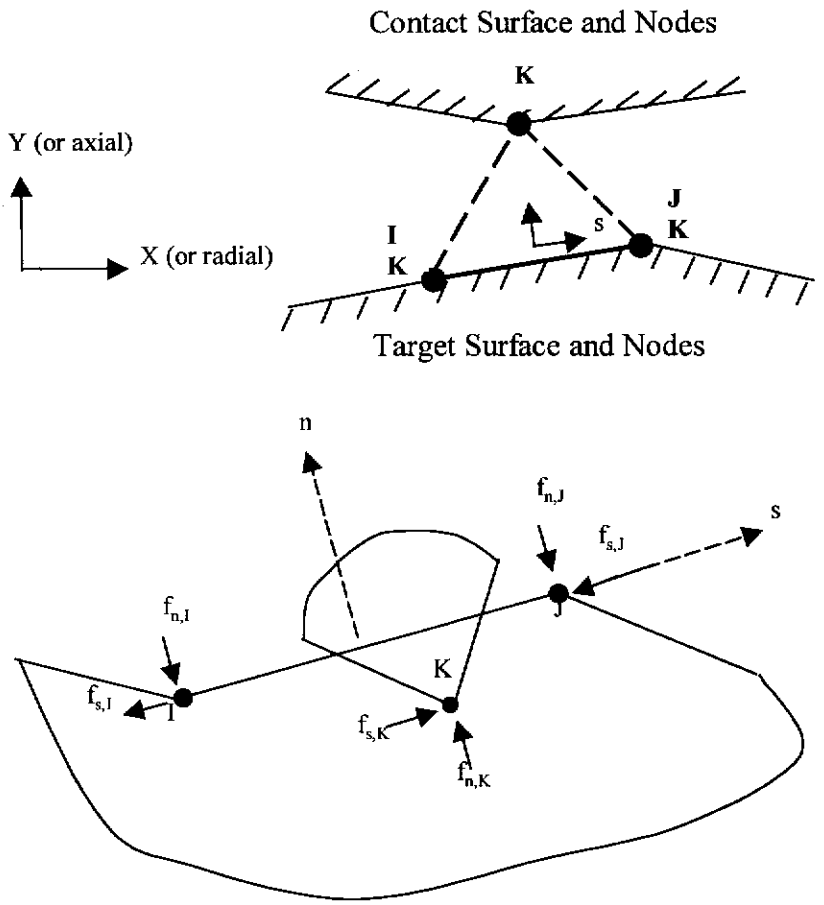

Figure 4.4.1. 2-D Point-to-surface contact elements and nodal contact forces.

In order to satisfy contact compatibility, forces are developed (see Figure 4.4.1, where, $f_{n,IJK}$ and $f_{s,IJK}$ are the normal and tangential forces at node I,J,K respectively.) in a direction n normal to the target plane that will tend to reduce the penetration to an acceptable numerical level. In addition to compatibility forces, friction forces are

developed in a direction s tangent to the target plane. Two methods of satisfying contact compatibility are available: (i) a penalty method, and (ii) a combined penalty plus Lagrange multiplier method. The penalty method enforces approximate compatibility by means of a contact stiffness. The combined penalty plus Lagrange multiplier approach satisfies compatibility to a user-defined precision by the generation of additional contact forces that are referred to as Lagrange forces.

4.5 Advantages and Disadvantages of Contact Elements

Because of the simplicity of their formulation, the advantages of using contact elements are,

- They are easy to use,
- They are simple to formulate,

and

- They are easily accommodated into existing FE codes.

However, using contact elements poses some difficulties such as the fact that their performance, in term of convergence and accuracy, depends on user defined parameters.

4.6 Penalty Parameters for Contact Elements

In order to handle a contact analysis with the finite element method, a stiffness relationship between the two contact areas must be established when contact occurs. This relationship can be established through a spring that is placed between the two contacting areas when contact occurs. This is essential to prevent the two areas from passing through each other. This method of enforcing contact compatibility is called the penalty method. The contact stiffness is the penalty parameter which is an element real constant of the contact element. There are two kinds of contact stiffness, the combined normal contact stiffness and the combined tangential or sticking contact stiffness.

4.6.1 The Combined Normal Contact stiffness

A major problem in the implementation of contact elements is the assignment of values to KN_c. The amount of penetration, or incompatibility, between the two surfaces is therefore dependent on the combined normal contact stiffness. Ideally there should be no penetration, but this implies a KN_c value equal to infinity. However, the use of an excessively high value of KN_c will also lead to ill-conditioning of the global stiffness matrix as well as convergence difficulties. Ill-conditioning of the stiffness matrix means that some terms of the matrix are very large compared to others. When these sets of equations are solved, the numerical round-off errors that occur can be significant so that sometimes the solution is grossly incorrect. On the other hand, the use of smaller values of the combined normal contact stiffness can result in convergence to the wrong solution allowing for interpenetration and wrong estimates of the stick and slip regions. In practice, a high enough stiffness is desired so that the contact penetration is acceptably small, but still low enough so that convergence or ill-conditioned problems do not arise. The contact stiffness value must be chosen with care in order to minimise both the penetration and the number of iterations needed.

4.6.2 The Combined Tangential Contact Stiffness

The Coulomb law states that the tangential force f_s transmitted between the two bodies cannot exceed a fraction of the normal force f_n as,

$$| f_s | \quad \leq \quad - \mu f_n \quad , \tag{4.6.1}$$

where μ is the coefficient of friction defined as a material property.

Once f_s is exceeded, the two bodies will slide relative to one another. The coefficient of dynamic friction is usually less than the coefficient of static friction. Two types of Coulomb friction models are available in ANSYS, (ANSYS 1995), the elastic coulomb friction model and the rigid coulomb friction model.

Elastic Coulomb Friction behavior allows both sticking and sliding conditions to occur. The axis u_s in Figure 4.6.1 is the relative sliding displacement. The two surfaces will deform tangentially if there is a sliding force applied. If the sliding force is less than μf_n, when the force is removed, the two surfaces will return to their original tangential location. When the sliding force exceeds μf_n, the surface will slide inelastically. The size of the elastic zone depends on the value of the combined tangential contact stiffness KT_c. Similar to the combine normal contact stiffness KN_c, a high value of KT_c is desired, but not so high that it conversely affects the convergence of the problem.

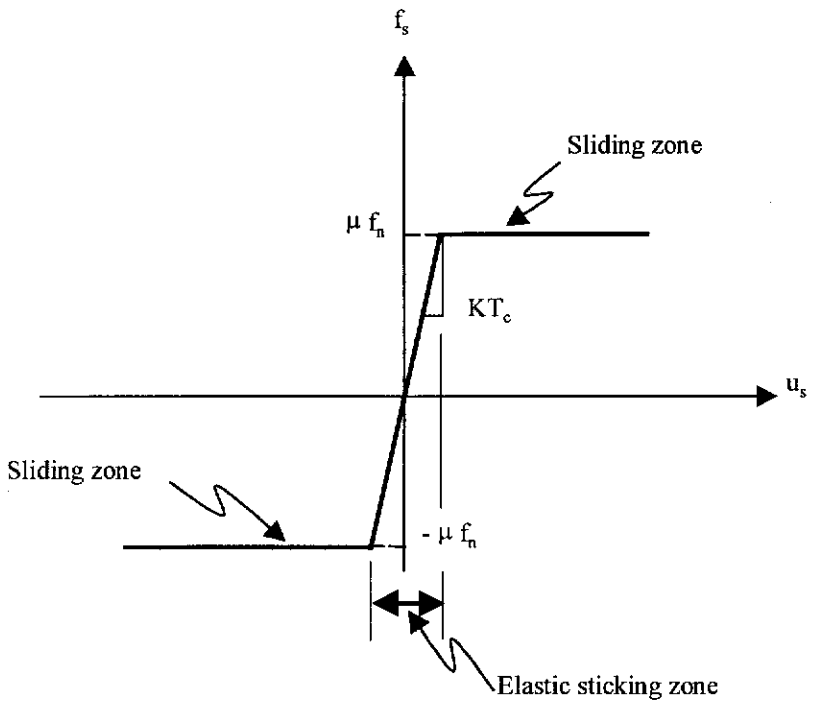

Figure 4.6.1. Contact zone relationship using elastic Coulomb friction.

Rigid Coulomb Friction behavior allows only sliding friction to occur. The sliding relationship between force and deflection behavior is as shown in Figure 4.6.2. This model is only good for analyses where the two surfaces are continuously sliding relative to one another. It always applies a resisting force against sliding, equal to μf_n and the direction of the force always opposes the motion.

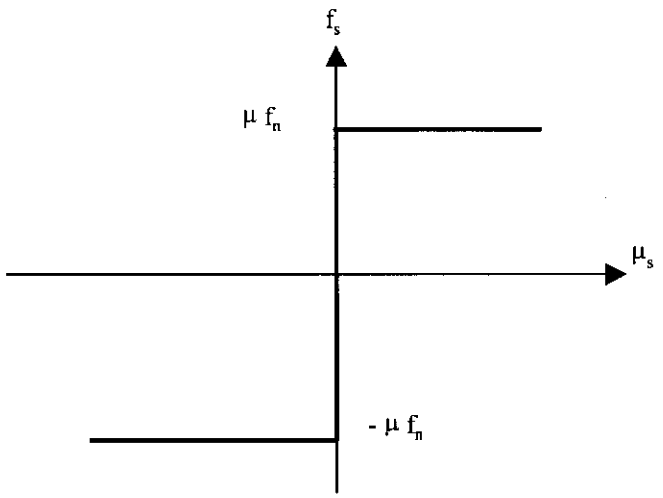

Figure 4.6.2. Contact zone relationship using rigid Coulomb friction.

4.7 A STRATEGY OF HOW TO DETERMINE THE PENALTY PARAMETER

In order to handle contact problems with the finite element method, the stiffness relationship between the two contact areas must be established through a contact element that is placed in between the two contacting areas where contact occurs. The accuracy of the solution which is obtained, depends on the choice of the contact stiffness. If the contact stiffness is too small, the surface penetration may be too large, which may cause unacceptable errors. On the other hand, if the contact stiffness is too large, the contact stiffness may produce severe numerical problems in the solution process or simply make a solution impossible to solve because of ill-conditioning with the stiffness matrix as some terms of the matrix are very large compared to others.

The underlying premise which has been used in this work is that to determine an appropriate value of the combined normal contact stiffness, KN_c, and the combined sticking or tangential contact stiffness, KT_c, the value of contact stiffness should be computed from the local compliance of the component in contact. The method by which this can be done depends on the kind of FEA models as given below.

1. For bulky solid models, the contact stiffness accounts for the flexibility of only the *local stiffness* of the materials at the point of contact.

2. For flexible models, such as beams, shells, and gears, the contact stiffness accounts for the flexibility of the *entire component* and not just the local stiffness of the material at the point of contact.

For both cases, the user-defined contact stiffness of the contact element can be seen as being equivalent to each component stiffness connected in series as given by,

$$KN_c = \frac{f(KN_1 * KN_2)}{(KN_1 + KN_2)}, \tag{4.7.1}$$

Where KN_1 and KN_2 are the normal contact stiffness of each component, f is the correction factor, which accounts for variations in contact problems such as mesh size, number of real nodes in contact, frictional effects, accuracy of contact nodal position, etc. In the case of translational stiffness, $KN_{1,2}$ are equivalent to translation load divide by translation deflection in the same load direction. For the case of the torsional stiffness of gears in mesh, $KN_{1,2}$ will be equal to the torsional load divided by the angular deflection. For either case, the load is applied at the potential contact nodes in a single-iteration (linear) analysis.

In the case of elastic Coulomb friction, convergence is usually adversely affected if the sticking zone is too small (see Figure 4.6.1), where KT_c is too large, because some of the points in contact oscillate between sliding and sticking or sliding left and right. Friction experiments do indicate that a sticking zone is a real behavior, but there has been no easy way to measure and quantify it. As a rule of thumb, the combined tangential contact stiffness KT_c should usually be 1, 2, or 3 orders of magnitude less than the combined normal contact stiffness KN_c, depending on the type of contact element.

4.8 Application and Convergence Study of Two Cylinders in Contact

The accuracy of contact problems depend on the choice of the penalty parameter which is not known at the start of any analysis, and which is verifiable only by the

amount of penetration in the solution. As mentioned above, a high value of the penalty parameter can lead to ill-conditioning of the global stiffness matrix as well as convergence difficulties, giving a very slow convergence rate and a large number of equilibrium iterations or a very small time step to generate a solution in each substep. Conversely, a low value of the penalty parameter can lead to over-penetration of the surfaces. In this section, a synthetic verification of how to select the appropriate value of the penalty parameter is presented using finite element analysis and a Hertzian comparison of two cylinders in contact.

Most of the previously published work on general contact problems has relied upon contact elements. However, it appears that the selected value of the combined normal contact stiffness has not been investigated in great detail. The primary purpose of this study was to determine an appropriate value for the penalty parameter.

The analysis was carried out by a model of two identical cylinders using a 2D point-to-surface contact element between the contact surface. A number of factors have been investigated in this study. Firstly, the effect of varying the combined normal contact stiffness on the approach deflection of the cylinders was studied. Secondly, the effect of other parameters such as using a smaller step size, the combined penalty plus Lagrange multiplier method, a more refined mesh over the contacting surface, and an asymmetric contact were also investigated. Finally, the results of the approach deflection were compared to analytical formulations based upon Hertzian stress theory (Boresi and Sidebottom 1985; Young 1985).

Hertzian theory for two cylinders in contact provides the equation for the approach deflection as,

$$\text{Approach deflection} = \frac{2F_y(1-\nu^2)}{\pi E}\left[\frac{2}{3}+\ln\left(\frac{D_1}{b}\right)+\ln\left(\frac{D_2}{b}\right)\right] , \qquad (4.8.1)$$

where,

F_y = compressive force per unit length (N/m),

ν = Poisson's Ratio,

$D_{1,2}$ = cylindrical diameter 1,2, and

b = half width of the rectangular contact area.

The question, which this work addresses, is how to model the approach deflection of two general surfaces in contact using finite element analysis. The ultimate aim is to be able to model two gear teeth in contact under a variety of tooth conditions. To assist this, an initial investigation was carried out on the contact between two identical cylinders as shown in Figure 4.8.1(a). A finite element model of the cylinders was constructed as shown. The cylinder parameters are shown in Table 4.8.1.

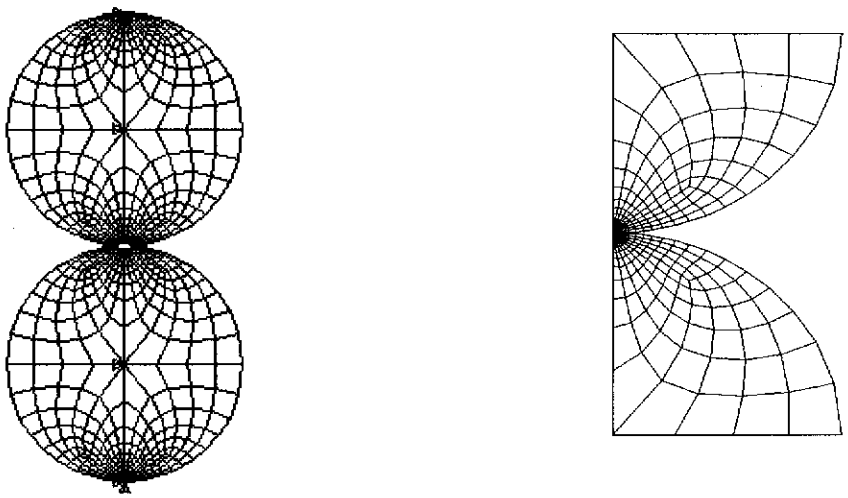

(a) (b)

Figure 4.8.1. Finite Element model. (a) two cylinders in contact. (b) a quarter model.

The cylinders were modelled by the quadratic plane-stress four-noded element through their thickness. The contact effect was modelled using 2D point-to-surface general contact elements, which consisted of a contact node and a target surface as shown in Figure 4.4.1. The contact element can be generated as a symmetric or as an asymmetric contact element. The symmetric contact element was created by two sets of contact elements between the contact surfaces as shown in Figure 4.8.2(a). The asymmetric contact element was created by using only one set of contact elements between the contact surfaces as shown in Figure 4.8.2(b). The assumption was made

that there was no friction or motion between the two cylinders when they were in contact.

Table 4.8.1. Cylinder parameters for the Finite Element Model

• material	Aluminium 2024-T3
• Young's Modulus, E	73 E 9 N/m^2
• Poisson's Ratio, ν	0.33
• Diameter, $D_{1,2}$	0.069 m.
• Length, h	0.015 m.

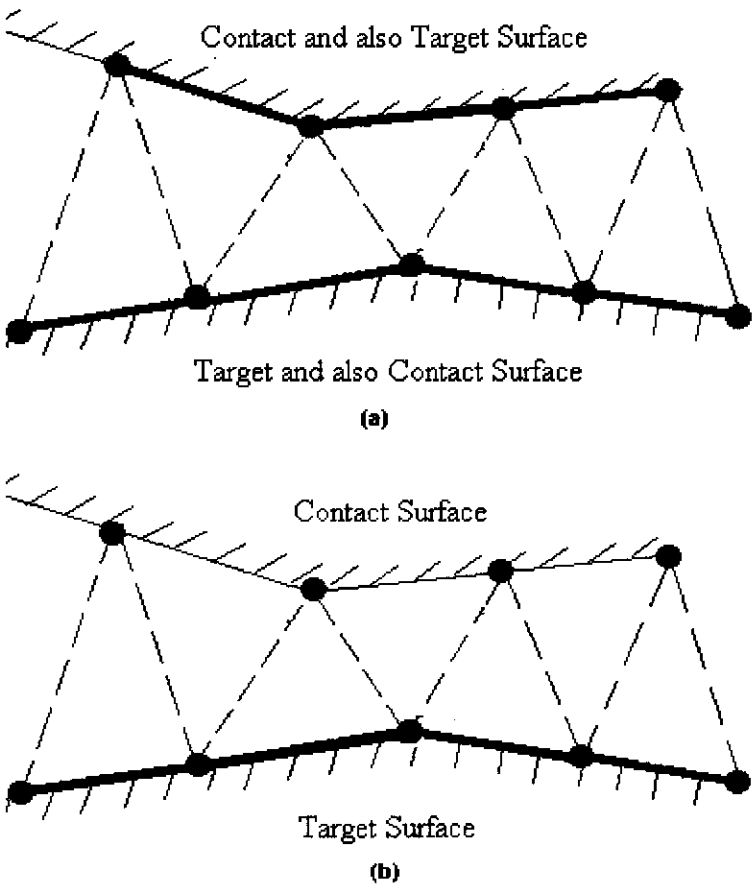

Figure 4.8.2. Finite element model of the contact surfaces (a) symmetric contact. (b) asymmetric contact.

In order to develop an accurate model of the cylinders in contact for the convergence study, an investigation of a large number of modelling variables was undertaken. Owing to double symmetry, only one quarter of the cylinder was modelled using the

finite element mesh shown in Figure 4.8.1(b). The major parameters, which were considered to have an effect on the finite element solution of the approach deflection, were,

1. the combined normal contact stiffness,
2. the number of substeps,
3. the combined penalty plus Lagrange multiplier method,
4. the mesh size,

and

5. the asymmetric contact.

Each of these variables was investigated in detail. The result of each of the convergence variables is presented below.

4.8.1 The Combined Normal Contact Stiffness

The penalty method allows surface penetrations, which can be controlled by changing the penalty parameter of the combined normal contact stiffness. If the combined normal contact stiffness is too small then the surface penetration may be too large, which may cause unacceptable errors. Thus the stiffness must be big enough to control the surface penetrations below a certain level. On the other hand, if the penalty parameter is too large, then the combined normal contact stiffness may produce severe numerical problems in the solution process or simply make a solution impossible to solve. For most contact analyses of bulky solid models, the value of the combined normal contact stiffness, KN_c, may be estimated (ANSYS 1995) as,

$$KN_c \approx f E h \qquad (4.8.2)$$

Where,

f = A factor that controls contact compatibility. This factor is usually be between 0.01 and 100,

E = smallest Young's Modulus of the contacting materials,

and

h = The characteristic contact length. This value depends on the particular geometry of the problem, h = "thickness" for plane stress with thickness.

To see the effect of varying the combined normal contact stiffness, eight models (KN_c = 0.05Eh, 0.1Eh, 0.5Eh, 1.0Eh, 5.0Eh, 10.0Eh, 50.0Eh, and 100Eh) of the combined normal contact stiffness given by equation (4.8.2) were investigated. The coefficient f was varied from 0.05 to 100 with the mesh size at the contact surface being 0.0001 m. In this study, the time-history results were used to define nodal displacements for the approach deflection and reaction forces as shown in Figure 4.8.3.

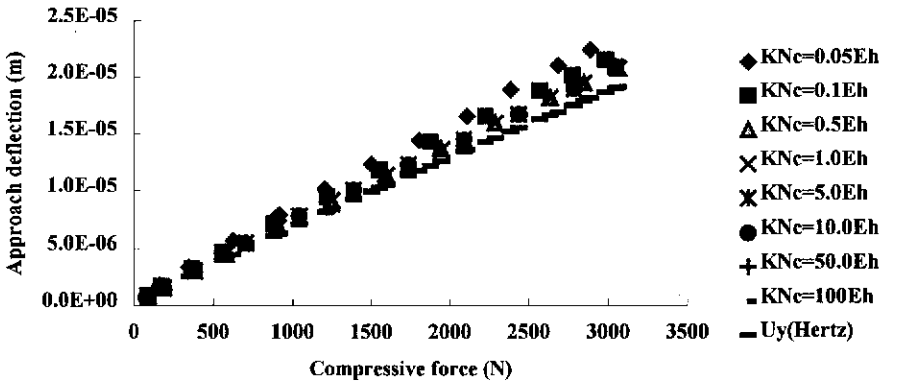

Figure 4.8.3. Effect of the combined normal contact stiffness.

It can be clearly seen that the gradient curve between the compressive force and the approach deflection starts to converge when KN_c is equal to 0.5Eh. Any further increase in the value of the combined normal contact stiffness appeared to yield the same gradient. It was found that the higher values of the combined normal contact stiffness caused a slower convergence rate with a significant increase in the CPU-time required to solve the problem. Therefore the optimum convergence due to the combined normal contact stiffness variation appeared to be KN_c equal to 0.5Eh.

4.8.2 The Number of Substeps

The optimal combined normal contact stiffness (KN_c equal to 0.5Eh) was further modified using smaller substeps by setting the minimum number of substeps equal to 20 in the FE model of the nonlinear analysis. The comparative results for the approach deflection is shown in Figure 4.8.4, which shows no significant difference. It was found however, that increasing the number of substeps from 10 to 20 caused a significant increase in the CPU-time require for problem solving. The results indicate that a minimum number of substeps equal to 10 was sufficient enough for this convergence study.

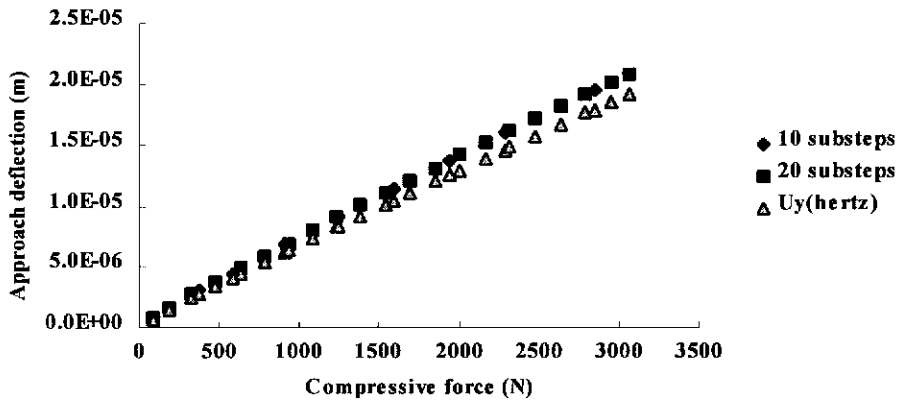

Figure 4.8.4. Effect of the number of substeps.

4.8.3 The Combined Penalty Plus Lagrange Multiplier Method

The two basic methods of contact constraint, the penalty and the combined penalty plus Lagrange multiplier method were compared. The results of the approach deflection are shown in Figure 4.8.5. Once again there was no significant difference in the results, however, the combined penalty plus Lagrange multiplier method caused a significant increase in the CPU-time required for problem solving. This was especially true when the number of new unknowns (user-defined) introduced into the solution was relatively large. The increase in CPU-time required by the new contact unknowns depended not only on the number of new unknowns but also on the node numbering of that part of the body where the unknowns were defined. It

would appear that the penalty method provides the best method appropriate for the problem being considered.

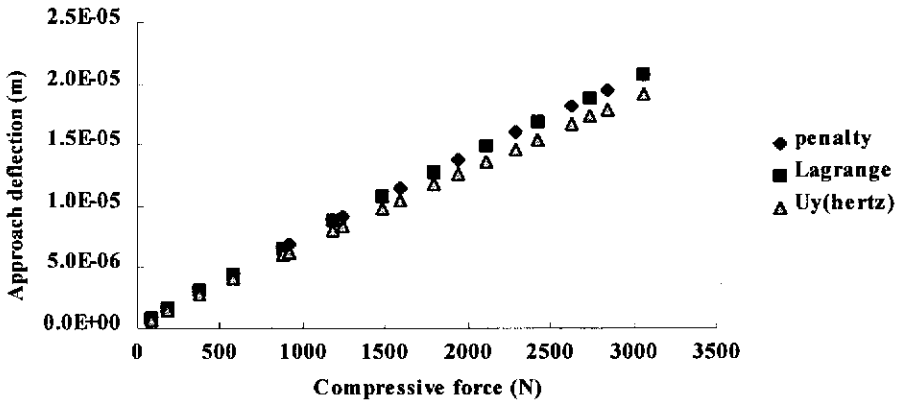

Figure 4.8.5. Effect of the contact constraint method.

4.8.4 The Mesh Size

The finite element model using the optimum contact stiffness was remeshed using a finer mesh size from 0.0001 m (imesh) to 0.00005 m (fmesh) at the contact surface. The comparative results of the approach deflection versus the normal contact force are shown in figure 4.8.6. The results showed that there appeared to be no significant difference in the deflection, although a finer mesh size was much more time-consuming for the nonlinear analysis and caused a significant increase in the CPU-time. The original mesh size of 0.0001m was thus seen to be very appropriate and was used for the remainder of the investigation.

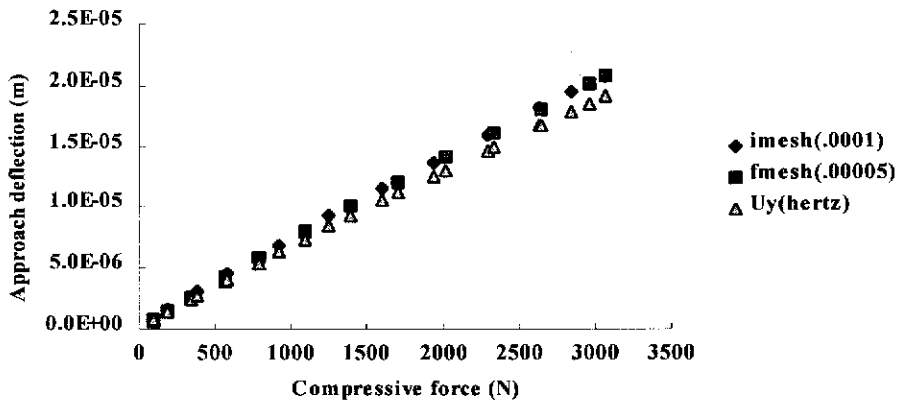

Figure 4.8.6. Effect of the mesh size.

4.8.5 The Symmetric/Asymmetric Contact

A comparative study between two sets of contact elements (symmetric contact) and one set of contact elements (asymmetric contact) was undertaken as shown in Figure 4.8.7 The results indicated that the stiffness for the asymmetric contact was too low when compared with symmetric contact. The asymmetric contact is usually the most efficient way to model surface-to-surface contact provided that it is clear which surfaces are designated to be the contact surface and target surface respectively. However, it has been found that under some circumstances, asymmetric contact does not perform satisfactorily, particularly if it is not clear which surface should be the contact and which should be the target. In these cases symmetric contact is required. In such cases, each surface can be designated to be a target and a contact surface. It is then possible to generate two sets of contact elements between the contacting surfaces. Specific situations that require symmetric contact include, (1) Both potential contact surfaces are identically symmetric. (2) If the choice between symmetric and asymmetric contact is not clear, then fully symmetric contact should be used. (3) The contact problem is one in which a node-to node model is employed, and (4) Both potential contact surfaces have nearly equal mesh densities and/or arbitrary shapes.

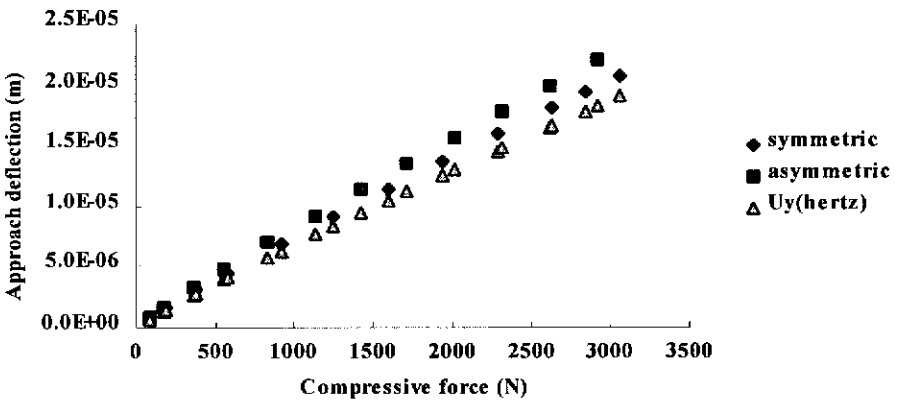

Figure 4.8.7. Effect of symmetric and asymmetric contact.

4.8.6 Comparison between 2-D Plain Strain and 3-D Brick Elements

The convergence study has shown that the approach deflection between the two cylinders can be accurately modelled using the penalty method with a mesh size of 0.0001m, a normal contact stiffness of $KN_c = 0.5Eh$, a minimum of 10 substeps and using the symmetric contact elements. For comparative purposes, the results of the approach deflection were further compared using 2-D plain stress elements, 2-D plain strain elements, and 3-D solid brick elements. The main reason explaining this further investigation lies in the fact that the Hertz contact theory of the tiny contact area is a 3 dimensional stress problem and the 2-D plain stress FEA analysis as outlined above is a 2 dimensional plane stress problem.

The comparison of results from FEA and the Hertzian theory are shown in Figure 4.8.8 and Figure 4.8.9. It can be clearly seen that the results from the approach deflection analysis using 2-D plane stress is about 10 percent higher when compare with the Hertzian theory.

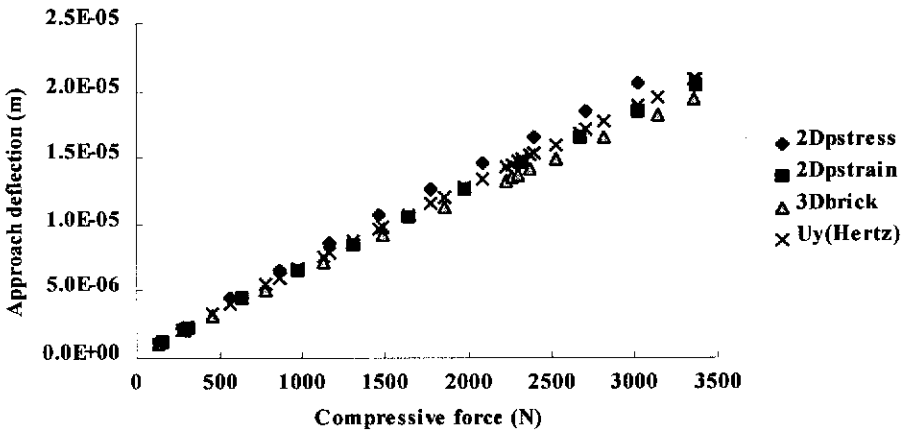

Figure 4.8.8. Comparison of approach deflection between 2D and 3D elements.

The results of the 2-D plane stress element analysis were further compared with 2-D plane strain elements and 3-D brick elements. As illustrated in Figure 4.8.9, the results of approach deflection of 2-D plane strain are very close, with less than 3 % difference from the Hertzian theory. The main reason why 3-D solid brick elements

were not closer to the Hertzian theory was most likely because this study did not mesh 3-D brick eight-node elements at the contact area as fine as 2-D plane stress or plane strain elements. A 3-D brick element analysis using fine elements is very time consuming and was not warranted given the high level of accuracy obtained using the 2-D plane strain element.

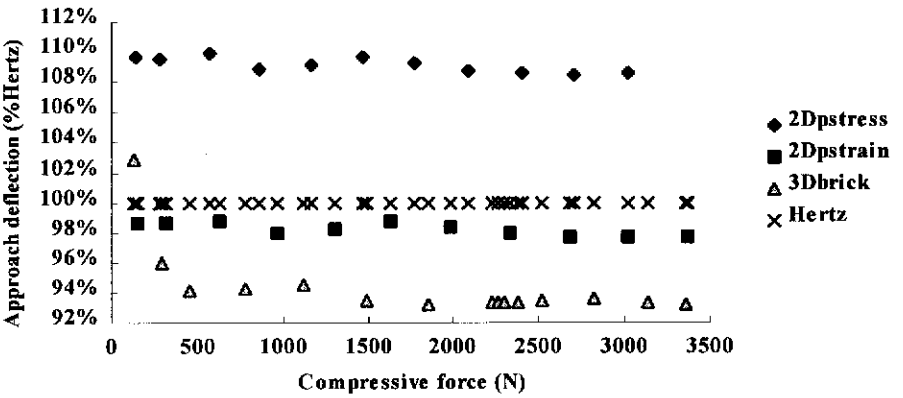

Figure 4.8.9. Comparison of approach deflection in percentage.

4.9 Verification of a Strategy on How to Determine the Penalty Parameter

The purpose of this verification was to confirm that the techniques, which have been developed for determining the contact stiffness, can be applied to general contact problems and to assess the accuracy of the results. In order to verify the validity of the procedure, the frictional contact between two identical cylinders, (Sirichai et al. 1997), as shown in Figure 4.9.1(a), was further analysed. The elastic properties of the cylinders were given as E=69 GPa., and ν= 0.33, with diameter 0.138 m. The coefficient of friction was taken as μ=0.4. The cylinders were modelled using the quadratic 2D *plain strain* four-node element with an increased number of elements at the candidate contact surface to 100 microns mesh size. The contacting area was modelled using 2D point-to-surface general contact elements with a symmetric contact. As the two cylinders in contact are bulky solids, the contact elements should be modelled by using only the local stiffness of the material at the point of contact. This can be achieved as shown in Figure 4.9.1(b), where only the first two potential

contact nodes with two elements on each cylinder are considered. By applying a concentrated compression load, F_y equal to 1×10^6 N, to both potential contact nodes in a single-iteration (linear) analysis, where the surrounding nodes are restrained, the combined normal contact stiffness, KN_c can be computed.

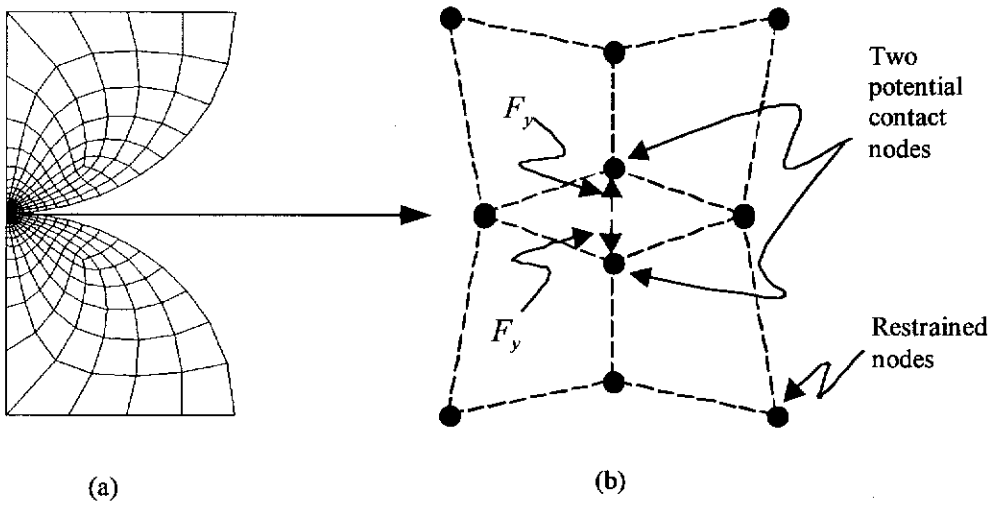

Figure 4.9.1. FEM (a) Two quarter cylinders in contact (b) the potential contact nodes.

From the applied load and the resulting deflections, equation (4.7.1) can be seen to give, using 1.0 for f,

$$
\begin{aligned}
KN_c &= \frac{f(KN_1 * KN_2)}{(KN_1 + KN_2)} \\
&= \frac{f(F_y)}{(Y_1 + Y_2)} \qquad (4.9.1) \\
&= \frac{1.0(1000000)}{(1.60773e-5 + 1.60773e-5)} \\
&= 3.11\ e10 \quad N/m \quad \approx \quad 0.5E \quad N/m.
\end{aligned}
$$

The comparison of the deflection results of the centre of the cylinders for various values of the normal contact stiffness, with Hertzian theory are shown in Figure

4.8.3, (Sirichai et al. 1997). It can be clearly seen that the gradient curve between the compressive force and the approach deflection starts to converge when the value of the combined normal contact stiffness KN_c is equal to 0.5E. Any further increase in the value of the combined normal contact stiffness KN_c yields the same gradient, showing that the combined normal contact stiffness KN_c is approximately equal to 0.5E. In addition, with further improvments resulting from using a cylinder body element from 2-D plain stress with thickness to be 2-D plain strain, the result of the approach deflection was less than 3 % different from the Hertzian theory, as shown in Figure 4.8.9. The technique for finding the normal contact stiffness for bulky solids as used above, therefore appears to be correct.

4.10 CONCLUSION

This chapter has dealt with an initial investigation of how to verify the value of the combined normal contact stiffness for surfaces in contact, which can have values of the combined normal contact stiffness in the range from 0.01Eh to 100Eh. The results of these investigations give a clear picture of what occurs when using different values of the combined normal contact stiffness and should be particularly useful for all kinds of contact elements. The value of the combined normal contact stiffness which must be defined by the user is generally not known at the start of the solution process, and in accordance with ANSYS (ANSYS 1995), the solution is verified by checking that the amount of penetration is not excessive - without any clear guidelines as to how much is considered excessive. This synthetic verification method and strategy of how to choose a correct value of the penalty parameter and the appropriate contact constraint method should be very useful in solving all kinds of general contact problems. In this chapter, a strategy for choosing an appropriate value of the combined normal contact stiffness has been presented. The method has been demonstrated to work well for bulky solids like two cylinders in contact. The method involves the creation of first potential contact nodes and keypoints. The keypoints are used for specifying the edge lengths of the elements and mesh sizes at the candidate contact surfaces. The results for the stiffness of two cylinders in contact have been shown to agree very closely with Hertzian theory, 3% different

when 2-D plane strain element were used with a mesh size of 10 μm at the contact point.

CHAPTER 5

FINITE ELEMENT ANALYSIS OF GEARS IN MESH: THE COMBINED TORSIONAL MESH STIFFNESS

5.1 INTRODUCTION

This chapter presents a finite element analysis of two spur gears in mesh. The model predicts the combined torsional mesh stiffness of the two gears in mesh when one of the gears is restrained from rotating, with the other gear having a torque input load, see section 5.1.1. The combined torsional mesh stiffness of two gears in mesh varies with the meshing position as the teeth rotate within the mesh cycle. In particular, the combined torsional mesh stiffness decreases and increases dramatically as the meshing of the teeth change from the double pair of teeth in contact, to the single pair of teeth in contact and vice-versa. The accuracy of finite element modelling of contact problems depends on the choice of the penalty parameter for the contact element, as seen in Chapter 4. For modelling of gear teeth in mesh, the penalty parameter also varies as the gear teeth rotate through the cyclic mesh. This chapter presents a simple strategy of how to determine an appropriate value of the penalty parameter as the gears rotate through the mesh cycle. The combined torsional mesh

stiffness is then predicted as a function of the position of the mesh point in the mesh cycle.

Gears are one of the most critical components in industrial rotating machinery. In recent years, many different procedures have been developed to model the behaviour of gears in mesh. Examples of this can be seen in references (Tordian and Geraldin 1967; Remmers 1978; Drago et al. 1979; Walford and Stone 1980; Hayashi and Hayashi 1981; Bahgat et al. 1983; Ozguven and Houser 1988; Kahraman and Singh 1991; Kuang and Yang 1992; Liou et al. 1992; Rebbechi et al. 1992; Vinayak and Houser 1992; Bard et al. 1994; Brousseau et al. 1994; Daniewicz et al. 1994; Kowalczyk 1994; Munro and Yildirim 1994; Refaat and Meguid 1994; Refaat and Meguid 1995; Velex et al. 1995; Liou et al. 1996; Litvin et al. 1996; Sirichai et al. 1996; Sweeney and Randall 1996; Velinsky 1996; Sirichai et al. 1997, Gargiulo, 1980 #399; Elkholdy et al. 1998, Tordion, 1967 #410; Gosselin et al. 1998; Nadolski and Pielorz 1998; Zhang and Fang 1998, Underhill, 1997 #12). One of the many factors which can be investigated, is the combined torsional mesh stiffness variation as the gear teeth rotate through the mesh cycle.

In order to model contact problems with the finite element method, the stiffness relationship between the two contact bodies must be established, otherwise the two bodies will pass through each other. One of the means of solving this problem is through the use of a contact element. The convergence and accuracy of contact problems depends on the choice of the penalty parameter for the contact element, which must be defined by the user, as demonstrated in Chapter 4. Some of the previously published work has used analytical techniques such as the variational inequality approach (see for more in: Panagiotopoulos 1975; Panagiotopoulos 1977; Kikuchi and Song 1980; Compos et al. 1982; Talaslidis and Panagiotopoulos 1982; Martins and Oden 1983; Pires and Oden 1983; May 1986; Sayegh and Tso 1986; Klarbring 1986a; Klarbring 1986b; Klarbring et al. 1988; Zhong and Sun 1988; Johnson and Quigley 1989; Lee and Kwak 1989; Kowalczyk 1994, Panagiotopoulos, 1987 #497; Refaat and Meguid 1994; Refaat and Meguid 1994; Refaat 1995; Refaat and Meguid 1995; Refaat and Meguid 1996; Refaat and Refaat 1997; Underhill et al. 1997), which tend to be complicated and difficult to use. This chapter presents a simple method for choosing an appropriate value of the penalty

parameter. The method has been verified using two cylinders in contact and the result compared with Hertzian theory in Chapter 4. The same strategy is used here to determine an appropriate value of the penalty parameter of gears in cyclic mesh.

5.1.1 Defining a Torque input Load

Two methods have been developed for applying an input torque load to the gears in mesh in this thesis.

The first method consists of an indirect approach where the gear is restrained from rotating by constraining all DOF of the master coupled node of the gear hub. A torque input load on the pinion hub is then generated by defining DOF angular constraints for the master coupled node of the pinion hub. This method is used in chapter 5, and the step-by-step procedure describing how the torque input load is used for finding the combined torsional mesh stiffness is outlined in section 5.9, followed by a flow chart shown in Figure 5.9.1.

The second method represents a direct method for developing a torque input load. The gear is restrained from rotating by constraining all DOF of the master coupled node of the gear hub, then a torque input load is applied to the pinion hub by defining a tangential force at the master coupled node of the pinion hub. This method is used in chapter 6 and 7, and the step-by-step procedure describing how the torque input load is used for finding the static transmission error is outlined in section 7.6, followed by a flow chart shown in Figure 7.6.1.

5.2 Tooth Profile

The finite element model of spur gears in mesh is based upon test gears which have been used in an experimental investigation (Sirichai et al. 1996), and the test gear parameters are shown in Table 5.2.1. The test gears have a ratio of 1:1. The involute and fillet tooth profile equations used in the finite element model have been introduced by references (Litvin 1989; Townsend 1991; Kuang and Yang 1992). For most of the other gears, profile equations can be found in references (Litvin and Hsiao 1993; Litvin and Lu 1993; Zhang et al. 1994; Litvin et al. 1995; Litvin and Lu

1995; Litvin and Feng 1996; Litvin and Seol 1996; Seol and Litvin 1996; Seol and Litvin 1996; Litvin and Kim 1997; Donno and Litvin 1998; Feng et al. 1998; Litvin et al. 1998; Litvin et al. 1998; Litvin et al. 1998). Gear tooth profiles and other gear tooth calculations can be performed on a personal computer by the use of a small computer program or by a purchased program developed by a gear consultant or others. This section show some of the basic equations used for calculating gear tooth involute profile coordinates and gear tooth fillet coordinates. A customised AutoLisp, (AUTODESK 1995), AutoCAD programming language was used to generate the profile of the teeth and the profile was then transferred from AutoCAD, to finite element code (ANSYS 1995), to generate the finite element model of gears in mesh. The equations for generating the involute and fillet tooth profile are given below. The customised AutoLisp program for generating the involute and fillet tooth profile is given in Appendix A.

Table 5.2.1 Test Gear Parameters

• gear type	standard involute, full-depth teeth
• material	aluminum
• modulus of elasticity, E	69 Gpa,
• Poisson's ratio, ν	0.33
• face width	0.015 m.
• module, m	6 mm.
• number of teeth	23
• pressure angle	20 degrees
• theoretical contact ratio	1.59
• theoretical angle of meshing cycle	24.912 degrees
• addendum	1.00m
• dedendum	1.25m

The following algorithm calculates the coordinates of an involute and fillet tooth profile based on the tooth profile generating method introduce by (Litvin 1989, Kuang, 1992 #34). The following equations for the generated involute (curve AB) and fillet (curve BC) tooth profile as shown in Figure 5.2.1 are valid for gears conjugate to the counterpart basic rack where,

- m is metric module, mm
- N is number of teeth
- Addendum, $a = \alpha\ m$ (usually $\alpha = 1.0$)
- Dedendum, $b = \beta\ m$ (usually $\beta = 1.25$)
- Tip radius, $r_c = \gamma\ m$ (usually $\gamma = 0.25$)
- ϕ is pressure angle
- Addendum modification coefficient $X = e/m$
- e is cutter offset

The parametric representation coordinates of the involute profile (curve AB) is,

$$\bar{r}(\theta) = \begin{Bmatrix} x(\theta) \\ y(\theta) \end{Bmatrix}, \tag{5.2.1}$$

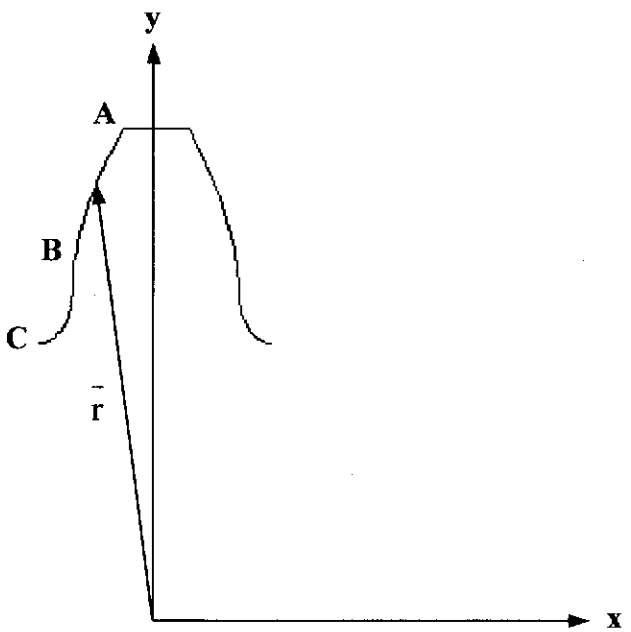

Figure 5.2.1. Coordinate system for generating involute and fillet tooth profiles.

where coordinates of the involute curve are given by equation (5.2.2) and (5.2.3),

$$x(\theta) = \frac{Nm}{2}\left\{\sin(\theta) - \left[\left(\theta + \frac{\pi}{2N}\right)\cos\phi + \frac{2X}{N}\sin\phi\right]\cos(\theta + \phi)\right\}, \tag{5.2.2}$$

and

$$y(\theta) = \frac{Nm}{2}\left\{\cos(\theta)+\left[\left(\theta+\frac{\pi}{2N}\right)\cos\phi+\frac{2X}{N}\sin\phi\right]\sin(\theta+\phi)\right\}. \quad (5.2.3)$$

The parameter θ, in radians, of the involute curve is limited to the following range,

$$\theta_{min} \le \theta \le \theta_{max} \quad , \quad (5.2.4)$$

where the parameters θ_{min} and θ_{max} of the involute curve are given by equation (5.2.5) and (5.2.6),

$$\theta_{min} = \frac{2}{N}\left[U+(V+X)\cot\theta\right] , \quad (5.2.5)$$

and

$$\theta_{max} = \frac{1}{N\cos\phi}\sqrt{(2+N+2X)^2-(N\cos\phi)^2}-\left(1+\frac{2X}{N}\right)\tan\phi-\frac{\pi}{2N}. \quad (5.2.6)$$

The parameters U and V of the involute curve are given by,

$$U = -\left[\frac{\pi}{4}+(\alpha-\gamma)\tan\phi+\frac{\gamma}{\cos\phi}\right] , \quad (5.2.7)$$

and

$$V = \gamma-\alpha \quad . \quad (5.2.8)$$

The parametric representation coordinates of the fillet profile (curve BC) is,

$$\bar{r}(\theta) = \begin{Bmatrix} x(\theta) \\ y(\theta) \end{Bmatrix}, \quad (5.2.9)$$

where coordinates of the fillet curve are given by equation (5.2.10) and (5.2.11),

$$x(\theta) = m(P\cos\phi+Q\sin\phi), \quad (5.2.10)$$

and

$$y(\theta) = m(-P\sin\phi + Q\cos\phi). \tag{5.2.11}$$

The parameter θ of the fillet curve is limited to the following range,

$$\theta_{min} \le \theta \le \theta_{max}, \tag{5.2.12}$$

where the parameters θ_{min} and θ_{max} of the fillet curve are given by equation (5.2.13) and (5.2.14),

$$\theta_{min} = \frac{2}{N}[U + (V + X)\cot\theta], \tag{5.2.13}$$

and

$$\theta_{max} = \frac{2U}{N}. \tag{5.2.14}$$

The parameters P, Q, and L of the fillet curve are given by,

$$P = \frac{\gamma}{L} + \left(U - \frac{N\theta}{2}\right), \tag{5.2.15}$$

$$Q = \frac{2\gamma}{L} + \left(\frac{V + X}{2U - N\theta}\right) + V + \frac{N}{2} + X, \tag{5.2.16}$$

and

$$L = \sqrt{1 + 4\left(\frac{V + X}{2U - N\theta}\right)^2}. \tag{5.2.17}$$

5.3 FINITE ELEMENT MODEL OF GEARS IN MESH

The involute and fillet tooth profile of the spur gears used in the finite element model were based on those developed in the AutoLisp file of appendix A, then transferred to ANSYS to generate the finite element model of the gears in mesh as shown in Figure 5.3.1.

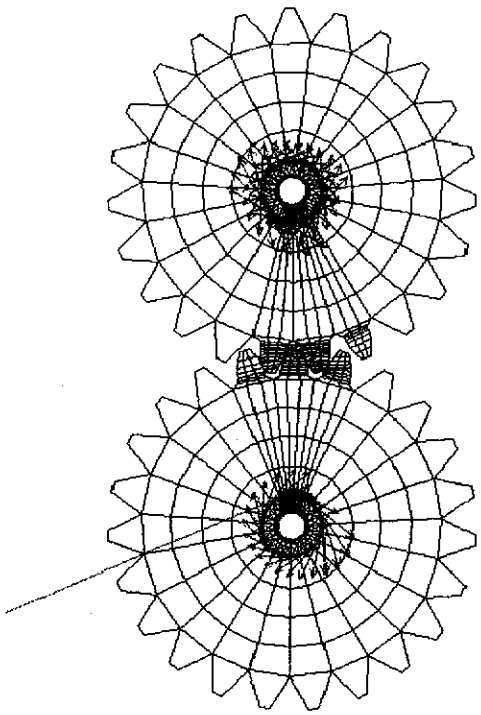

Figure 5.3.1. Finite Element Model of the spur gears in mesh.

Most of the previously published finite element work with gear models has involved only partial teeth models. In an investigation of gear transmission errors using factors such as variational combined torsional mesh stiffness, the whole body of the gears in mesh must be modelled. This ensures that the penalty parameter of the contact element accounts for the flexibility of the entire body of the gear not just the local stiffness at the contact point and tooth body, (see more detail in: ANSYS 1995; ANSYS 1997; Sirichai et al. 1997). A finite element model of the spur gears in mesh, without any tooth damage, is shown in Figure 5.3.1. The gear body was modelled using quadratic 2D plane strain elements and the contact surface area was modelled using 2D point-to-surface general contact elements, which included elastic Coulomb frictional effects. The contact element was generated as a symmetric contact.

The combined torsional mesh stiffness of gears in mesh at particular positions throughout the mesh cycle was obtained by rotating both solid gears then creating a finite element model in that particular position. In order to develop representative

results, a large number of finite element models at different meshing positions were undertaken for this investigation.

5.4 THE PENALTY PARAMETER ANALYTICAL MODEL

In order to handle gears in mesh with the finite element method using contact elements, the stiffness relationship between the two contact areas of the gear teeth must be established. The stiffness of the contact element is composed of the combined normal contact stiffness, KN_c, and the combined tangential contact stiffness, KT_c. The method of enforcing contact compatibility used in this thesis was based on the penalty parameter plus Lagrange multiplier method. The accuracy of the solution obtained depends on the choice of the combined normal contact stiffness, KN_c. If the combined normal contact stiffness is too small, the surface penetration may be too large, which may cause unacceptable errors. On the other hand, if the combined normal contact stiffness is too large, the combined normal contact stiffness may produce severe numerical problems in the solution process or simply make a solution impossible to solve because of ill conditioning.

The combined tangential contact stiffness, KT_c, as with the combined normal contact stiffness, ideally should be high, but not so high that it adversely affects convergence. As a guideline, the combined tangential contact stiffness should be between 1 and 3 orders of magnitude less than the combined normal contact stiffness, (see more detail in: ANSYS 1995). A default value for the elastic Coulomb friction is KT_c equal to $KN_c/100$. However, recent experimental work on gear tooth friction by Rebbechi (Rebbechi and Crisp 1981; Rebbechi and Crisp 1983; Rebbechi et al. 1992; Rebbechi et al. 1996), especially the results of the measurement of gear tooth dynamic friction (Rebbechi et al. 1996), has shown typical friction coefficient results of 0.06. A value for the elastic Coulomb friction of KT_c equal to $0.067 * KN_c$ was thus used in this research.

The main strategy behind the determination of an appropriate value of the combined normal contact stiffness was that the combined normal contact stiffness should be

computed from the local compliance of the component. It should account for the flexibility of the entire gear body and not just the local stiffness of the teeth material at the point of contact.

5.5 THE COMBINED NORMAL CONTACT STIFFNESS VARIATION

The combined normal contact stiffness of the contact elements for gears in mesh at particular positions throughout the mesh cycle was generated by rotating both solid gears then creating a finite element model in each particular position. The gear body was modelled using quadratic 2D plane strain elements and the contact surface areas were modelled using 2D point-to-surface general contact elements, including elastic Coulomb frictional effects. The contact element was generated as a symmetrical contact. The difficulty of determining the combined normal contact stiffness of the contact element at each contact position was then overcome, so that it could be user-defined in the finite element model for further determination of the combined torsional mesh stiffness and the transmission error.

The technique by which the tooth normal contact stiffness of the contact elements was obtained involved restraining the first potential contact nodes, one node for each gear for a single tooth pair in contact and two nodes for each gear for the double tooth pair in contact. A torsional load was then developed by rotating both gear hubs in a single-iteration analysis. The tooth normal contact stiffness of the contact elements of the pinion and gear, KN_p and KN_g, was then computed from the applied torque and the corresponding angle of rotation of the pinion and gear hub, θ_p and θ_g, for the pinion and gear respectively.

As the mesh geometry of the gear teeth changes over each mesh cycle, the user-defined value of the combined normal contact stiffness of the contact element must also vary within each meshing cycle. The combined normal contact stiffness KN_c must therefore be computed at each meshing position. This can be computed from the tooth normal contact stiffness for the full completed meshing cycle as shown in Figure 5.5.1. Having computed the combined normal contact stiffness at each

meshing position, the combined torsional mesh stiffness of the pinion and gear in mesh can then be determined as shown in section 5.7.

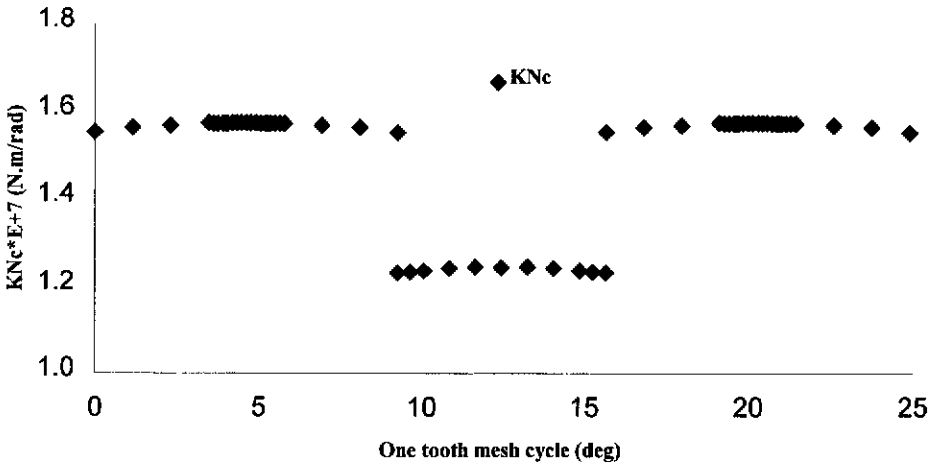

Figure 5.5.1. The variation of the combined normal contact stiffness of the contact element with the undamaged tooth.

5.6 Comparison of the Variation of Combined Normal Contact Stiffness with and Without a Cracked Pinion Tooth

One of the more difficult areas for gear fault detection is the correct diagnosis of localised tooth damage, where the important distinction between a tooth crack and a tooth spall must be made. To aid in the development of improved diagnostic techniques, finite element modelling of gear teeth in mesh with and without local teeth cracks should ultimately improve the understanding of the influence of localised teeth cracks on the resulting gearcase vibration. This section presents the results of FEA modelling of the comparison of the normal contact stiffness with and without a cracked pinion tooth including the modelling of a 2, 5, and 10 mm crack at the root of one of the pinion teeth.

A finite element model of the spur gears in mesh as shown in Figure 5.3.1, with the pinion have a single cracked tooth with through thickness of depth 2, 5, and 10 mm, was also developed in the investigation. The crack was assumed to have been

initiated at the point of the highest fillet stress (see for example: Fredriksson 1984; Mcfadden 1986; Abersek et al. 1994; Daniewicz et al. 1994; Ding et al. 1995; Flasker et al. 1995; Andersson 1996; Yang et al. 1996; Blarasin et al. 1997; Brie et al. 1997; Park et al. 1997; Glodez et al. 1998; Howard et al. 1998; Ramamurti and Neogy 1998; Sirichai et al. 1998; Sirichai et al. 1998; Tradegard et al. 1998; Xu and Saigal 1998). A finite element model of a tooth with a through thickness crack of depth 5 mm in the fillet region is shown in Figure 5.6.1.

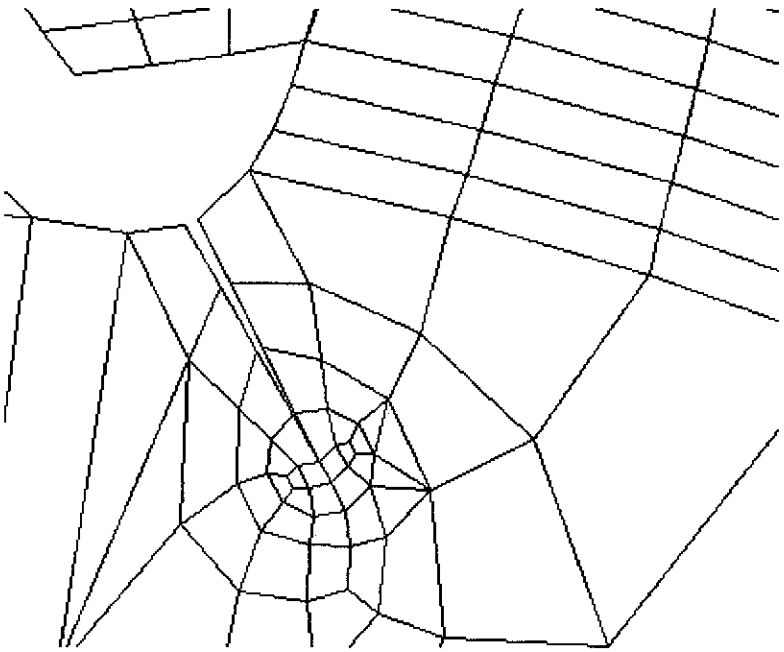

Figure 5.6.1. Finite element mesh of a cracked pinion tooth.

The same procedure, as outlined in section 5.5, was followed for the cracked pinion model. The computed value of the combined normal contact stiffness of the contact elements of gears in mesh, with one pinion tooth cracked, at particular positions throughout the mesh cycle was generated by rotating both solid gears then creating a finite element model in each particular position.

The procedure as developed in section 5.5 was followed with various tooth crack sizes, for calculation of the tooth normal contact stiffnesses with tooth damage. The first potential contact nodes were again created exactly on the intersection point between the line of action and the involute curve of the contacting teeth of both

gears. A torsional load was then applied by rotating both gear hubs in a single-iteration analysis. The tooth normal contact stiffness of the contact elements of both the pinion and gear was thus computed from the applied torque and the corresponding angle of rotation of the pinion and gear hub respectively.

Figure 5.6.2 shows the comparison results of the combined normal contact stiffness of the contact element with/without the cracked pinion tooth with the through thickness crack depth of 5 mm. The combined normal contact stiffness of the gear mesh with the damaged tooth gradually decreases after the damaged pinion tooth starts to come in contact during the double pair contact zone. The maximum decrease in stiffness is clearly seen at the end of the single pair contact zone of the damaged pinion tooth. Finally, during the second half of the double pair contact zone, the combined normal contact stiffness of the gear mesh with the damage tooth decreases slightly because most of the contact load is shared with the other undamaged tooth contact pair. This is discussed in more detail in Chapter 7.

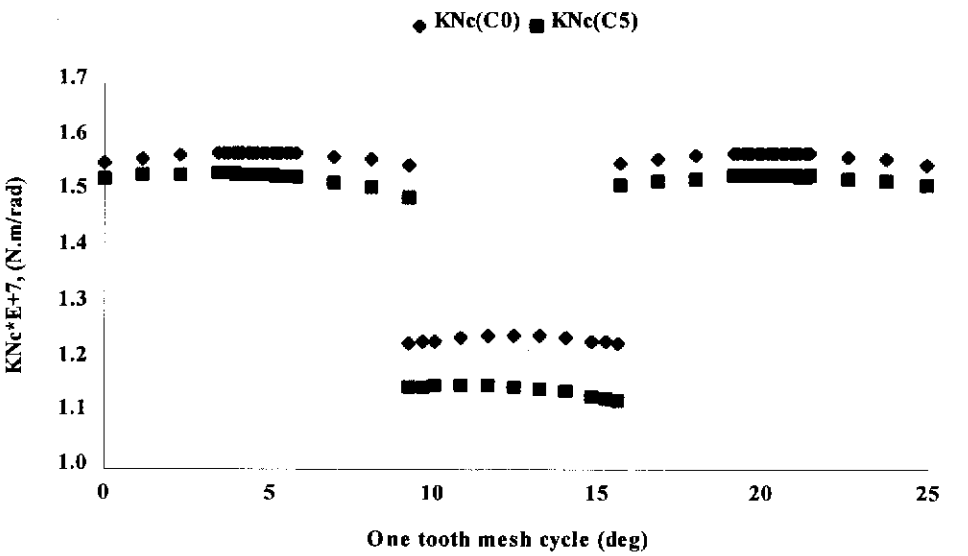

Figure 5.6.2. The comparison of the combined normal contact stiffness of the contact element with/without a damaged tooth.

5.7 THE VARIATION OF COMBINED TORSIONAL MESH STIFFNESS

Having computed the combined normal contact stiffness's of the pinion and gear at various mesh positions, the combined torsional mesh stiffness of the gears in mesh was able to be determined. The combined torsional mesh stiffness of the gears in mesh, K_p, can be obtained by introducing a prescribed rotation of the coupled nodes of the input gear hub, while restraining all nodes of the output gear hub. The computed value of the combined normal contact stiffness, KN_c for the uncracked model at each particular meshing position was used in the FE model. The result of the combined torsional mesh stiffness of the input gear at each particular meshing position was obtained by calculating the gradient of the linear relationship between torque and angular displacement at each meshing position, as shown in Figure 5.7.1. In this manner the combined torsional mesh stiffness of the input gear over the entire meshing cycle was obtained using FEA, giving the result shown in Figure 5.7.2.

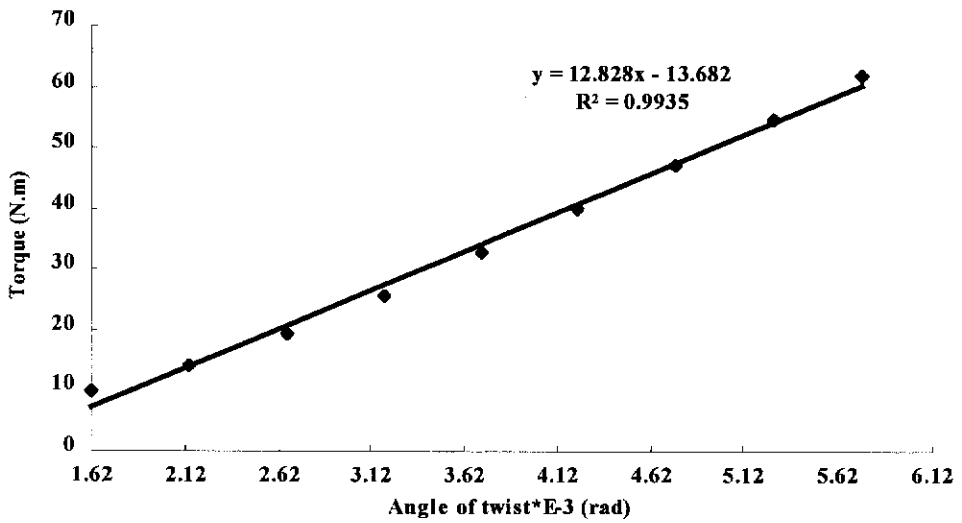

Figure 5.7.1. The combined torsional mesh stiffness, K_p, at one meshing position.

As expected, the resulting combined torsional mesh stiffness of the input gear varies dramatically throughout the meshing cycle, and it appears to be periodic with the tooth position. As the number of teeth in mesh changes from two to one and then back to two teeth in contact, the combined torsional mesh stiffness decreases and

increases respectively. At the middle of the double pair of teeth in contact, a small variation in the combined torsional mesh stiffness also appears.

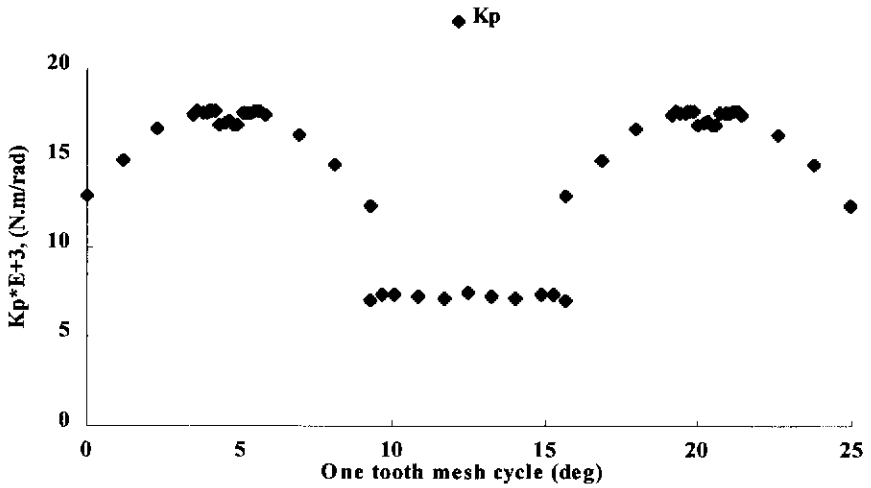

Figure 5.7.2. The combined torsional mesh stiffness of the undamaged gears in mesh over one mesh cycle.

A second model of the combined torsional mesh stiffness of the gears in mesh was also developed by considering gear rotation instead of the pinion rotation, K_g. A prescribed rotation of the coupled nodes of the output gear hub was introduced, while restraining all nodes of the input gear hub. The computed value of the combined normal contact stiffness, KN_c, at each particular meshing position was again used in the FE model. The result of the combined torsional mesh stiffness of the gears at particular meshing positions was obtained by the same process as outlined above. Figure 5.7.3 shows the comparative results of the combined torsional mesh stiffness at one meshing position between the two models.

Using the same procedure as for the first model, the combined torsional mesh stiffness of the gears in mesh over the entire meshing cycle was obtained using FEA. Figure 5.7.4 shows the comparative results from the two procedures of the combined torsional mesh stiffness of the gears in mesh. As expected, the results of both models are very similar as the same actual system is being considered in both models. The slight differences between the model results could reasonably be due to numerical error.

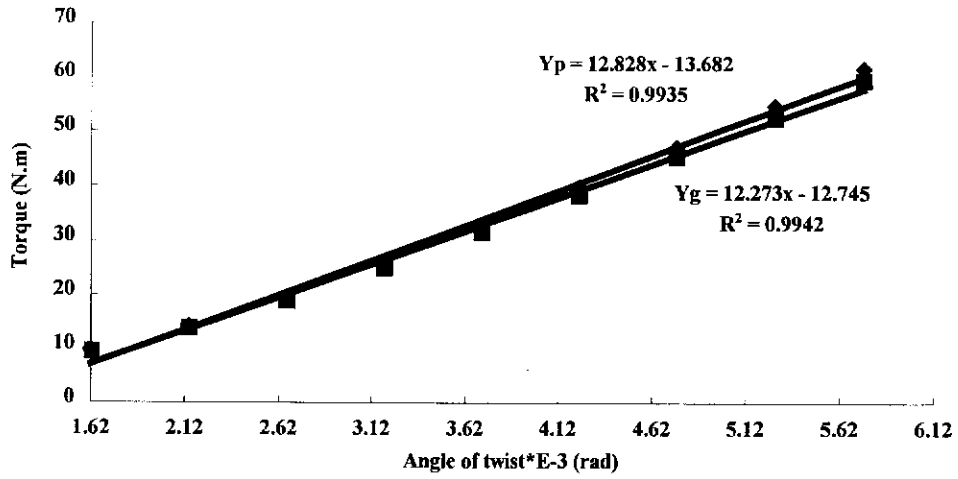

Figure 5.7.3. Comparison of the combined torsional mesh stiffness, K_p, and K_g.

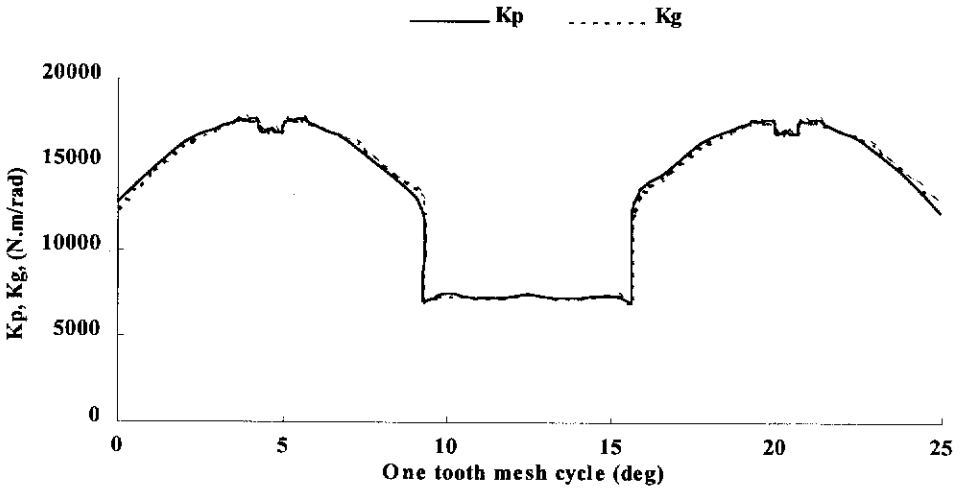

Figure 5.7.4. Comparison of the combined torsional mesh stiffness of the gears in mesh from the two models, K_p, and K_g.

5.8 Comparison of Combined Torsional Mesh Stiffness With/Without Cracked Pinion Tooth

The same procedure as used in section 5.7 was followed for the cracked pinion model, although the computed value of the combined normal contact stiffness of the cracked pinion was used in the FE model. The result of the combined torsional mesh stiffness of the input gear with the cracked pinion tooth of 5 mm for the entire meshing cycle was obtained, and the comparison results with the undamaged pinion are shown in Figure 5.8.1.

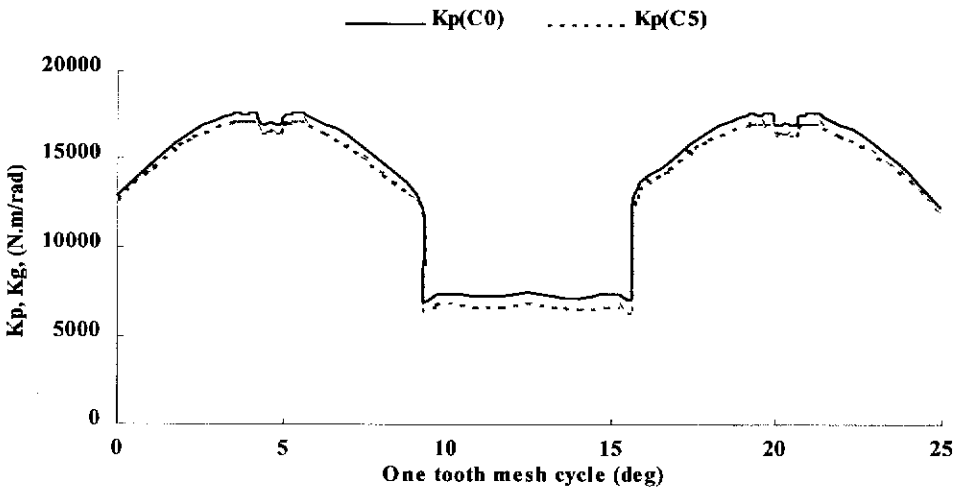

Figure 5.8.1. Comparison of the combined torsional mesh stiffness of the pinion with (C5) / without (C0) damaged tooth.

As clearly seen in Figure 5.8.1, the combined torsional mesh stiffness for the pinion with the cracked tooth is slightly smaller than the undamaged results. The difference of the combined torsional mesh stiffness values between the uncracked and cracked pinion are shown in Figure 5.8.2.

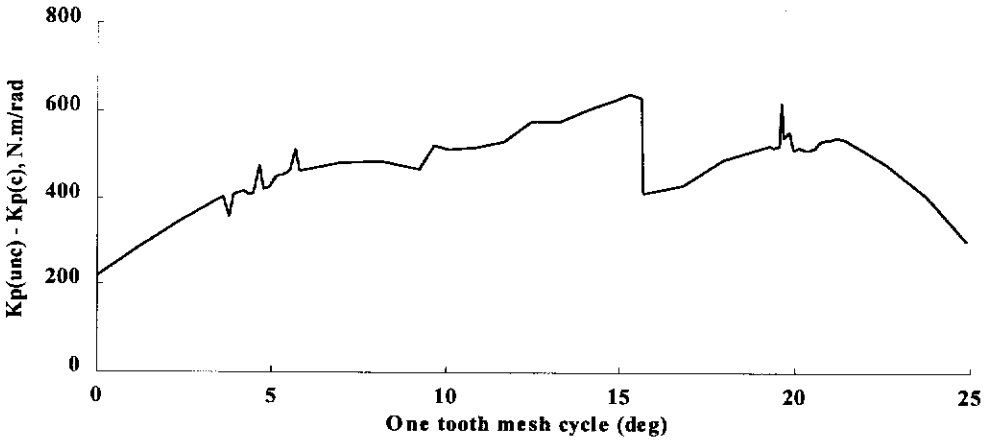

Figure 5.8.2. The difference of the combined torsional mesh stiffness between the uncracked and cracked pinion, K_p.

It can be seen from the comparison that the combined torsional mesh stiffness for the cracked pinion starts reducing gradually until the end of the single tooth pair in contact, where its value increases suddenly as another uncracked tooth starts to come into contact. Before the cracked pinion leaves the mesh, its combined torsional mesh stiffness starts to decrease because the tooth is being loaded closer to its tip.

5.9 The Procedure for Modelling the Combined Normal Contact Stiffness and the Combined Torsional Mesh Stiffness

The procedure for modelling the combined normal contact stiffness of the contact elements and the combined torsional mesh stiffness is outlined by a step-by-step description followed by a flow chart shown in Figure 5.9.1. The program was written using the ANSYS Parametric Design Language and the entire program is provided in appendix B for the undamaged tooth and in appendix C for the damaged tooth.

The step-by-step procedures for the determination of the combined normal contact stiffness of the contact elements and the combined torsional mesh stiffness of the gears in mesh with and without a damaged tooth are described below.

Define array parameters:

1. Define a basic array parameter and its meshing position dimensions such as angle of rotation and keypoints, then save it as a parameter file.

Do-loop:

2. Do-loop of meshing position covering a complete mesh cycle. For the undamaged gear mesh the loop will run from Figure 3.3.1(a) to (d) because the procedure for the loop in Figure 3.3.1(d) to (e) is just the same as that for (a) to (b). However, for the damaged gear mesh, the loop procedure must run over the completed cyclic mesh as shown in Figure 3.3.1(a) to (e) because of the change in the damaged tooth stiffness.

Resume FE model: (preprocessor)

3. Resumes the model and database, as shown in Figure 5.3.1, at the start of the mesh cycle, see Figure 3.3.1(a).

Resume array parameters: (preprocessor)

4. Reads array parameters from a parameter file to extend the current parameters in the database.

Rotate FE model: (preprocessor)

5. Sets the element type, element material, element real constant, and element coordinate system of the gear body.
6. Activates a global cylindrical coordinate system of the pinion. Selects subset areas of the pinion only, then rotates the FE model through particular meshing position in degrees.
7. Activates a local cylindrical coordinate system of the gear. Selects subset areas of the gear only, then rotates the FE model through the same angular meshing position as the pinion.

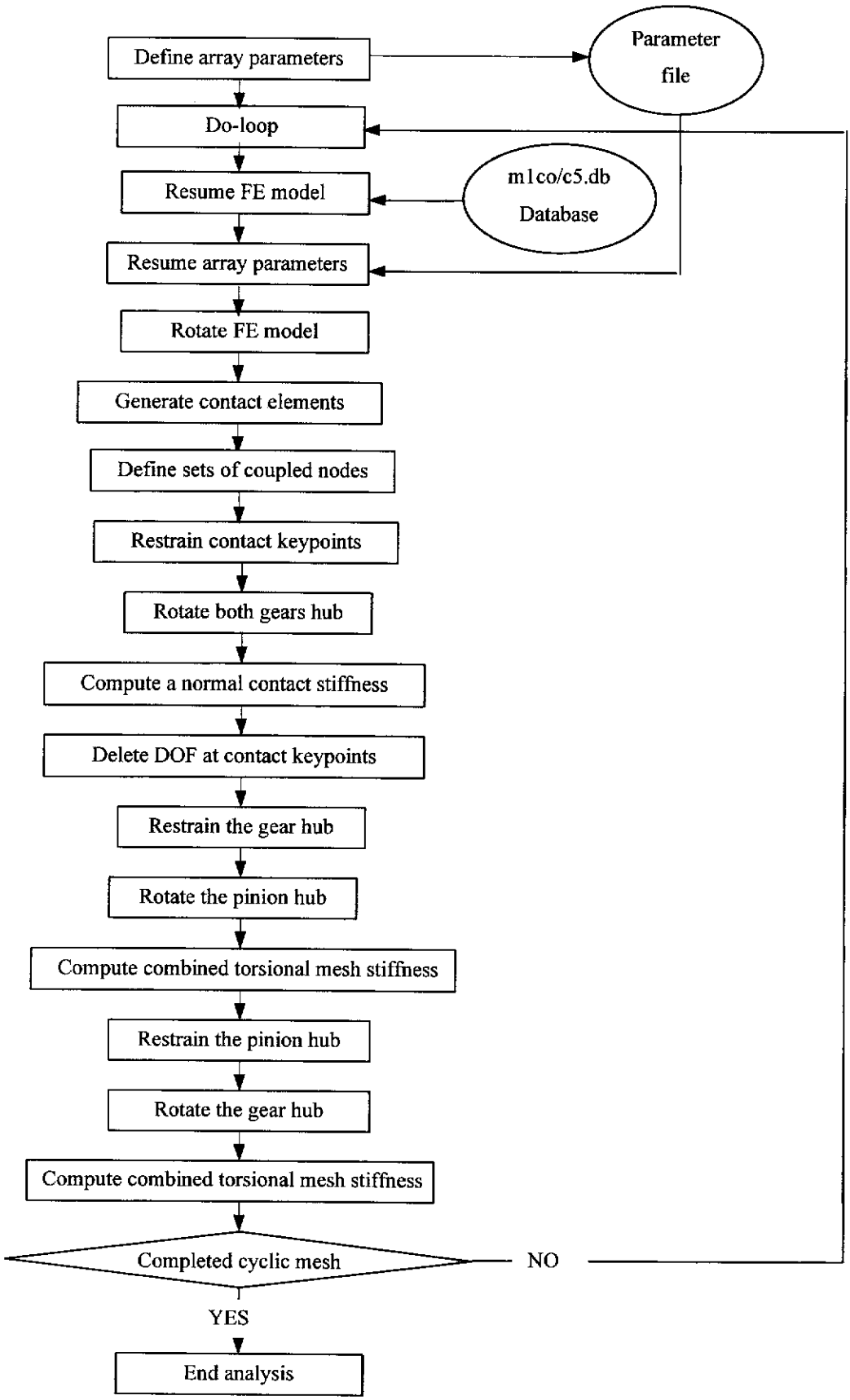

Figure 5.9.1. Procedure for modelling the combined normal contact stiffness of the contact element and the combined torsional mesh stiffness.

Generate contact elements: (preprocessor)

8. Do loop condition of meshing position for the single pair or double pair of teeth in mesh.
9. Deletes nodes and area elements associated with the contact teeth of both gears.
10. Specifies the division and spacing ratio on unmeshed lines of each contact tooth.
11. Concatenates multiple lines into one line for mapped meshing.
12. Generates nodes and area elements within the contact tooth area.
13. Groups potential contact nodes of the contact tooth into components for further generation of the contact elements.
14. One of the most important criteria for each meshing position was that the first potential contact nodes of both contact teeth, in step 10-12, must be created exactly on the intersection point between the pressure line or line of action and the involute curve. This strategy will activate contact nodes on the run by moving nodes to every meshing position.
15. Sets the element type, element material, element real constant, and element coordinate system of the contact element. Then generates symmetric contact elements on potential contact nodes.

Define sets of couple nodes: (preprocessor)

16. Activates a global cylindrical coordinate system of the pinion. Selects the subset nodes of the pinion hub then rotates nodal coordinate systems into the global cylindrical coordinate system. Defines a set of coupled nodes DOF. Stores master node number of coupled set of the pinion hub.
17. Activates a local cylindrical coordinate system of the gear. Selects a subset node of the gear hub then rotates nodal coordinate systems into the local cylindrical coordinate system. Defines a set of coupled nodes DOF. Stores master node number of coupled set of the gear hub.

Restrain contact keypoints: (preprocessor)

18. Defines gear material properties.
19. Restrains all DOF at the contact keypoints of the pinion and the gear. The technique restrains the first potential contact nodes which are generated exactly at contact keypoints in steps 9-11, one node for each gear for a single tooth pair in contact and two nodes for each gear for the double tooth pair in contact.

Rotate both gear hubs: (preprocessor)

20. Define DOF constraints at master coupled nodes of the pinion and gear hubs.
21. Applies loads to both gear hubs in a single-iteration analysis.

Compute the combined normal contact stiffness: (postprocessor)

22. Specifies the total reaction force at the pinion hub and the gear hub.
23. Computes the combined torsional stiffness, defined as the ratio between the torsional load and the angular rotation of the gear body, for the pinion model, K_p, and the gear model, K_g.
24. Computes the combined normal contact stiffness of that particular meshing position and stores it as a user-defined array parameter for further use.

Delete DOF at contact keypoints: (preprocessor)

25. Deletes DOF constraints at contact keypoints
26. Sets element key options.
27. Defines the element real constants with Lagrange multiplier.

Restrain the gear hub: (preprocessor)

28. Restrains all DOF at the master coupled nodes of the gear hub.

Rotate the pinion hub: (preprocessor)

29. Applies the load to the pinion hub by defining DOF constraints to the master coupled nodes of the pinion hub.
30. Specifies the optimized nonlinear solution and some enhanced internal solution algorithms, such as number of substeps, etc.

Compute pinion torsional mesh stiffness: (postprocessor)

31. Specifies the nodal rotation and the total reaction force at the pinion hub to be stored.
32. Computes the angular rotation of the pinion hub and the torsional load of each substep in the nonlinear solution. Computes the combined torsional mesh stiffness of the pinion defined as the gradient of relationship between torque and angle of rotation. Redirects the results to a file in specific directory. The further

analysis of gradients for the combined torsional mesh stiffness is also to be done in Microsoft Excel.

Restrain the pinion hub: (preprocessor)

33. Restrains all DOF at master coupled nodes of the pinion hub.

Rotate the gear hub: (preprocessor)

34. Applies the load to the gear hub by the defined DOF constraints to master coupled nodes of the gear hub.
35. Specifies optimized nonlinear solution and some enhanced internal solution algorithms, such as number of substeps, etc.

Compute gear torsional mesh stiffness: (postprocessor)

36. Specifies nodal rotation and the total reaction force at the gear hub to be stored.
37. Computes the angular rotation of the gear hub and the torsional load of each substep using the nonlinear solution. Computes the combined torsional mesh stiffness of the gear defined as the gradient relationship between torque and angle of rotation. The result is also redirected to a file in a specific directory. The further analysis of gradient of the combined torsional mesh stiffness is also to be done in Microsoft Excel.

Completed cyclic mesh:

38. End a do loop when the cyclic mesh is completed and exit the program.

5.10 Conclusion

A strategy for choosing an appropriate value of the combined normal contact stiffness of contact elements at particular meshing positions, over the whole mesh cycle, has been presented. The method has been demonstrated to work well for two spur gears in mesh. The method involves the creation of potential contact nodes and keypoints. The keypoints are used for specifying the edge lengths of the elements and mesh sizes at the candidate contact surface. The first potential contact node was restrained and the combined normal contact stiffness at each particular meshing

position over the gear mesh cycle was then computed. The application of the technique to two gears in mesh appears to have been successful, with the resulting combined torsional mesh stiffness being periodic over each mesh cycle.

This chapter has also presented a general formulation for the combined torsional mesh stiffness which takes into account the angular rotation of the gear blank caused by tooth bending, shearing and contact deformation as calculated by FEA through the use of contact elements. Geometrical error effects such as profile errors and runout has not been considered in the calculation.

The combined torsional stiffness of the gears in mesh was obtained by introducing a prescribed rotation of the coupled nodes of the input gear hub, while restraining all nodes of the output gear hub. The computed value of the combined normal contact stiffness of the contact elements with and without a damaged tooth at each particular meshing position was used in each specific FE model. The result of the combined torsional stiffness of the gear mesh at particular meshing positions was obtained by calculating the gradient of the linear relationship between torque and angular displacement and in this manner the combined torsional stiffness of the gears in mesh for the entire meshing cycle was obtained. As expected, the resulting combined torsional mesh stiffness of the gears in mesh varies dramatically throughout the meshing cycle, and it appears to be periodic with the tooth position. As the number of teeth in mesh changes from two to one and then back to two teeth in contact, the combined torsional mesh stiffness decreases and increases. At the middle of the double pair of teeth in contact, an abrupt change in the combined torsional stiffness also appears and is the subject of an ongoing investigation.

The presence of a single cracked tooth has decreased the combined normal contact stiffness of the contact element as well as modifying the overall combined torsional mesh stiffness. When a single cracked tooth is in mesh it can be clearly seen, with the largest effect occurring as the single tooth contact changes to the double tooth contact. In the double pair contact zone, the effect was less because other undamaged tooth pairs share the torque load. These results provide valuable insight into the effect a single tooth crack has on torsional mesh stiffness, and should aid in

the development of gear dynamic models aimed at modelling the resulting gear vibration where teeth cracks are present.

CHAPTER 6

FINITE ELEMENT ANALYSIS OF GEARS IN MESH: THE STATIC TRANSMISSION ERROR

6.1 INTRODUCTION

The transmission error of gears in mesh is a term used to describe the difference between the theoretical and actual angular position between a pinion and a gear. Transmission error is considered to be one of the main important causes of gear noise and vibration. Numerous works have been published on gear transmission error measurement (Gregory et al. 1963; Hayashi and Hayashi 1979; Hayashi and Hayashi 1981; Mcfadden 1986; Vinayak and Houser 1992; Daniewicz et al. 1994; Munro and Yildirim 1994; Yau et al. 1994; Velex et al. 1995; Munro 1997). Experimentally, transmission error testing has been accomplished by rolling gears together with backlash, and at their proper operating center distance. The input and output angular motion characteristics of the gears are normally measured by encoders and associated electronics. The data can be presented in graphical analog form or can be further processed by Fast Fourier Transform (FFT) techniques to aid in pinpointing the source of excitation. However, the measurement of transmission

errors from test rigs has traditionally not shown a great amount of detail within each meshing cycle. The primary purpose of this chapter is to develop the detailed static loaded transmission error over one completed cycle of mesh.

Two types of transmission error are commonly referred to in the literature.

The first is the manufactured transmission error, which can be obtained for unloaded gear sets when they rotate in single flank contact. The manufactured transmission error is affected most by profile inaccuracies, spacing errors, and gear tooth runout. Gears that have perfect involute profiles and no spacing or runout error should produce a perfectly straight transmission error trace, which would result in a spectrum with no peaks at discrete frequencies. It has been shown that there is a direct relation between the manufactured transmission error and noise, (Welbourn 1972; Welbourn 1979; Smith 1983; Smith 1987; Smith 1987; Baron et al. 1988).

The second is the loaded transmission error, which is similar in principle to the manufacturing transmission error but takes into account tooth bending deflection, shearing displacement and contact deformation due to load. When gears operating at low speed are loaded, two additional factors contribute to the transmission error (Townsend 1991),

- A constant component due to the mean tooth compliance. This component is of major significance in choosing appropriate profile modifications, but of much less significance with regard to its contribution to mesh frequency noise,

and

- A time-varying component that is a function of gear tooth geometry and torsional mesh stiffness variation, as well as the manufactured transmission error. This component contributes heavily to mesh frequency noise.

As gears are run at higher speeds, a dynamic component that is a function of the system dynamics, (Ozguven and Houser 1988), must be included along with the low speed effects aforementioned.

When gears are unloaded, a pinion and gear with involute profiles should theoretically run with zero transmission error. However, when gears with involute profiles are loaded, the combined torsional mesh stiffness of each gear changes, as shown in chapter 5, causing variations in angular rotation of the gear body. The combined torsional mesh stiffness is defined as the ratio between the torsional load and the angular rotation of the gear body. At each particular meshing position, the angular rotation of the pinion due to tooth bending, shearing and contact displacement is calculated in the gear reference frame by restraining the gear from rotating, with the pinion having a torque input load. In relation to the pinion reference frame, the pinion is restrained from rotating, with the gear having the torque input load and the resulting angular rotation of the gear is computed. The difference between these two angular rotations is the static transmission error of gears under load at low speed, which can be expressed in angular units as shown in equations (3.6.1).

One of the deficiencies in the measurement of the transmission error from test rigs is that the detailed behaviour of each tooth meshing cycle isn't present. Secondly the manufactured transmission error such as spacing errors and runout error is much greater than the loaded transmission error. Therefore the results of gear transmission error measurement from the test rig is greatly influenced by the manufacturing transmission errors (see for example of test rig results: Gregory et al. 1963; Tordian and Geraldin 1967; Tordion and Gerardin 1967; Hayashi and Hayashi 1981; Houser and Blankenship 1989; Rebbechi et al. 1992; Vinayak and Houser 1992; Bard et al. 1994; Barnett and Yildrim 1994; Munro and Yildirim 1994; Velex et al. 1995; Houser et al. 1996; Sweeney and Randall 1996). In this chapter, a detailed investigation of the variation of the loaded transmission error throughout the mesh cycle is presented. Many different positions within the meshing cycle have been investigated and then compared with the effect of a pinion having a single cracked tooth. For modelling of gear teeth in mesh, the penalty parameter of the combined normal contact stiffness of the contact element is user-defined and it varies through the cyclic mesh. The simple strategy of how to overcome this difficulty was also used.

6.2 THE STATIC TRANSMISSION ERROR ANALYTICAL MODEL

The development of a static combined torsional mesh stiffness model of gears in mesh, as developed in chapter 5, can be used to determine the static transmission error throughout the mesh cycle. Consider the two identical spur gears in mesh as shown in Figure 3.3.1, part (a) of which is enlarged here as shown in Figure 6.2.1. Point A along the path of contact indicates the initial tooth contact where the addendum circle of the output gear intersects the line of action. For involute gears, the line of action is the common tangent line to the base circle. When the first tooth pair contacts at point A, between the tooth tip of the output gear and the root of the pinion, a second tooth pair is already in contact at point D. As the gear rotates, the point of contact will move along the line of action APE. When the first tooth pair reaches point B, the second tooth pair disengages at point E leaving only the first tooth pair in the single contact zone. When this first tooth pair rotates to point D, the next tooth pair begins engagement at point A and starts another mesh cycle, as shown in Figure 3.3.1.

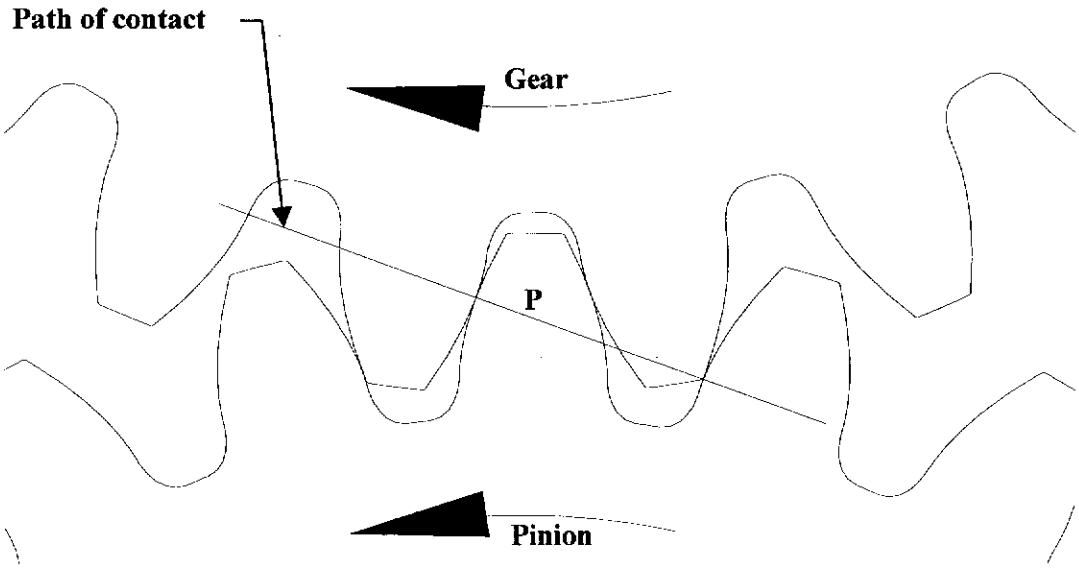

Figure 6.2.1. Expansion of Figure 3.3.1(a) at the start of the meshing cycle.

Considering the start of the meshing cycle of the two contact pairs at A and D as shown in Figure 6.2.1, and using the equilibrium constraint that the sum of the

torque contributions of each meshing tooth pair must equal the total applied torque, then the torque equation will be given as shown below.

For the pinion, the torque equilibrium equation becomes,

$$\begin{aligned} T_{tot,p}^{A,D} &= T_p^A + T_p^D, \\ &= \left(R_p^A * F_p^A\right) + \left(R_p^D * F_p^D\right), \end{aligned} \tag{6.2.1}$$

and for the gear,

$$\begin{aligned} T_{tot,g}^{A,D} &= T_g^A + T_g^D \quad , \\ &= \left(R_g^A * F_g^A\right) + \left(R_g^D * F_g^D\right), \end{aligned} \tag{6.2.2}$$

where T_p^A, T_p^D, T_g^A, T_g^D are the torque vectorial contributions to the total applied torque of tooth pairs at A and D of the pinion and gear respectively, and $T_{tot,p}^{A,D}$, and $T_{tot,g}^{A,D}$ are the total applied torque vectors of the pinion and gear respectively. The transverse plane contact radius vectors on the pinion and gear tooth pair A and D are given by R_p^A, R_p^D, R_g^A, R_g^D and the load sharing vectors F_p^A, F_p^D, F_g^A, F_g^D are part of the total applied force vectors $F_{tot,p}^{A,D}$, and $F_{tot,g}^{A,D}$, at the contact points A and D of the pinion and gear respectively. The equations relating the load share vectors to the total applied force vectors $F_{tot,p}^{A,D}$ and $F_{tot,g}^{A,D}$ are given by $F_{tot,p}^{A,D} = F_p^A + F_p^D = -F_{tot,g}^{A,D} = -F_g^A - F_g^D$. The equations relating the load sharing vectors at each tooth pair in contact are $F_p^A = -F_g^A$ and $F_p^D = -F_g^D$ for the contact at points A and D of the pinion and gear respectively.

The transmission error, TE, of gears in mesh with involute profile under load can be defined as the difference between the actual position of the output gear and the theoretical position it should occupy. In angular units, this can be expressed as,

$$TE = \theta_g - (Z)\theta_p \quad , \quad \text{rad} \tag{6.2.3}$$

where Z represents the gear ratio, $\theta_{p,g}$ denotes the angular rotation of the input and output gears in radians. The foregoing developments of equation (6.2.3) are appropriate for both loaded and unloaded gears, and static or dynamic situations. When gears are unloaded, transmission error contributions arise from manufacturing inaccuracies such as profile errors, spacing errors, and runout. When gears are loaded, the changes in angular rotation due to torsional mesh stiffness variations must be accounted for in the evaluation of transmission error.

From previous experimental results, the time varying component of transmission error, which is periodic at the tooth mesh frequency, has been shown to be related to gear noise amplitude (Smith 1983; Smith 1987). In fact, it has been shown that the transmission error of spur gears, which have large changes in torsional mesh stiffness, can be reduced significantly by applying appropriate profile modifications (Gregory et al. 1963; Welbourn 1979; Baron et al. 1988; Alattass et al. 1994; Oswald et al. 1994; Litvin et al. 1995; Wang and Tong 1996).

6.3 THE STATIC TRANSMISSION ERROR FINITE ELEMENT MODEL

The static transmission error analysis developed here using the finite element model of spur gears in mesh was based upon the same analytical model of the combined torsional mesh stiffness, as shown in chapter 5. The steps involved are essentially the same as for modelling the normal contact stiffness of the contact element and the combined torsional mesh stiffness, except that a postprocessor solution was required to calculate the transmission error.

The transmission error of gears in mesh at particular positions throughout the mesh cycle was generated by rotating both solid gears then creating a finite element model in that particular position using the appropriate value of the normal contact stiffness of the contact element. Next, in the postprocessor solution, the static transmission error of the gears in mesh was obtained from the FEA model by introducing a prescribed load to the master coupled nodes of the pinion hub, while restraining all

the nodes of the gear hub. The analysis then computes the angular rotation of the pinion hub and the reaction gear torque from the reaction forces at the gear contact teeth. The converse analysis was also done in a second model by introducing a prescribed load, equal to the reaction gear torque from the previous calculation, to the master coupled nodes of the gear hub, while restraining all the nodes of the pinion hub. Finally, the values of the angular rotation of the pinion and gear were used in equation (6.2.3) to compute the static transmission error at each particular meshing position. The transmission error given by equation (6.2.3) was obtained by the summation of the absolute angular rotations of the pinion and gear from the two models divided by two, to get the true transmission error. In order to develop representative results, a large number of finite element models at different meshing positions were undertaken for this investigation.

6.3.1 The Static Transmission Error of Undamaged Gears

The procedure for modelling the static transmission error of gears in mesh is outlined in the flow chart in Figure 7.6.1. The step-by-step description procedures are described in section 7.6 and the program batch file is listed in appendix D for the uncracked pinion tooth and in appendix E for a cracked pinion tooth.

The stiffness of the contact elements, being user-defined, was composed of the combined normal contact stiffness, KN_c, and the combined tangential contact stiffness, KT_c. A default value for the elastic Coulomb friction $KT_c = KN_c/100$ was used in this investigation, as discussed in section 4.6.2.

Having computed the combined normal contact stiffness at each meshing position, the transmission error of the pinion and the gear in mesh can then be determined. At each particular meshing position, the angular rotation of the pinion and the gear due to tooth bending, shearing and contact displacement was calculated in the gear reference frame and the pinion reference frame in separate models respectively. The angular rotation of the pinion, θ_p, and the *output torque* can be obtained by introducing a prescribed torque input load at the master coupled nodes of the pinion hub, while restraining the master coupled nodes of the gear hub. Conversely, in

relation to the pinion reference frame, the angular rotation of the gear, θ_g, can be obtained by restraining the pinion hub from rotating, with the gear having the torque input load at the master coupled nodes of the gear hub. Each of these angular rotations gives the static TE, however in this case, the average of these two angular rotations was used to give the static transmission error of gears under load. In this manner the static transmission error of gears in mesh over the entire meshing cycle was obtained using FEA, giving the result as shown in Figure 6.3.1 using a constant applied torque load of 76.2 N.m.

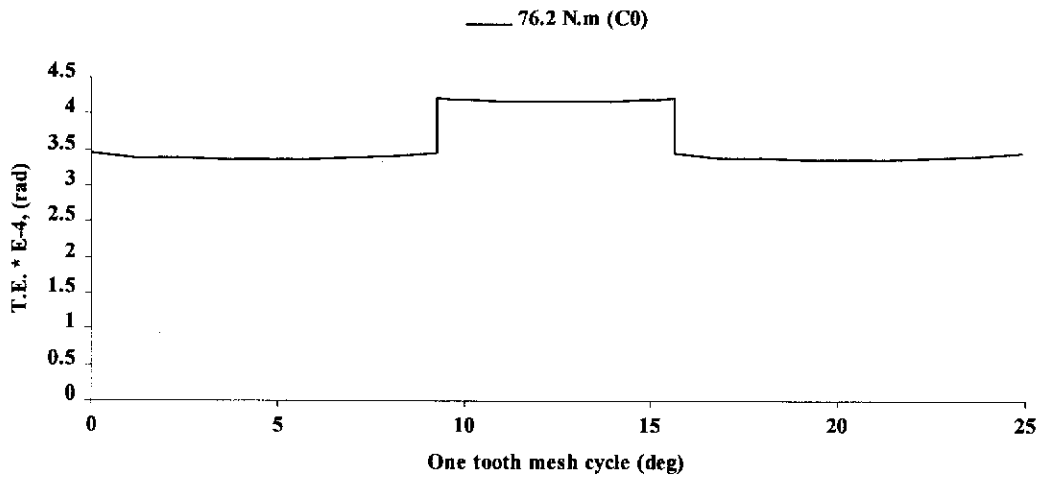

Figure 6.3.1. The static transmission error of undamaged gears in mesh.

As expected, when perfect involute gears mesh under static load, the transmission error is caused by the torsional mesh stiffness variations. In one complete cycle of the undamaged gear mesh, the gear body rotation variations due to tooth bending deflection, shearing displacement and contact deformation cause the transmission error of each half of the mesh cycle to reflect at the pitch point. The static transmission error shown in Figure 6.3.1 shows that the abrupt T.E. changes occur at the transitional positions between two teeth to one tooth in mesh, and conversely, at the transitional positions from one tooth to two teeth in mesh. These sudden changes in the transmission error generate vibration and noise.

6.3.2 The Static Transmission Error With/Without Cracked Pinion Tooth

A finite element model of the spur gears with the pinion having a single cracked tooth, was developed for the investigation of the static transmission error. The crack was assumed to have been initiated at the point of the highest fillet stress with a through thickness crack of depth 5 mm in the fillet region.

The resulting combined normal contact stiffness, KN_c, was shown in chapter 5. The presence of the pinion tooth crack results in a decrease in the combined normal contact stiffness. The reduction in the combined normal contact stiffness of the cracked gear is greatest at the end of the single tooth pair contact zone because the pinion tooth crack is being loaded closer to its tip.

The preprocessor involved here was essentially the same as for modelling the static transmission error of the uncracked gear mesh outlined above. Having computed the combined normal contact stiffness of the damaged gear at each meshing position, the transmission error of the pinion and gear in mesh can then be determined. At each particular meshing position, the angular rotation of the pinion due to tooth bending, shearing and contact displacement is calculated in the gear reference frame by restraining the gear from rotating, with the pinion having a torque input load. In relation to the pinion reference frame, the pinion is restrained from rotating, with the gear having the torque input load and the resulting angular rotation of the gear is computed. The average between these two angular rotations provides the static transmission error of the involute profile gears under load with the tooth damage. The computed value of the combined normal contact stiffness for the cracked model at each particular meshing position, as shown in chapter 5, was user-defined in the FE model. In this manner the static transmission error of the gears in mesh over the entire meshing cycle was obtained, giving the result shown in Figure 6.3.2 using a constant applied torque of 76.2 N.m.

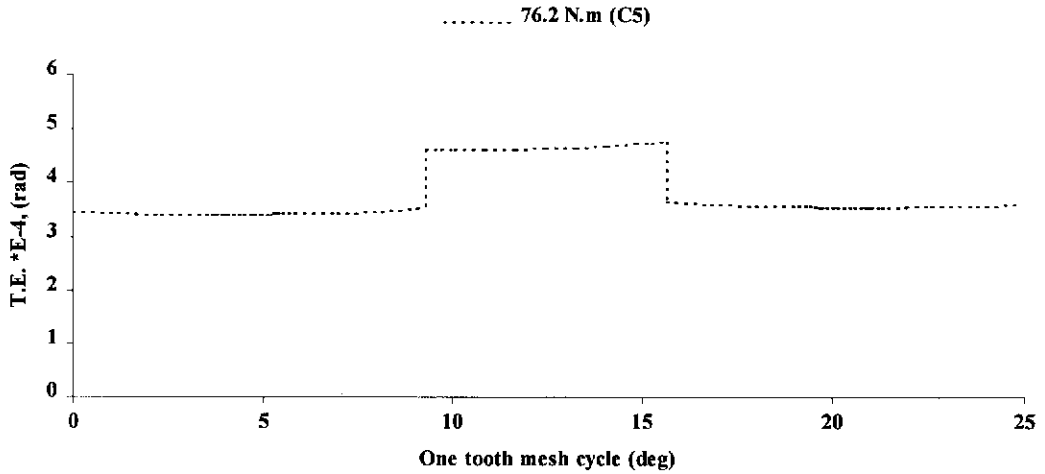

Figure 6.3.2. The static transmission error of gears in mesh with a cracked tooth.

The result of the static transmission error of damaged gears in mesh is similar to that of the undamaged gear shown in Figure 6.3.1. However, the transmission error of each half of the cyclic mesh is not reflected at the pitch point but now varies throughout the entire mesh cycle. For the second half of the double pair contact zone, the transmission error is slightly higher than the first half of the double pair contact zone. This is because the contact point of the cracked tooth moves closer to its tip. Again the abrupt transmission error changes take place at the entry and exit of mesh, and at the transition point between two teeth to one tooth in contact, and vice-versa. These sudden changes are higher than for the undamaged gear mesh so it should generate more vibration and noise.

The comparison of results of the static transmission error for the undamaged/damaged model are shown in Figure 6.3.3. The greatest distinguishing difference between the two occurs during the single pair contact zone, especially at the end of the single tooth pair in contact where the cracked tooth is being loaded closer to its tip. This is in agreement with the comparison of the combined torsional mesh stiffness with/without the cracked pinion tooth as shown in chapter 5. In the double tooth pair contact zone, the difference is small during the first half of the double pair contact zone, when the damaged tooth first appears in mesh, but increases during the second half of the double pair contact zone.

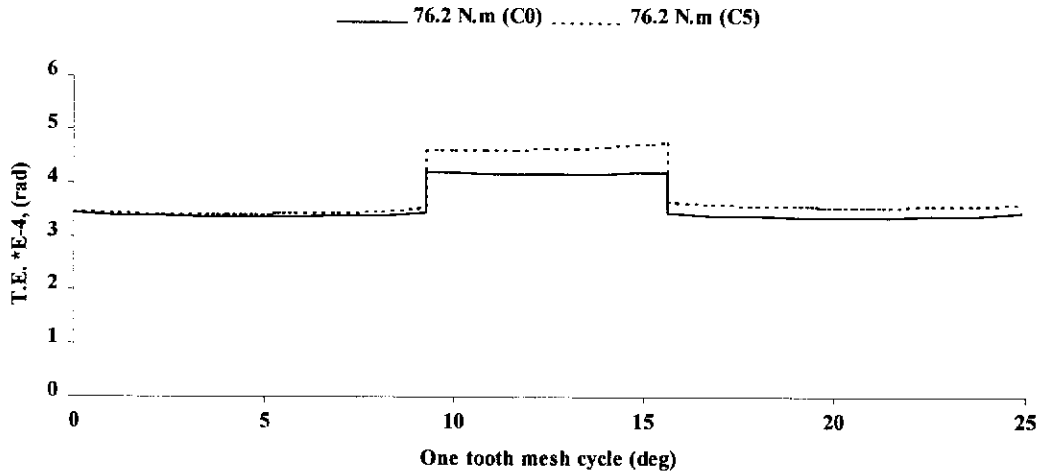

Figure 6.3.3. Comparison of the static transmission error of undamaged/damaged gears in mesh.

6.4 THE EFFECT OF INPUT LOAD ON THE STATIC TRANSMISSION ERROR

Further results of the static transmission error of the gears in mesh, as given by equation (6.2.3), including different applied torques of 38.1, 76.2, 114.3, and 152.4 N.m, were computed over the full meshing cycle. The step procedures involved were essentially the same as those in section 6.3.1, except that the solution required the addition of 3 more do-loops for the variation of the input torque load.

The comparison of results of the effect of the input torque load on the static transmission error of undamaged gears mesh is shown in Figure 6.4.1. As expected, the amplitude of the transmission error is directly related to the magnitude of applied torque, which is similar to other published work on the static and dynamic transmission error measurements (Gregory et al. 1963; Houser and Blankenship 1989; Barnett and Yildrim 1994; Munro and Yildirim 1994; Velex et al. 1995). It should be noted however, that the resulting transmission error over one tooth mesh cycle as shown in Figure 6.4.1 is for the case where there are no runout or profile errors on the teeth. The only variation being included in the model is the change in the torsional mesh stiffness of the teeth in mesh over the complete tooth mesh cycle.

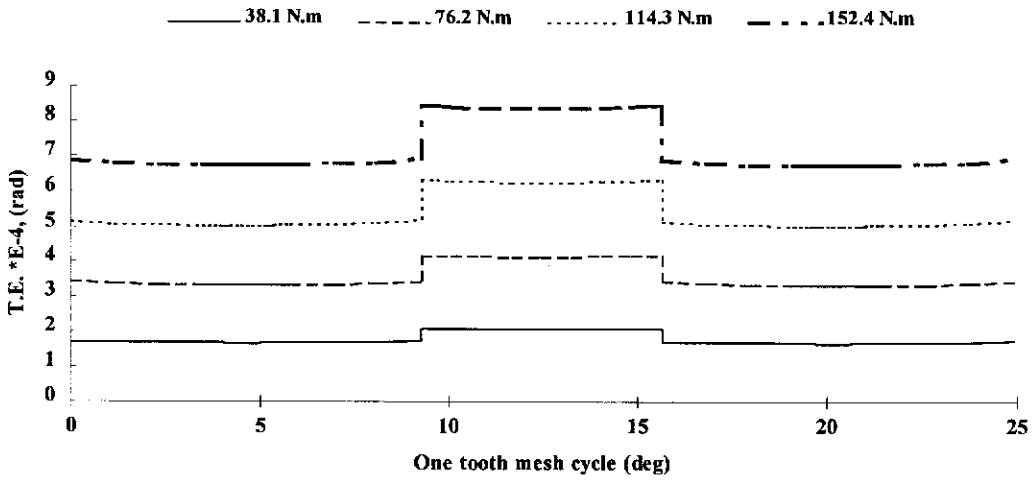

Figure 6.4.1. The effect of different applied torques on the transmission error.

6.5 CONCLUSION

This chapter has presented a general finite element formulation of the static transmission error of gears in mesh. The formulation has taken into account the angular rotation of the gear blank caused by tooth bending, shearing and contact deformation and has been calculated by FEA through use of non-linear contact elements based on a Newton-Raphson algorithm and using the Frontal Solver method for equation solution. A strategy for choosing an appropriate value of the combined normal contact stiffness of contact elements at particular meshing positions, over the whole mesh cycle, has been presented. The method has been demonstrated to work well for two spur gears in mesh. The method involves the creation of potential contact nodes and keypoints. The keypoints are used for specifying the edge lengths of the elements and mesh sizes at the candidate contact surfaces. The first potential contact node was restrained and the normal contact stiffness at each particular meshing position over the gear mesh cycle was then computed. The application of the technique to two gears in mesh appears to have been successful, with the resulting combined torsional mesh stiffness being periodic over each mesh cycle. Geometrical error effects such as profile inaccuracies, spacing and runout errors have not been considered in the calculation. Furthermore, it has been assumed that the physical contact between teeth occurs along the line of contact. For localised damage to the tooth profile, the physical contact point between

teeth in mesh may deviate from the line of action, necessitating a modification to the FE model presented here.

The resulting static transmission errors are consistent with the results obtained in other research publications. The slight variations in transmission error can cause enhanced noise and vibration if the excitation frequency matches a resonance of the gearbox.

The presence of a single cracked tooth has decreased the combined torsional mesh stiffness of each gear and the resulting changes to the transmission error when a single cracked tooth is in mesh can be clearly seen, with the largest effect occurring as the single tooth contact changes to the double tooth contact. In the double pair contact zone, the effect was less because other undamaged tooth pairs share the torque load.

These results provide valuable insight into the effect a single tooth crack has on the combined torsional mesh stiffness and on transmission error and should aid in the development of gear dynamic models aimed at modelling the resulting gear vibration where teeth cracks are present.

CHAPTER 7

FINITE ELEMENT ANALYSIS OF GEARS IN MESH: THE LOAD SHARING RATIO ALONG THE PATH OF CONTACT

7.1 INTRODUCTION

For involute gears under normal operating conditions, the main source of vibration excitation is from the periodic change in tooth stiffness due to non-uniform load distributions over the double and single contact zone in each meshing cycle of the mating teeth. Previous results have indicated that the variation in mesh stiffness can significantly affect the vibration and dynamic loading (Nakada and Utagawa 1956; Harris 1958; Utagawa and Harada 1962; Gregory et al. 1963) of gear teeth in mesh. This chapter reports on the study of the load-sharing ratio of gears in mesh. In the spur involute teeth gears being studied, the load was transmitted by one and two pairs of teeth alternately. The torsional stiffness of the two spur gears in mesh varied within the meshing cycle as the number and position of teeth in mesh changed from two to one tooth in contact. In general, the torsional stiffness decreased as the meshing of the teeth changed from two to one in contact. If the gears were absolutely rigid, devoid of all inaccuracies and changes in meshing geometry were

ignored, the tooth load in the zone of the double tooth contact would be half that of the single tooth contact. However, in reality the teeth become deformed under the influence of the teeth bending and shear stresses, and the tooth flanks become flattened at the points of contact as the mesh geometry changes, and these factors alter the load variation along the path of contact. Furthermore, every gear contains surface finishing and pitching errors, which alter the load variation yet again. Since the teeth are comparatively stiff, even small errors have a notable influence. The effect of the elastic tooth deformation can be shock loading. In order to avoid shock loading as the gear teeth move into and out of mesh, the tooth flanks are generally tip relieved. The tip relief is normally designed so that as the tooth passes through the mesh zone, the load increases uniformly and then reduces back to zero again.

7.2 Analytical Model of Load Sharing Ratio

The development of the static transmission error model of gears in mesh can be used to determine the load sharing ratio throughout the mesh cycle. Consider the two identical spur gears in mesh, as shown in Figure 7.2.1(a), where two gears are in mesh at the start of the double tooth pair contact zone. As shown, two pair of teeth are in the double contact zone AB and DE, and one pair of teeth are in the single contact zone BD. The distance AD and BE corresponds to the transverse base pitch of the gears. Point A indicates the initial contact where the addendum circle of the output gear intersects the line of action. For involute gears the line of action is in the common tangent line to the base circles. When the first tooth pair contacts at point A, between the tooth tip of the output gear and the root of input gear, a second tooth pair is already in contact at point D. As the gear rotates, the point of contact will move along the line of action APE. When the first tooth pair reaches point B, the second tooth pair disengages at point E leaving only the first tooth pair in the single contact zone. When the first tooth pair rotates to point D the next tooth pair begins engagement at point A, starting another tooth mesh cycle.

The meaning of load sharing ratio in this chapter is the ratio between the shared force of one meshing tooth pair and the sum of the force contributions of each meshing tooth pair. All normal contact forces considered here are in the direction of the path of contact, as shown in force diagrams of Figure 7.2.1(b).

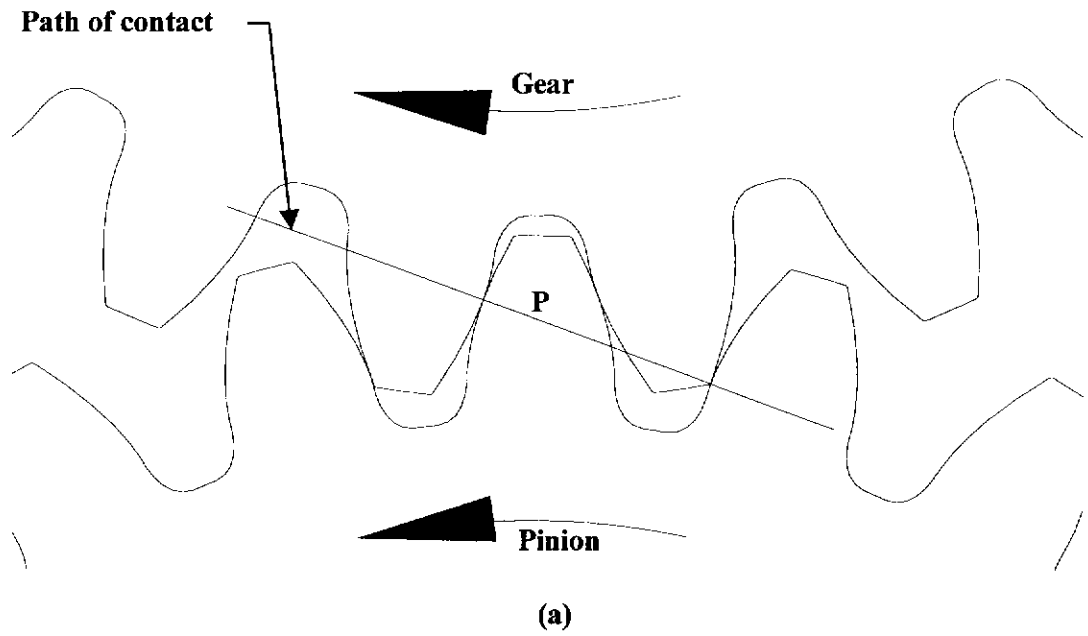

(a)

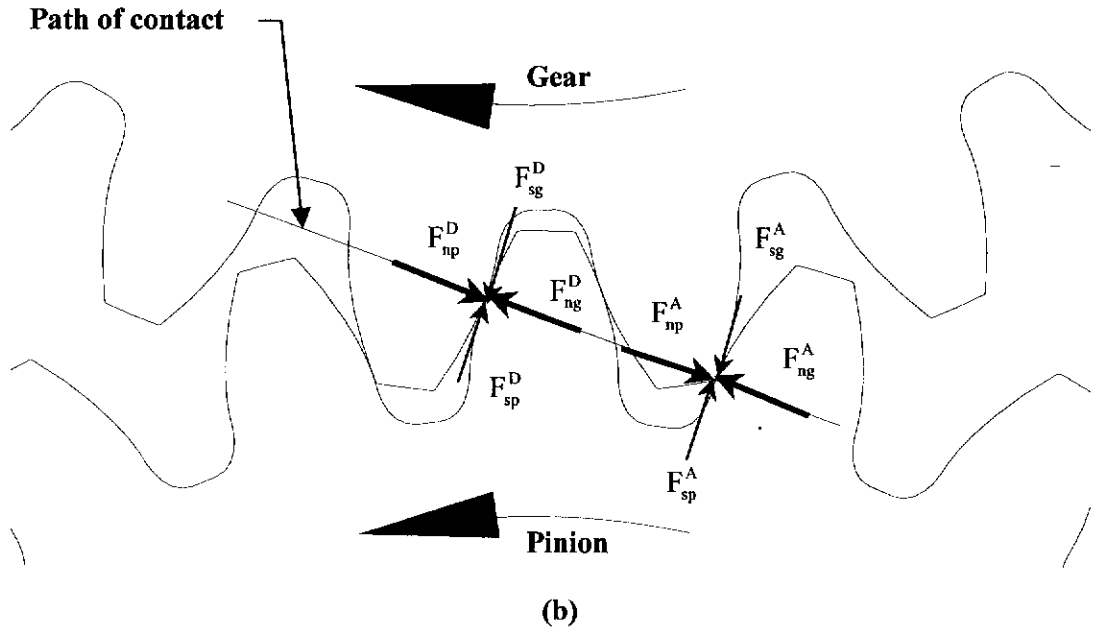

(b)

Figure 7.2.1. (a) Start of meshing position for the double pair contact zone (b) forces diagram.

In order to simplify the complexity of the problem, the load sharing compatibility condition is based on the fact that the sum of the force contributions of each meshing

tooth pair must equal the total applied force. Considering the two contact pairs at A and D as shown in Figure 7.2.1(b), the force will then be given by,

for the pinion,

$$F_{tot,np}^{A,D} = F_{np}^{A} + F_{np}^{D}, \tag{7.2.1}$$

and for the gear,

$$F_{tot,ng}^{A,D} = F_{ng}^{A} + F_{ng}^{D}, \tag{7.2.2}$$

where F_{np}^{A}, F_{np}^{D}, F_{ng}^{A}, F_{ng}^{D} denote the normal forces as a part of the total normal applied forces $F_{tot,np}^{A,D}$, and $F_{tot,ng}^{A,D}$, at the contact points A and D of the pinion and gear respectively. While F_{sp}^{A}, F_{sp}^{D}, F_{sg}^{A}, F_{sg}^{D} as shown in Figure 7.2.1(b) denote the friction forces at the contact points A and D of the pinion and gear respectively. The normal force equilibrium condition at each tooth pair in contact gives $F_{np}^{A} = F_{ng}^{A}$ and $F_{np}^{D} = F_{ng}^{D}$ at the contact points A and D of the pinion and gear respectively.

The load sharing ratio between the gear teeth is dependent on the tooth torsional mesh stiffness at each particular contact position A and D. Furthermore the load sharing compatibility condition arises from the fact that the pinion and gear body rotation, caused by the displacement of any tooth under load, is assumed to be the same for all simultaneously meshing tooth pairs (see section 6.2). This includes the effects of tooth bending deflection, shearing displacement and contact deformation. The resultant load sharing ratio for the gear pair at A and the gear pair at D is then given by,

for the pinion,

$$L_{np}^{A} = \frac{F_{np}^{A}}{F_{tot,np}^{A,D}}, \tag{7.2.3}$$

$$L_{np}^{D} = \frac{F_{np}^{D}}{F_{tot,np}^{A,D}}, \tag{7.2.4}$$

and

$$L_{np}^{A} + L_{np}^{D} = \frac{F_{np}^{A}}{F_{tot,np}^{A,D}} + \frac{F_{np}^{D}}{F_{tot,np}^{A,D}} = 1.0. \tag{7.2.5}$$

and for the gear, this gives,

$$L_{ng}^{A} = \frac{F_{ng}^{A}}{F_{tot,ng}^{A,D}}, \tag{7.2.6}$$

$$L_{ng}^{D} = \frac{F_{ng}^{D}}{F_{tot,ng}^{A,D}}, \tag{7.2.7}$$

and

$$L_{ng}^{A} + L_{ng}^{D} = \frac{F_{ng}^{A}}{F_{tot,ng}^{A,D}} + \frac{F_{ng}^{D}}{F_{tot,ng}^{A,D}} = 1.0, \tag{7.2.8}$$

where L_{np}^{A}, L_{np}^{D}, L_{ng}^{A}, L_{ng}^{D} are the corresponding load sharing ratios.

7.3 FINITE ELEMENT MODEL OF LOAD SHARING RATIO

The finite element load sharing ratio model of spur gears in mesh is based upon the same analytical model of the combined torsional mesh stiffness and the static transmission error, as developed in chapter 5 and chapter 6. The gear arrangement is similar to that which has been used in an experimental investigation with a ratio of 1:1, see appendix F (Sirichai et al. 1996), the major parameters of which are shown in Table 5.2.1. The procedural steps involved are essentially the same as for the model of the static transmission error, except that a processor solution is required to calculate the load sharing ratio. The flow chart outline and step-by-step description are described in section 7.6. A customised batch file program written in the ANSYS Parametric Design Language was used to generate the load sharing ratio finite

element model of the gears in mesh, as detailed in appendix D for the uncracked gear and appendix E for the cracked gear.

The load sharing ratio of gears in mesh at particular meshing positions throughout the mesh cycle was generated by rotating both solid gears, then creating a finite element model in that particular position. In the postprocessor solution, the load sharing ratio of each contact tooth in mesh, $F_{np}^{A,D}$, was obtained from the FEA model by introducing a prescribed torque load to the master coupled nodes of the pinion hub, while restraining all the nodes of the gear hub. Finally, the computed value of the load sharing ratio, $F_{np}^{A,D}$, at each particular meshing position was used to compute the full meshing cycle of the load sharing ratio, L_{np}. A large number of finite element models at different meshing positions, under different constant applied torques of 38.1, 76.2, 114.3, and 152.4 N.m, were undertaken for this investigation.

7.4 The Load Sharing Ratio of Undamaged Gears

The variable torsional mesh stiffness of the mating gears results in a varying load share cycle on the teeth of the gears. The load share ratio is dependent largely upon the effective torsional mesh stiffness of the revolving gears and the assumed load sharing compatibility condition that the pinion and gear body rotation, caused by the displacement of any tooth under load, must be the same for all simultaneously meshing tooth pairs.

The load sharing ratio result of the pinion teeth at particular meshing positions under different constant applied torques of 38.1, 76.2, 114.3, and 152.4 N.m, were obtained using FEA and computed for the full meshing cycle as shown in Figure 7.4.1.

The variation of load sharing ratio along the path of contact shown in Figure 7.4.1 is plotted against the travel of the engaged contact point, from right to left through one completed meshing cycle. The region of unit load sharing ratio implies that a single tooth pair carries the whole load, in the interval between B through D as expected.

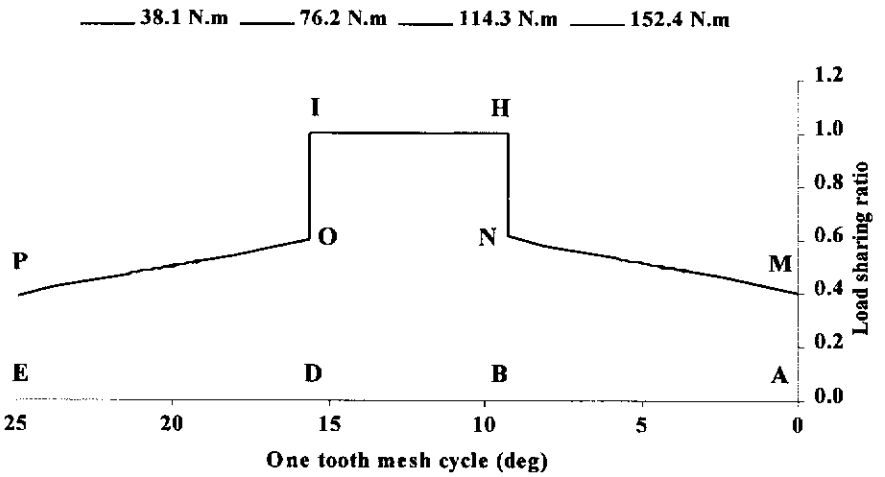

Figure 7.4.1. Variation of load sharing ratio along the path of contact for the undamaged pinion tooth.

The above load sharing ratio result is similar to other published work (Chabert et al. 1974; Kuang and Yang 1992), where shared loads between tooth pairs in mesh are not equally borne while two pairs of teeth are brought into contact, but rather the loads vary throughout the double pair contact zone. As one tooth pair increases its load share, the other tooth pair decreases load share linearly and vice-versa, etc. Furthermore, within the elastic range, the load share ratio has been shown to be almost independent of the amount of applied torque. As shown in Figure 7.4.1 the load sharing ratio result under different constant applied torques of 38.1 to 152.4 N.m, were collinear.

7.5 THE LOAD SHARING RATIO WITH/WITHOUT A CRACKED PINION TOOTH

A finite element model of the spur gears with the pinion having a single through thickness crack of length 5 mm in the fillet region, was also developed for the investigation. The crack was assumed to have been initiated at the point of the highest fillet stress. The same procedure, as outlined in section 7.4, was followed for the cracked pinion model, although the computed value of the combined normal contact stiffness of the cracked pinion was used in the FE model. The result of the load sharing ratio of the cracked pinion tooth for the entire meshing cycle under the

different applied torques of 38.1, 76.2, 114.3, and 152.4 N.m, were obtained as shown in Figure 7.5.1. The load sharing ratio result is similar to that shown in Figure 7.4.1 for the uncracked pinion, which varied throughout the double pair contact zone. Again, within the elastic range the results are almost independent of the amount of applied torque between 38.1 to 152.4 N.m, and were collinear.

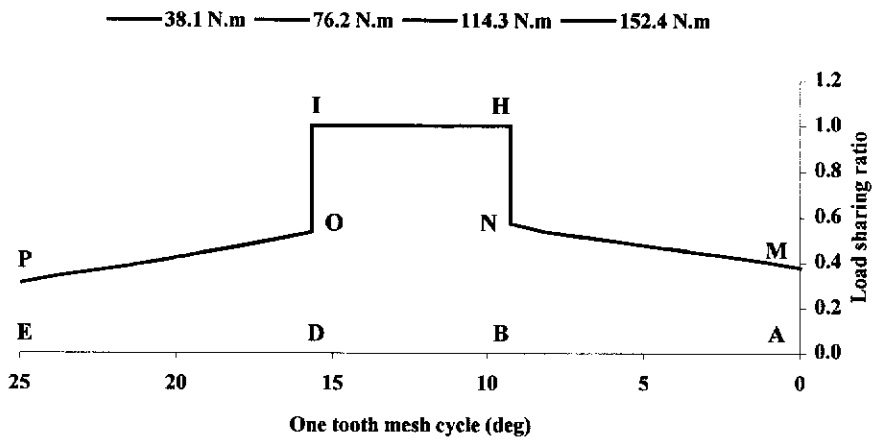

Figure 7.5.1. Variation of load sharing ratio along the path of contact for the cracked pinion tooth.

The comparison of the load sharing ratio results along the path of contact of the uncracked/cracked pinion tooth under constant applied torque of 76.2 N.m are shown in Figure 7.5.2. As expected, the load sharing ratio for the pinion with the cracked tooth, 76.2 N.m (C5), is smaller than the uncracked tooth, 76.2 N.m (C0). It can be seen that the load sharing ratio for the cracked pinion starts reducing gradually from A to B. This is because along the path of contact from A to B of the double pair contact zone, the front tooth pair in contact is undamaged while the back tooth pair in contact has the cracked tooth.

These load sharing ratio results are an outcome of the load sharing compatibility condition which arises from the fact that the gear body rotation, caused by the effects of tooth bending deflection, shearing displacement and contact deformation of any tooth under load, must be the same for all simultaneously meshing tooth pairs, as discussed in section 6.2. Therefore the cracked tooth with the reduced stiffness must carry less of the load in order to meet load sharing compatibility

condition. Along the recessing path DE of the double pair contact zone, the front pair of teeth has the cracked tooth while the back pair has the undamaged teeth. The load sharing ratio of the cracked tooth is further reduced because the cracked tooth is being loaded closer to its tip, so the tooth stiffness in further reduced.

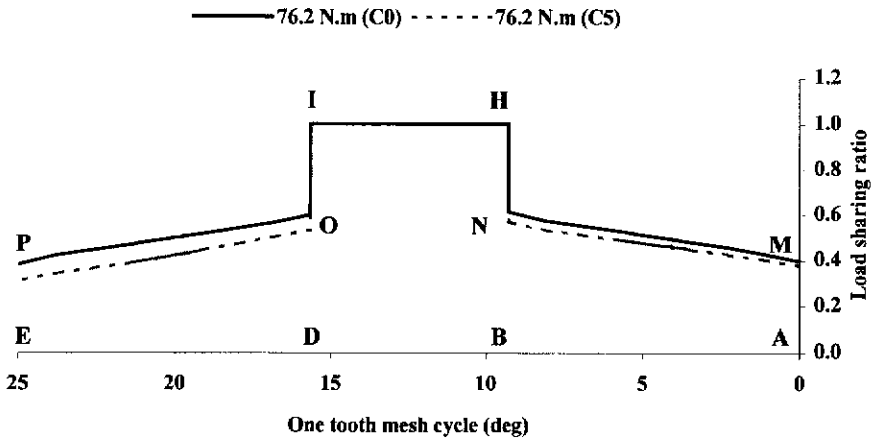

Figure 7.5.2. Comparison of load sharing ratio along the path of contact between the uncracked/cracked pinion tooth.

7.6 THE PROCEDURE FOR MODELLING THE STATIC TRANSMISSION ERROR AND THE LOAD-SHARING RATIO

The procedure for modelling the static transmission error and the load sharing ratio with variable applied torques of 38.1, 76.2, 114.3, and 152.4 N.m, is outlined in the flow chart below (Figure 7.6.1), followed by a step-by-step description. The program was written using the ANSYS Parametric Design Language and is listed in appendix D for the undamaged tooth model and in appendix E for the damaged tooth model.

The step procedures for modelling the static transmission error and the load-sharing ratio of gears in mesh with/without tooth damage are also described below. The steps involved are essentially the same as for modelling the normal contact stiffness

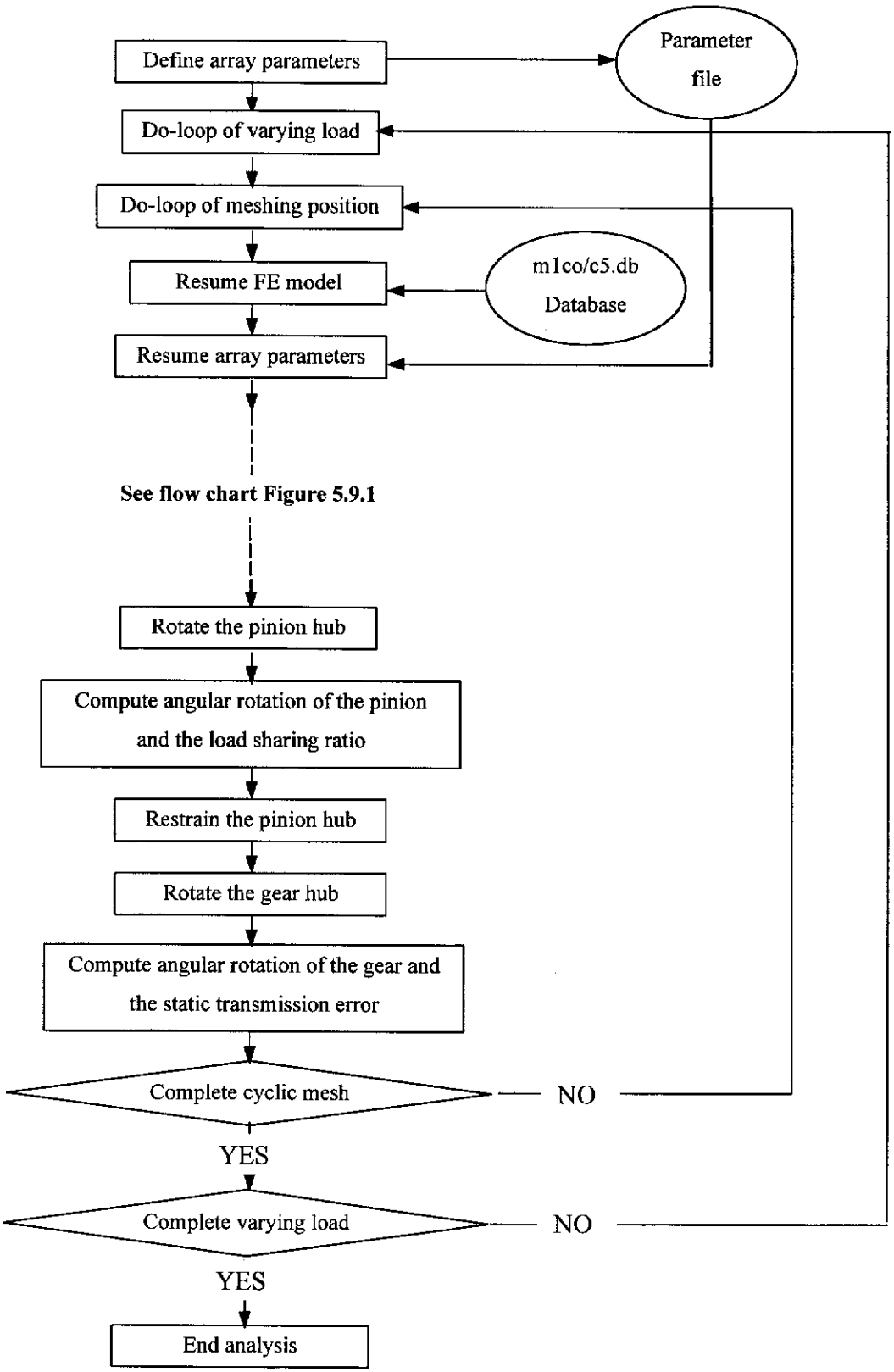

Figure 7.6.1. Procedure for modelling the static transmission error and the load sharing ratio.

of contact elements and the combined torsional mesh stiffness, except that a postprocessor solution was required to calculate the transmission error and the load sharing ratio. An additional do-loop was required to allow for a varying input load. Thus, steps 1-28 are the same as for modelling the normal contact stiffness of the contact elements and the combined torsional mesh stiffness. Steps 29 to 60 of the procedure are thus described below.

Rotate the pinion hub: (preprocessor)

29. The procedure of how to compute the transmission error and load sharing ratio is, firstly, restrain the gear hub from rotating then input a torque load into the pinion hub.
30. Activate a cylindrical coordinate system of the pinion. Restraint all DOF of the master coupled node of the gear hub and restrain all DOF in radian-axis of the master coupled node of the pinion hub. Define initial pre-defined DOF constraints of the master coupled node of the pinion hub and solve in a single iteration.
31. Delete initial pre-defined DOF constraints of the master coupled node of the pinion hub.
32. Apply a load to the pinion hub by specifying tangential forces of the master coupled node of the pinion hub.
33. Specify optimized nonlinear solution and some enhanced internal solution algorithms, such as number of substeps, etc.

Compute angular rotation of the pinion and the load sharing ratio: (postprocessor)

34. Define the last data set to be read from the result file.
35. Select a subset of potential contact nodes on the first pinion tooth contact pair.
36. Retrieve sum force values, FXP1 () and FYP1 (), of the contact nodal force in global Cartesian coordinate system and sum moment values, MZP1, due to these nodal forces.
37. Select a subset of potential contact nodes on the second pinion tooth contact pair.
38. Retrieve sum force values, FXP2( ) and FYP2( ), of the contact nodal force in the global Cartesian coordinate system and sum moment values, MZP2, due to these nodal forces.

39. Select a subset of potential contact nodes on the first gear tooth contact pair.
40. Retrieve sum force values, FXG1( ) and FYG1( ), of the contact nodal force in global Cartesian coordinate system and sum moment values, MZG1, due to these nodal forces.
41. Select a subset of potential contact nodes on the second gear tooth contact pair.
42. Retrieve sum force values, FXG2 () and FYG2 (), of the contact nodal force in the global Cartesian coordinate system and sum moment values, MZG2, due to these nodal forces.
43. Compute the total pinion torque.
44. Compute the total gear torque.
45. Compute the equivalent tangential force at the gear hub.
46. Retrieve the displacement of the pinion hub then compute the angular rotation of the pinion hub.

Restrain the pinion hub: (preprocessor)

47. In relation to the pinion reference frame, the angular rotation of the gear hub was generated by restraining the pinion from rotating, while the gear has an input load and the resulting angular rotation of the gear was computed.
48. Delete all DOF constraints.
49. Activate a local cylindrical coordinate system of the gear.
50. Restrain all DOF at the master coupled node of the pinion hub.

Rotate the gear hub: (preprocessor)

51. Define initial pre-defined DOF constraints at the master coupled node of the gear hub and solve in a single iteration.
52. Delete initial pre-defined DOF constraints at the master coupled node of the gear hub.
53. Define equivalent tangential force at master coupled node of the gear hub.
54. Specify optimized nonlinear solution and some enhanced internal solution algorithms, such as number of substeps, etc.

Compute angular rotation of the gear and the static transmission error: (postprocessor)

55. Define the last data set to be read from the result file.

56. Retrieve a displacement value of the gear hub, UYG.
57. Compute angular rotation of the gear hub, ANGG( ).
58. Compute the transmission error at each particular meshing position, TE( ).

Complete cyclic mesh:

59. End a do-loop when each cyclic mesh is completed and start the variable load loop.

Complete variable load:

60. End a do-loop when the variable load loop is completed and exit the program.

7.7 CONCLUSION

In spur gears, the load is transmitted by one pair and two pairs of teeth alternately. Figure 7.7.1 shows the tooth load sharing ratio along the path of contact, MNHIOP. Two pairs of teeth are in contact in the zones AB and DE and one pair only throughout the zone BD. If the gears were absolutely rigid and devoid of all inaccuracies, the tooth load in the zone of the double tooth contact would be exactly half of that in the single tooth contact zone. This load variation is represented by the curve AFGHIKLE.

However, in reality the teeth become deformed under the influence of the teeth bending and shear stresses, and the tooth flanks become flattened at the points of contact, and these factors alter the load variation along the path of contact, according to the curve AMNHIOPE.

The effect of the elastic tooth deformation can be shock loading. In order to avoid shock loading as the gear teeth move into and out of the mesh, the tooth flanks are normally tip relieved. The tip relief being designed so that as the tooth passes through the mesh zone, the load increases uniformly and then reduces back to zero again.

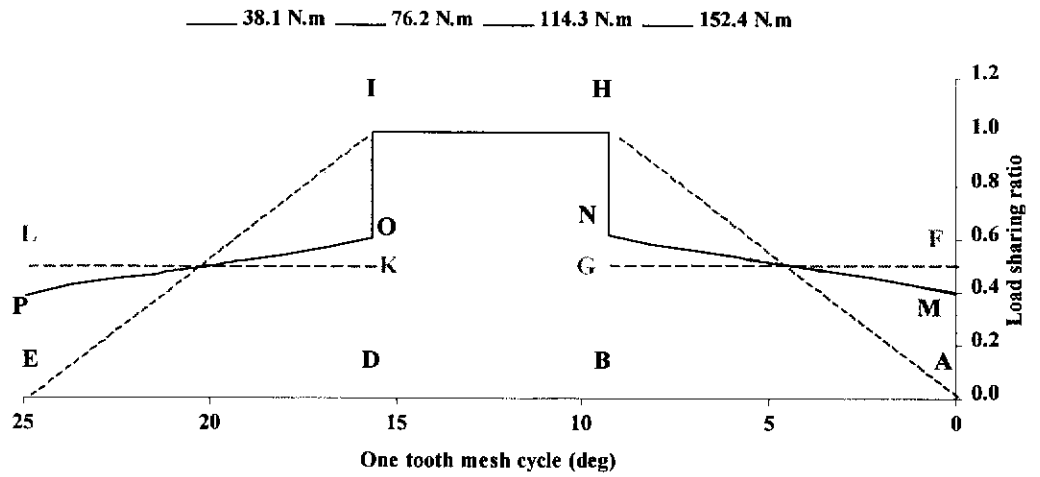

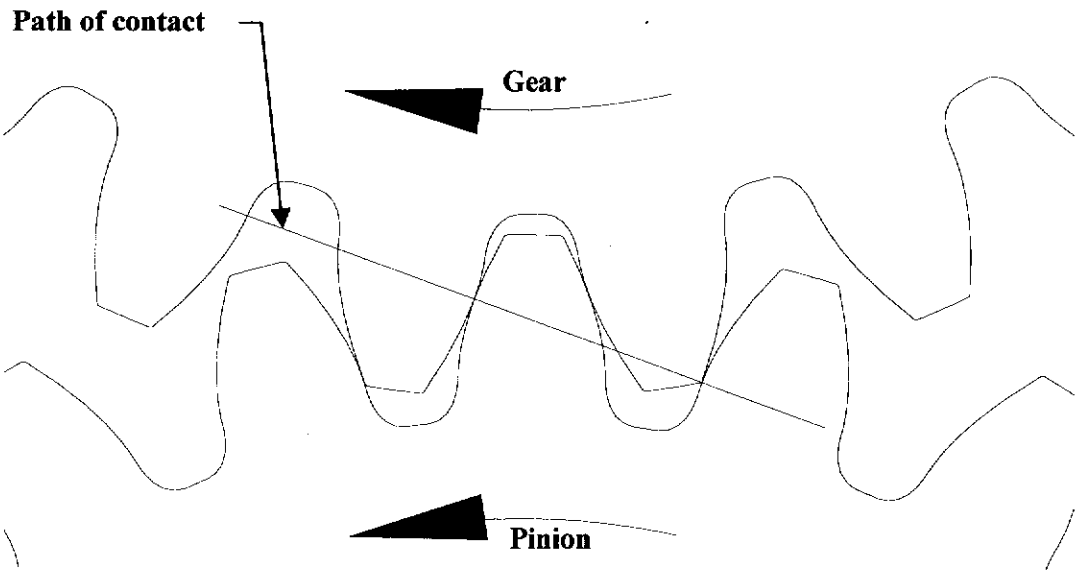

Figure 7.7.1. Load variation along the path of contact.

The load sharing diagram in Figure 7.7.1 shows that the abrupt load sharing changes not only take place at the entry and exit points M and P, but also at the points N and O, where the load share changes between two teeth to one tooth, and conversely, from one tooth to two teeth. These sudden changes in load share can lead to the generation of vibration and noise. This phenomena also occurs in the static transmission error as shown in Figure 6.4.1 where abrupt changes of T.E. have been shown to take place both when gear teeth move into and out of mesh and also

between the double pair contact to single pair contact and vice-versa. The tip relief must be so designed that the load increases as uniformly as possible, and gradually sinks back to zero again. The desired theoretical load variation is shown in Figure 7.7.1, as the dotted line AHIE.

CHAPTER 8

CONCLUSIONS AND FUTURE WORK

8.1 General Conclusions

The main aims of this thesis have been to use a numerical approach to develop theoretical models to predict the effect of gear tooth damage on torsional mesh stiffness, transmitted load sharing ratio, and transmission error. The main focuses of the study have been on the development of efficient and reliable solution techniques as well as on the understanding of the penalty parameter of the contact element at each contact position through the mesh cycle. The numerical approach enabled the development of a software program based on the ANSYS FEA package to predict the effect of gear tooth damage on torsional mesh stiffness, transmission error, and the load sharing ratio of the gear mesh, provided that the tooth damage was outside of the contact zone.

(i) Penalty Parameter of Contact Element

A new strategy for choosing an appropriate value of the normal contact stiffness of the contact element has been presented. The results gave a clear picture of what occurs when using different values of the normal contact stiffness of different

contact elements which should prove to be particularly useful for all kinds of contact elements and contact problems.

(ii) Torsional Mesh Stiffness

A strategy for obtaining the torsional mesh stiffness of gears in mesh was developed by introducing a prescribed rotation of the input gear hub, while restraining the output gear hub and vice-versa. The resulting combined torsional mesh stiffness of the gear mesh at particular meshing positions was obtained by calculating the gradient of the linear relationship between torque and angular displacement. Both gears were then rotated to a new meshing position and in this manner the torsional mesh stiffness of the input and the output gear over the entire meshing cycle was obtained. The resulting combined torsional mesh stiffness of the gears in mesh was shown to dramatically change throughout the meshing cycle, increasing and decreasing as the number of teeth in mesh changes from two to one and then back to two teeth in contact.

(iii)Transmission Error

This thesis has presented a general formulation for obtaining the transmission error which takes into account the different angular rotations of the gear blank caused by tooth bending, shearing and contact deformation as calculated by FEA through the use of non-linear contact elements. The geometrical effects of runout, profile and pitch errors have not been included in this analysis. The presence of a single cracked tooth was shown to have changed the results of the transmission error. When a single cracked tooth is in mesh its effect can be clearly seen, with the largest effect occurring as the single tooth contact changes to the double tooth contact. In the double tooth pair contact, the effect was less because other undamaged tooth pairs share the torque load. These results provide valuable insight into the effect a single tooth crack has on the transmission error. The thesis also presented the effect of four different values of input torque on the spur gear transmission error, the result of which is in general agreement with measured gear transmission error as published by many well known research workers (Gregory et al. 1963; Tordian and Geraldin 1967; Tordion and Gerardin 1967; Hayashi and Hayashi 1981; Houser and

Blankenship 1989; Rebbechi et al. 1992; Vinayak and Houser 1992; Bard et al. 1994; Barnett and Yildrim 1994; Munro and Yildirim 1994; Velex et al. 1995; Houser et al. 1996; Sweeney and Randall 1996).

(iv)Load Sharing Ratio

The results of load sharing ratio shows that abrupt changes take place at both the entry and exit points of the single and double tooth pairs in contact. However the load sharing ratio within the elastic range has been shown to change an insignificant amount when the input torque varies. The presence of a single cracked tooth has changed the results of the load sharing ratio, in much the same way as it changed the transmission error results.

8.2 THESIS CONTRIBUTION

The main contribution of the thesis work presented here can be summarised as follows:

- Verification of contact element stiffness of cylinders in contact, in comparison with Hertzian theory.

- The development of a new numerical method for modelling the whole gear body rotation in mesh including frictional contact.

- The development of a strategy to determine an appropriate value of the penalty parameter of the contact elements as the gears rotate through the mesh cycle.

- The development of a finite element method program written in ANSYS Parametric Design Language for defining the torsional mesh stiffness of the gear mesh with and without the presence of a cracked tooth.

- The development of a finite element method program written in ANSYS Parametric Design Language for modelling the static transmission error of spur gears in mesh with and without a cracked tooth.

- The development of a finite element method program written in ANSYS Parametric Design Language for defining the load-sharing ratio of the gear mesh, with and without a cracked tooth.

8.3 FUTURE WORK

The following areas are noted as being worthy of further research, in the light of this thesis.

- Further numerical method investigation and study should be conducted on gears in mesh under dynamic situations with and without cracked teeth, surface pitting and wear using the finite element method.

- Further numerical method investigation and study should be conducted on the transmission error for all types of gears in mesh with and without tooth damage. This could include helical, spiral bevel and other gear tooth forms.

- Further numerical method investigation and study should be conducted on a whole gearbox with all elements in the system including the gear casing with and without tooth damage.

- Further testing and analysis should be conducted on the effect of gear tooth profile modifications, with and without artificial tooth cracks.

REFERENCES

Abersek, B., Flasker, J. and Balic, J. (1994). "Theoretical Model for Fatigue Crack Propagation on Gears." *3rd International Conference on Computer-Aided Assessment and Central Localized Damage '94*, pp 63-70.

Aguilera, E. (1995). "The Torsional Stiffness of Two gears Whilst in Mesh," B. Eng. Project Report, Curtin University of Technology, Perth.

Aida, T. (1968). "Fundamental Research on Gear Noise and Vibration I." *Transaction of the Japanese Society of Mechanical Engineers*, **34**, pp 2226-2264.

Aida, T. (1969). "Fundamental Research on Gear Noise and Vibration II." *Transaction of the Japanese Society of Mechanical Engineers*, **35**, pp 2113-2119.

Aida, T., Sato, S. and Fukuma, H. (1967). "Properties of Gear Noise and Its Generating Mechanism." *Proceedings of the Japanese Society of Mechanical Engineers Semi-International Gearing Symposium*, pp 151-160.

Alattass, M. et al. (1994). "Experimental Study of Fault Influence on Vibration and Noise Measurements in a Gear Transmission Mechanism." *International Gearing Conference*, UK, pp 469-474.

andersson, M. (1996). "Stress Distribution and Crack Initiation for an Elastic Contact Including Friction." *International Journal of Solids and Structures*, **33**(25), pp 3673-3696.

ANSYS. (1995). *User's Manual Elements*, ANSYS, Inc.

ANSYS. (1995). *User's Manual Procedures*, ANSYS, Inc.

ANSYS. (1995). *User's Manual Theory*, ANSYS, Inc.

ANSYS. (1997). *Structural Analysis Guide*, ANSYS, Inc.

Arikan, M.A.S. (1991). "Dynamic Load and Contact Stress Analysis of Spur Gears." *Advance in Design Automation*, USA, pp 85-91.

Arikan, M.A.S. and Kaftanoglu, B. (1989). "Dynamic Load and Root Stress Analysis of Spur Gears." *Annal of the CIRP*, **38**, pp 171-174.

Arikan, M.A.S. and Tamar, M. (1992). "Tooth Contact and 3-D Stress Analysis of Involute Helical Gears." *6th International Power Transmission and Gearing Conference*, pp 461-468.

Arya, S.K. and Hegemier, G.A. (1982). "Finite Element Method for Interface Problems." *J. of the Stru. Div. ASCE*, **108**, pp 327-42.

AUTODESK. (1995). *AutoCad Command Reference: Release 13.0*, Elan Computer Group, Inc.

AUTODESK. (1995). *AutoCad User's Guide: Release 13.0*, Elan Computer Group, Inc.

AUTODESK. (1997). *AutoCAD: Release 14.0*, CAD Software, AUTODESK, USA.

Bahgat, B.M., Osman, M.O.M. and Sankar, T.S. (1981). "On the Dynamic Gear Tooth Loading as Effected by Bearing Clearances in High Speed Machinery." *Journal of Mechanical Design*, pp 81-DET-112.

Bahgat, B.M., Osman, M.O.M. and Sankar, T.S. (1983). "On the Spur-Gear Dynamic Tooth-Load under Consideration of System Elasticity and Tooth Involute Profile." *Journal of Mechanisms, Transmissions, and Automation in Design*, **105**(September), pp 302-309.

Bard, C., Remond, D. and Play, D. (1994). "New Transmission Error Measurement for Heavy Load Gears." *International Gearing Conference*, UK, pp 393-400.

Baret, C., Coccolo, G. and Raffa, F.A. (1994). "3d Stress Analysis of Spur Gears with Profile Errors and Modifications Using P-Fem Models." *International Gearing Conference*, UK, pp 1.

Barnett, O.W. and Yildrim, N. (1994). "Loaded Transmission Error Predictions Using a Computer Model and Its Verification." *International Gearing Conference*, UK, pp 57-62.

Baron, E., Favre, B. and Mairesse, P. (1988). "Analysis of Relation between Gear Noise and Transmission Error." *Proc. Internoise, '88*, pp 611-614.

Bathe, K.J. (1982). *Finite Element Procedures in Engineering Analysis*, Prentice-Hall, New Jersey.

Bathe, K.J. and Chaudhary, A. (1985). "A Solution Method for Planar and Axisymmetric Contact Problems." *International Journal for Numerical Methods in Engineering*, **21**, pp 65-88.

Blarasin, A., Guagliano, M. and Vergani, L. (1997). "Fatigue Crack Growth Prediction in Specimens Similar to Spur Gear Teeth." *Fatigue Fract. Engng. Mater Struct.*, **20**(8), pp 1171-1182.

Blazakis, A. and Houser, D.R. (1994). "Finite Element and Experimental Analysis of the Effect of Thin-Rimmed Gear Geometry on Spur Gear Fillet Stresses." *International Gearing Conference*, UK, pp 41-46.

Bollinger, J.G. and Harker, R.J. (1967). "Instability Potential of High Speed Gearing." *The Journal of the Industrial Mathematics Society*, **17**, pp 39-55.

Boresi, P. and Sidebottom, O.M. (1985). *Advanced Mechanics of Materials*, John Wiley & Sons, Inc, New York.

Brie, D. et al. (1997). "Gear Crack Detection by Adaptive Amplitude and Phase Demodulation." *Mechanical Systems and Signal Processing*, **11**(1), pp 149-167.

Brousseau, J., Gosselin, C. and Cloutier, L. (1994). "Reference Point, Mesh Stiffness, and Gear Dynamic Models." *1994 International Gearing Conference*, University of Newcastle, UK, pp 139-144.

Chabert, G., Tran, T.D. and Mathis, R. (1974). "An Evaluation of Stresses and Deflection of Spur Gear Teeth under Strain." *Journal of Engineering for Industry*, **February 1974**(February), pp 85-93.

Chan, S.K. and Tuba, I.S. (1971a). "A Finite Element Method for Contact problems for Solid Bodies-part 1. Theory and Validation." *International journal of mechanical sciences.*, **13**, pp 615-25.

Chan, S.K. and Tuba, I.S. (1971b). "A Finite Element Method for Contact problems for Solid Bodies-part 2. Application to Turbine Blade Fastenings." *International journal of mechanical sciences.*, **13**, pp 627-39.

Chaudhary, A. and Bathe, K.J. (1986). "A Solution Method for Static and Dynamic Analysis of Three-Dimensional Contact Problems with Friction." *Computers and Structures*, **24**(6), pp 855-73.

Chen, C.-H., Wang, Y. and Colbourne, J.R. (1992). "A General formula for Determining the Normal to the Path of Contact in Parallel-Axis Gearing." *6th International Power Transmission and Gearing Conference*, pp 529-534.

Chen, J.S., Litvin, F.L. and Shabana, A.A. (1994). "Computerized Simulation of Meshing and Contact of Loaded Gear Drives." *International Gearing Conference*, UK, pp 161-166.

Chen, W.-H. and Pwu, T. (1986). "Finite Element Analysis of Elastodynamic Sliding Contact Problems with Friction." *Computers and Structures*, **22**(6), pp 925-38.

Cheng, Y. and Lim, T.C. (1998). "Dynamic Analysis of High Speed Hypoid Gears with Emphasis on Automotive Axle Noise Problem." *1998 ASME Design Engineering Technical Conference*, Atlanta, GA, USA, pp DETC98/PTG-5784.

Childs, D.B., et al. (1980). "Estimation of Seal Bearing Stiffness and Damping Parameters from Experimental Data." *Second International Conference: Vibration in Rotating Machinery*, IME, pp 175-179.

Choy, F.K. et al. (1996). "Vibration Signature Analysis of a Faulted Gear Transmission System." *Journal of Propulsion and Power*, **12**(2), pp 289-295.

Choy, F.K. and Polyshchuk, V. (1995). "Dynamic Analysis and Experimental Correlation of a Gear Transmission System." *International Journal of Turbo and Jet Engines*, **12**, pp 269-281.

Choy, F.K. et al. (1996). "Analysis of the Effects of Surface Pitting and Wear on the Vibrations of a Gear Transmission System." *Tribology International*, **29**(1), pp 77-83.

Choy, F.K. et al. (1993). "Modal Simulation of Gear Box Vibration with Experimental Correlation." *Journal of Propulsion and Power*, **9**(2), pp 301-306.

Choy, F.K. et al. (1992). "Modal Analysis of Multistage Gear Systems Coupled with Gearbox Vibrations." *Journal of Mechanical Design*, **114**(September), pp 486-496.

Choy, F.K. et al. (1991). "Effect of Gear Box Vibration and Mass Imbalance on the Dynamics of Multistage Gear Transmission." *Journal of Vibration and Acoustics*, **113**, pp 333-344.

Compos, L.T., Oden, J.T. and Kikuchi, N. (1982). "A Numerical Analysis of a Class of Contact Problem with Friction in Elastostatics." *Computer Methods in Applied Mechanics and Engineering*, **34**, pp 821-845.

Cook, R.D. (1995). *Finite Element Modeling for Stress Analysis*, John Wiley & Sons, New York.

Cook, R.D., Malkus, D.S. and Plesha, M.E. (1989). *Concepts and Applications of Finite Element Analysis*, John Wiley and Sons, New York.

Daly, K.J. and Smith, J.D. (1979). "Using Gratings in Driveline Noise Problems." *Proc., Noise & Vib. of Engineering and Transmissions*, Cranfield, pp 15-20.

Daniewicz, S.R., Collins, J.A. and Houser, D.R. (1994). "The Stress Intensity Factor and Stiffness for a Cracked Spur Gear Tooth." *Journal of Mechanical Design*, **116**(September), pp 697-700.

Ding, Y., Jones, R. and Kuhnell, B. (1995). "Numerical Analysis of Subsurface Crack Failure Beneath the Pitch Line of a Gear Tooth During Engagement." *Wear*, **185**, pp 141-149.

Donno, M.D. and Litvin, F.L. (1998). "Computerized Design, Generation and Simulation of Meshing of a Spiroid Worm-Gear Drive with Double-Crowned Worm." *1998 ASME Design Engineering Technical Conference*, Atlanta, GA, USA, pp DETC98/PTG-5779.

Dooner, D.B. and Seireg, A.A. (1998). "Concurrent Engineering of Toothed Bodies for Generalized Function Transmission." *1998 ASME Design Engineering Technical Conference*, Atlanta, GA, USA, pp DETC98/PTG-5780.

Doudoumis, I.N. and Mitsopoulou, E.N. (1988). "On the Evolution of the Unilateral Contact Frictional Problem for General Static Loading Conditions." *Computers and Structures*, **30**(5), pp 1111-26.

Drago, R.J., Lenski, J.W. and Royal, A. (1979). "An Analytical Approach to the Source Reduction of Noise and Vibration in Highly Loaded Mechanical Power Transmission Systems." *Proceeding of the Fifth World Congress on Theory of Machines and Mechanisms*, ASM, pp 910-913.

Du, S. (1997). "Dynamic Modelling and Simulation of Gear Transmission Error for Gearbox Vibration Analysis." Ph.D. Thesis 1997, University of New South Wales, Sydney, Australia.

Du, S., Randall, R.B. and Kelly, D.W. (1998). "Modelling of Spur Gear Mesh Stiffness and Static Transmission Error." *Proc. Instn Mech. Engrs*, **212**(Part C), pp 287-297.

Dudley, D.W. et al. (1995). *Gear Motor Handbook*, Springer-Verlag Berlin Heidelberg, Neyork.

Elkholdy, A.H., Elsharkawy, A.A. and S., Y.A. (1998). "Effect of Meshing Tooth Stiffness and Manufacturing Error on the Analysis of Straight Bevel Gears." *Mechanics of Structures and Machines.*, **21**(1), pp 41-.

El-Saeidy Fawzi, M.A. (1991). "Effect of Tooth Backlash and Ball Bearing Deadband Clearance on Vibration Spectrum in Spur Gear Boxes." *Journal of Acoustical Society of America*, **89**(6), pp 2766-2773.

Feng, P.-H. et al. (1998). "Determination of Principal Curvatures and Contact Ellipse for Profile Crowned." *1998 ASME Design Engineering Technical Conference*, Atlanta, GA, USA, pp DETC98/PTG-5778.

Flasker, J., Glodez, S. and Pehan, S. (1995). "Influence of Contact Area on Service Life of Gears with Crack in Tooth Root." *Communications in Numerical Methods in Engineering*, **11**, pp 49-58.

Forrester, B.D. (1996). "Advance Vibration Analysis Techniques for Fault Detection and Diagnosis in Geared Transmission System," Ph.D. Thesis 1996, Swinburne University of Technology, Melbourne, Australia.

Fredriksson, B. (1976a). "On Elastostatic Contact Problems with Friction," Linkoping University, Linkoping.

Fredriksson, B. (1976b). "Finite Element Solution of Surface Nonlinearities in Structural Mechanics with Special Emphasis to Contact and Fracture Mechanics Problems." *Computers and Structures*, **6**, pp 281-90.

Fredriksson, B. (1984). "Numerical Solution to Contact Friction and Crack Problems with Applications." *Engineering Computations*, **1**, pp 133-143.

Fujio, H. et al. (1992). "Laser Holographic Measurement of Tooth Flank form of Cylindrical Involute Gear: Part 2- for Helical Gear Tooth." *6th International Power Transmission and Gearing Conference, DE-Vol. 43-1*, pp 185-192.

Gargiulo, E.P.J. (1980). "A Simple Way to Estimate Bearing Stiffness." *Machine Design*, pp 107-110.

Gladwell, G.M.L. (1980). *Contact Problems in the Classical Theory of Elasticity*, Alphen aan den Rijn, The netherlands.

Glodez, S., Pehan, S. and Flasker, J. (1998). "Experimental results of the fatigue crack growth in a gear tooth root." *International. Journal. Fatigue*, **20**(9), pp 669.

Goldsmith, W. (1960). *Impact-the Theory and Physical Behaviour of Colliding Solids*, Edward Arnold, London.

Goodman, L.E. (1954). "Contact Stress Analysis of Normally Loaded Rough Spheres." *Journal of Applied Mechanics*, **29**, pp 515-522.

Goodman, L.E. and Keer, L.M. (1965). "The Contact Stress Problem for an Elastic Sphere Indenting an Elastic Cavity." *International Journal of Solids and Structures*, pp 407-422.

Gosselin, C., Cloutier, L. and Nguyen, Q.D. (1995). "A General formulation for the Calculation of the Load Sharing and Transmission Error under Load of Spiral Bevel and Hypoid Gears." *Mech. Mach. Theory*, **30**(3), pp 433-450.

Gosselin, C., Gagnon, P. and Cloutier, L. (1998). "Accurate Tooth Stiffness of Spiral Bevel Gear Teeth by the Finite Strip Method." *Journal of Mechanical Design*, **120**(4), pp 599.

Gosselin, C. et al. (1994). "A Review of the Current Contact Stress and Deformation formulations Compared to Finite Element Analysis." *International Gearing Conference*, UK, pp 155-160.

Goudreau, G.L. and Hallquist, J.O. (1982). "Recent Developments in Large-Scale Finite Element Lagrangian Hydrocode Technology." *Computer Methods in Applied Mechanics and Engineering*, **33**, pp 725-57.

Gregory, R.W., Harris, S.L. and Munro, R.G. (1963). "Dynamic Behaviour of Spur Gears." *Proceedings of the Institute of Mechanical Engineers*, pp 207-218.

Gregory, R.W., Harris, S.L. and Munro, R.G. (1963). "A Method of Measuring Transmission Error in Spur Gear of 1:1 Ratio." *J. SCI. INSTRUM.*, **40**, pp 5-9.

Gregory, R.W., Harris, S.L. and Munro, R.G. (1963). "Torsional Motions of a Pair of Spur Gears." *Proc. I. Mech. E.*, pp 166-173.

Haber, R.B. and Abel, J.F. (1983). "Contact-Slip Analysis Using Mixed Displacements." *J. of the Eng. Mech. Div., ASCE*, **109**(2), pp 411-29.

Hallquist, J.O., Goudreau, G.L. and Benson, D.J. (1985). "Sliding Interfaces with Contact-Impact in Large-Scale Lagrangian Computations." *Computer Methods in Applied Mechanics and Engineering*, **51**, pp 107-37.

Harris, S.L. (1958). "Dynamic Loads on the Teeth of Spur Gears." *Proc. I. Mech. E.*, pp 87-112.

Hayashi, I. and Hayashi, T. (1979). "New measuring Method of a Single Flank Transmission Error of a pair of Gears." *Proc., Fifth World Congress on Theory of Machines and Mechanisms*, pp 359-362.

Hayashi, I. and Hayashi, T. (1981). "Development of the Dynamic Measurement Method of Transmission Error of a Gear Pair." *International Symposium on Gearing & Power Transmissions*, Tokyo, JAPAN, pp 491-502.

Hertz, H. (1881). "Uber die Beruhrung Fester Elastischer Korper und Uber die Harte." *Journal Fur Die Reine Und Angewandte Mathematik*, **92**, pp 156-171.

Hertz, H. (1882). *Uber die Beruhrung Fester Elastischer Korper und Uber die Harte*, Verhandlungen des Vereins zur Beforderung des Gewerbfleifses, Berlin.

Heyliger, P.R. and Reddy, J.N. (1987a). "A Mixed Computational Algorithm for Plane Elastic Contact Problems-I, formulation." *Computers and Structures*, **26**(4), pp 621-34.

Heyliger, P.R. and Reddy, J.N. (1987b). "A Mixed Computational Algorithm for Plane Elastic Contact Problems-II, Numerical Examples." *Computers and Structures*, **26**(4), pp 635-53.

Hinton, E. and Owen, D.R.J. (1977). *Finite Element Programming Academic Press.*, London.

Houser, D.R. (1990). "Research of the Ohio State University Gear Dynamics and Gear Noise Research Laboratory." *First International Conference, Gearbox Noise and Vibration, Proceeding of the Institute of Mechanical Engineers*, pp 19-26.

Houser, D.R. and Blankenship, G.W. (1989). "Methods for Measuring Gear Transmission Error under Load and At Operating Speeds." *SAE Technical Paper No. 891869*, pp 1-8.

Houser, D.R., Bolze, V.M. and Graber, J.M. (1996). "A Comparison of Predicted and Measured Dynamic and Static Transmission Error for Spur and Helical Gear Sets." *14th Intl. Modal Anal. Conf.*, USA, pp 1057-1062.

Howard, I., Sirichai, S. and Morgan, I. (1998). "A Simplified Model of the Effect of a Crack in a Spur Gear on the Resultant Gear Vibration." *Condition Monitoring and Diagnostic Engineering Management*, Tasmania, Australia, pp 397- 406.

Hughes, T.J.R. et al. (1976). "A Finite Element Method for a Class of Contact-Impact Problems." *Computer Methods in Applied Mechanics and Engineering*, **8**, pp 249-76.

Iida, H. and Tamura, A. (1984). "Couple Torsional-Flexural Vibration of a Shaft in a Geared System." *Proceeding of the Third international Conference on Vibrations in Rotating Machinery*, pp 67-72.

Iida, H. et al. (1980). "Coupled Torsional-Flexural Vibration of a Shaft in a Geared System of Rotors." *Bulletin of the JSME*, **23**(186), pp 2111-2117.

Iida, H., Tamura, A. and Yamamoto, H. (1986). "Dynamic Characteristics of a Gear Train System with Softly Supported Shafts." *Bulletin of the JSME*, **29**(252), pp 1811-1817.

Inoue, K., Townsend, D.P. and Coy, J.J. (1992). "Optimum Design of Gearbox for Low Vibration." *6th International Power Transmission and Gearing Conference*, USA, pp 497-504.

Iwatsubo, T., Arii, S. and Kawai, R. (1984). "Couple Lateral-Torsional Vibration of Rotor System Trained by Gears." *Bulletin of the JSME*, **27**(224), pp 271-277.

Iwatsubo, T., Arii, S. and Kawai, R. (1984). "The Coupled Lateral Torsional Vibration of a Geared Rotor System." *Proceeding of the Third international Conference on Vibrations in Rotating Machinery*, pp 59-66.

Johnson, A.R. and Quigley, C.J. (1989). "Frictionless Geometrically Non-Linear Contact Using Quadratic Programming." *International Journal for Numerical Methods in Engineering*, **28**, pp 127-144.

Johnson, D.C. (1962). "Modes and Frequencies of Shafts Coupled by Straight Spur Gears." *Journal of Mechanical Engineering Science*, **4**(3), pp 241-250.

Johnson, K.L. (1985). *Contact Mechanics*, Cambridge University Press.

Kahraman, A. (1993). "Effect of Axial Vibrations on the Dynamics of a Helical Gear Pair." *Journal of Vibration and Acoustics*, **115**(1), pp 33-39.

Kahraman, A. et al. (1992). "Dynamic Analysis of Geared Rotors by Finite Elements." *Journal of Mechanical Design*, **114**(September), pp 507-514.

Kahraman, A. and Singh, R. (1991). "Interaction between Time-Varying Mesh Stiffness and Clearance Non-Linearities in a Geared System." *Journal of Sound and Vibration*, **146**(1), pp 135-156.

Kahraman, A. and Singh, R. (1991). "Non-Linear Dynamics of a Geared Rotor-Bearing System with Multiple Clearances." *Journal of Sound and Vibration*, **144**(3), pp 469-506.

Kalluri, R. and Houser, D.R. (1998). "A Possible Strategy for Incorporating Edge Effects in Root Stress Estimation of Helical Gears." *1998 ASME Design Engineering Technical Conference*, Atlanta, GA, USA, pp DETC98/PTG-5796.

Kasuba, R. (1961). "An Analytical and experimental Study of Dynamic Loads on Spur Gear Teeth," Ph.D., University of Illinois.

Kasuba, R. (1971). "Dynamic Loads on Spur Gear Teeth by Analog Computation." *American Society of Mechanical Engineers*, pp 71-DE-26.

Kato, M. et al. (1994). "Evaluation of Sound Power Radiated by a Gearbox." *1994 International Gearing Conference*, University of Newcastle, UK, pp 69-74.

Kikuchi, N. and Oden, J.T. (1988). *Contact Problem in Elasticity: A Study of Variational Inequalities and Finite Element Methods.*, SIAM Publication, Philadelphia.

Kikuchi, N. and Song, Y.J. (1980). "Contact Problem Involving forces and Moments for Incompressible Linearly Elastic Materials." *Int. J. Eng. Sci.*, **39**, pp 1-22.

Kim, H.C., de Vaujany, J.P. and Play, D. (1998). "Stress Analysis of Cylindrical Webbed Spur Gears: Parametric Study." *Journal of Mechanical Design*, **120**(2), pp 349.

Kin, V. (1992). "Computerized Analysis of Gear Meshing Based on Coordinate Measurement Data." *6th International Power Transmission and Gearing Conference*, USA, pp 543-550.

Kissling, U.L. (1994). "Improving Gearbox Design by Highly Integrated Calculation Programs." *1994 International Gearing Conference*, University of Newcastle, UK, pp 221-226.

Klarbring, A. (1986a). "General Contact Boundary Condition and the Analysis of Frictional Systems." *International Journal of Solids Structures*, **22**(12), pp 1377-98.

Klarbring, A. (1986b). "A Mathematical Programming Approach to Three-Dimensional Contact Problems with Friction." *Computer Methods in Applied Mechanics and Engineering*, **58**, pp 175-200.

Klarbring, A., Mikelic, A. and Shillor, M. (1988). "Frictional Contact Problems with Normal Compliance." *Int. J. Eng. Sci.*, **26**(8), pp 811-32.

Kleiber, M. (1989). *Incremental Finite Element Modelling in Non-linear Solid mechanics*, Ellis Horwood Ltd., New York.

Kobler, H.K., Pratt, A. and Thomson, A.M. (1970). "Dynamics and Noise of Parallel Axis Gearing." *Proceedings of the Institute of Mechanical Engineers*, pp 111-121.

Kohler, H. and Regan, R. (1985). "The Derivation of Gear Transmission Error from Pitch Error Records." *Journal of Mechanical Engineering Science*, **199**(c3), pp 195-201.

Kowalczyk, P. (1994). "Finite-Deformation Interface formulation for Frictionless Contact Problems." *Communications in Numerical Methods in Engineering*, **10**, pp 879-893.

Kuang, J.H. and Yang, Y.T. (1992). "An Estimate of Mesh Stiffness and Load Sharing Ratio of a Spur Gear Pair." *6th International Power Transmission and Gearing Conference*, USA, pp 1-9.

Kubo, A. et al. (1992). "Laser Holographic Measurement of Tooth Flank form of Cylindrical Involute Gear: Part 1- Principle and Measurement of Spur Gear." *6th International Power Transmission and Gearing Conference*, pp 177-184.

Kurokawa, S., Ariura, Y. and Tachikake, K. (1994). "Gear Transmission Errors of Cylindrical Gears." *International Gearing Conference*, UK, pp 407-412.

Laschet, A. and Troeder, C. (1984). "Torsional and Flexural Vibrations in Drive Systems: A Computer Simulation." *Computers in Mechanical Engineering 3*, pp 32-43.

Lee, G.B. and Kwak, B.M. (1989). "Formulation and Implementation of Beam Contact Problems under Large Displacement by Mathematical Programming." *Computers and Structures*, **31**(3), pp 365-76.

Lee, K. (1989a). "An Accelerated Iterative Method for Contact Analysis." *International Journal for Numerical Methods in Engineering*, **28**, pp 279-93.

Lee, K. (1989b). "An Efficient Solution Method for Frictional Contact problems." *Computers and Structures*, **32**(1), pp 1-11.

Lewicki, D. et al. (1994). "Improvements in Spiral-Bevel Gears to Reduce Noise and Increase Strength." *1994 International Gearing Conference*, University of Newcastle, UK, pp 341-346.

Lim, T.C. and Singh, R. (1990). "Vibration Transmission through Rolling Element Bearings, Part I: Bearing Stiffness formulation." *Journal of Sound and Vibration*, **139**(2), pp 179-199.

Lim, T.C. and Singh, R. (1990). "Vibration Transmission through Rolling Element Bearings, Part II: System Studies." *Journal of Sound and Vibration*, **139**(2), pp 201-225.

Lim, T.C. and Singh, R. (1991). "Vibration Transmission through Rolling Element Bearings, Part III: Geared Rotor System Studies." *Journal of Sound and Vibration*, **151**(1), pp 31-54.

Lim, T.C. and Singh, R. (1992). "Vibration Transmission through Rolling Element Bearings, Part IV: Statistical Energy Analysis." *Journal of Sound and Vibration*, **153**(1), pp 37-50.

Lin, H.H., Huston, R.L. and Coy, J.J. (1988). "On Dynamic Loads in Parallel Shaft Transmissions: Part 1." *Journal of Mechanisms, Transmissions, and Automation in Design*, **110**(June), pp 221-225.

Liou, C.-H. et al. (1992). "Effect of Contact Ratio on Spur Gear Dynamic Load." *6th International Power Transmission and Gearing Conference*, USA, pp 29-33.

Liou, C.-H. et al. (1996). "Effect of Contact Ratio on Spur Gear Dynamic Load with No Tooth Profile Modifications." *Journal of Mechanical Design*, **118**(September), pp 439-443.

Litvin, F.L. (1989). *Theory of Gearing*, NASA Reference Publication, NASA.

Litvin, F.L. et al. (1996). "Application of Finite Element Analysis for Determination for Load Share, Real Contact Ratio, Precision of Motion, and Stress Analysis." *Journal of Mechanical Design*, **118**(December), pp 556-567.

Litvin, F.L., Chen, N.X. and Chen, J.S. (1995). "Computerized Determination of Curvature Relations and Contact Ellipse for Conjugate Surfaces." *Computer Methods in Applied Mechanics and Engineering*, **125**, pp 151-170.

Litvin, F.L. et al. (1995). "Computerized Design and Generation of Low-Noise Helical Gears with Modified Surface Topology." *Journal of Mechanical Design*, **117**(June), pp 254-261.

Litvin, F.L., Egelja, A.M. and De Donno, M. (1998). "Computerized determination of singularities and envelopes to families of contact lines on gear tooth surfaces." *Computer Methods in Applied Mechanics and Engineering*, **158**(1/2), pp 23.

Litvin, F.L. and Feng, P.-H. (1996). "Computerized Design and Generation of Cycloidal Gearings." *Mech. Mach. Theory*, **31**(7), pp 891-911.

Litvin, F.L. and Hsiao, C.L. (1993). "Computerized Simulation of Meshing and Contact of Enveloping Gear Tooth Surfaces." *Computer Methods in Applied Mechanics and Engineering*, **102**, pp 337-336.

Litvin, F.L. and Kim, D.H. (1997). "Computerized Design, Generation and Simulation of Meshing of Modified Involute Spur Gears with Localized Bearing Contact and Reduced Level of Transmission Errors." *Journal of Mechanical Design*, **119**(March), pp 96-100.

Litvin, F.L. and Lu, J. (1993). "Computerized Simulation of Generation, Meshing and Contact of Double Circular-Arc Helical Gears." *Mathl. Comput. Modelling*, **18**(5), pp 31-47.

Litvin, F.L. and Lu, J. (1995). "Computerized Design and Generation of Double Circular-Arc Helical Gears with Low Transmission Errors." *Computer Methods in Applied Mechanics and Engineering*, **127**, pp 57-86.

Litvin, F.L., Lu, J. and Howkins, M. (1998). "Computerized simulation of meshing of conventional helical involute gears and modification of geometry." *Mechanism and machine theory.*, **34**(1), pp 123.

Litvin, F.L. and Seol, I.H. (1996). "Computerized Determination of Gear Tooth Surface as Envelope to Two Parameter Family of Surfaces." *Computer Methods in Applied Mechanics and Engineering*, **138**, pp 213-225.

Litvin, F.L., Wang, A.G. and Handschuh, R.F. (1998). "Computerized generation and simulation of meshing and contact of spiral bevel gears with improved geometry." *Computer Methods in Applied Mechanics and Engineering*, **158**(1/2), pp 35.

Lu, J., Litvin, F.L. and Chen, J.S. (1995). "Load Share and Finite Element Stress Analysis for Double Circular-Arc Helical Gears." *Mathl. Comput. Modelling*, **21**(10), pp 13-30.

Mahalingam, S. (1968). "Couple Vibration of Gear Systems." *Journal of the Royal Aeronautical Society*, **72**, pp 522-526.

Mahmoud, F.F., Salamon, N.J. and Marks, W.R. (1982). "A Direct Automated procedure for Frictionless Contact problems." *International Journal for Numerical Methods in Engineering*, **18**, pp 245-57.

Mark, W.D. (1987). "The Role of the Discrete Fourier Transform in the Contribution to Gear Transmission Error Spectra from Tooth-Spacing Errors." *Journal of Mechanical Engineering Science*, **201**(c3), pp 227-9.

Mark, W.D. (1992). "Elements of Gear Noise Prediction." Noise and Vibration Control Engineering: Principles and Applications, L.L. Beranek and I.L. Ver, eds., John Wiley & Sons, Inc., pp 735-770.

Martins, J.A.C. and Oden, J.T. (1983). "A Numerical Analysis of a Class of Problems in Elastodynamics with Friction." *Computer Methods in Applied Mechanics and Engineering*, **40**, pp 327-60.

Maruyama, N., Morikawa, K. and Hitomi, N. (1992). "Gear Case Shape and Rib Distribution for Reducing Automobile Transmission Gear Noise." *6th International Power Transmission and Gearing Conference*, Scottdale, Arizona, USA, pp 583-588.

May, H.O. (1986). "The Conjugate Gradient Method for Unilateral Problems." *Computers and Structures*, **22**(4), pp 595-8.

Mcfadden, P.D. (1985). "Analysis of the Vibration of the Input Bevel Pinion in RAN Wessex Helicopter Main Rotor Gearbox Wak143 Prior to Failure." *Propulsion Report 169*, Department of Defence, Aeronautical Research Laboratory.

Mcfadden, P.D. (1986). "Detecting Fatigue Cracks in Gears by Amplitude and Phase Demodulation of the Meshing Vibration." *Journal of Vibration, Acoustics, Stress, and Reliability in Design*, **108**(April), pp 165-170.

Meguid, S.A. and Refaat, M.H. (1997). "Finite Element Analysis of the Deep Drawing Process Using Variational Inequalities." *Finite Elements in Analysis and Design*, pp 1-17.

Milenkovic, V. and Shmuter, S. (1982). "An Angular Sensor for Transmission Error Inspection." *International Congress & Exposition*, Michigan, USA, pp 1-18.

Moriwaki, I. et al. (1993). "Global Local Finite Element Method (Glfem) in Gear Tooth Stress Analysis." *Journal of Mechanical Design*, **115**(December), pp 1008-1012.

Munro, R.G. (1997). "The Use of Optical Gratings in Gear Metrology." *Third International Conference on Laser Metrology and Machine Performance*, UK, pp 243-252.

Munro, R.G. and Yildirim, N. (1994). "Some Measurements of Static and Dynamic Transmission Error of Spur Gears." *International Gearing Conference*, UK, pp 371-376.

Nadolski, W. and Pielorz, A. (1998). "The influence of variable stiffness of teeth on dynamic loads in single-gear transmission." *Archive of applied mechanics = ingenieur-archiv*, **68**(3/4), pp 185.

Nakada, T. and Utagawa, M. (1956). "The Dynamic Loads on Gears Caused by the Varying Elasticity of the Mating Teeth of Spur Gears." *Proceeding of the Sixth Japanese National Congress on Applied Mechanics*, pp 493-497.

Neriya, S.V., Bhat, R.B. and Sankar, T.S. (1985). "Coupled Torsional-Flexural Vibration of a Geared Shaft System Using Finite Element Analysis." *Shock and Vibration Bulletin*, **55**(3), pp 13-25.

Noor, A.K. and Kim, K.O. (1989). "Mixed Finite element formulation for Frictionless Contact Problems." *Finite Elements in Analysis and Design*, **4**, pp 315-32.

Nour-Omid, B. and Wriggers, P. (1986). "A Two-Level Iteration method for Solution of Contact Problems." *Computer Methods in Applied Mechanics and Engineering*, **54**, pp 131-44.

Oden, J.T. (1972). *Finite Elements of Nonlinear Continua*, McGRAW-Hill, New York.

Okamoto, N. et al. (1994). "Creep in Connections Between Gears and Shafts." *1994 International Gearing Conference*, University of Newcastle, UK, pp 189-194.

Ong, J.H. (1992). "Finite Elements for Vibration of Vehicle Transmission System." *Computers in Industry*, **18**, pp 257-263.

Oswald, F.B. et al. (1992). "Comparison of Analysis and Experiment for Gearbox Noise." *6th International Power Transmission and Gearing Conference*, USA, pp 675-679.

Oswald, F.B. et al. (1994). "Influence of Gear Design Parameters on Gearbox Radiated Noise." *1994 International Gearing Conference*, University of Newcastle, UK, pp 81-86.

Oswald, F.B. et al. (1992). "Effect of Operations Condition on Gearbox Noise." *6th International Power Transmission and Gearing Conference*, Scottdale, Arizona, USA, pp 669-674.

Ozguven, H.N. and Houser, D.R. (1988). "Dynamic Analysis of High Speed Gears by Using Loaded Static Transmission Error." *Journal of Sound and Vibration*, **125**, pp 71-83.

Ozguven, H.N. and Houser, D.R. (1988). "Mathematical Models Used in Gear Dynamics- A Review." *Journal of Sound and Vibration*, **121**(3), pp 383-411.

Padovan, J., Tovichakchaikul, S. and Zeid, I. (1984). "Finite Element Analysis of Steadily Moving Contact Fields." *Computers and Structures*, **18**(2), pp 191-200.

Panagiotopoulos, P.D. (1975). "A Nonlinear Programming Approach to the Unilateral Contact and Friction-Boundary Value Problem in the Theory of Elasticity." *Ingenieur-Archiv*, **44**, pp 421-32.

Panagiotopoulos, P.D. (1977). "On the Unilateral Contact Problem of Structures with a Non-Quadratic Strain Energy Density." *International Journal of Solids Structures*, **13**, pp 253-61.

Panagiotopoulos, P.D. and Lazaridis, P.P. (1987). "Boundary Minimum Principles for the Unilateral Contact Problem." *International Journal of Solids Structures*, **23**(11), pp 1465-84.

Park, S.J., Earmme, Y.Y. and H., S.J. (1997). "Determination on the Most Appropriate Mesh Size for a 2-D Finite Element Analysis of Fatigue Crack Closure Behaviour." *Fatigue & Fracture of Engineering Materials & Structures*, **20**(4), pp 533-545.

Perret-Liaudet, J. and Sabot, J. (1992). "Dynamics of Truck Gearbox." *6th International Power Transmission and Gearing Conference*, Scottdale, Arizona, USA, pp 249-258.

Pires, E.B. and Oden, J.T. (1983). "Analysis of Contact Problems with Friction under Oscillating Loads." *Computer Methods in Applied Mechanics and Engineering*, **39**, pp 337-62.

Pittman, J.F.T. et al. (1984). *Numerical Analysis of forming Processes*, John Wiley and Sons, New York.

Prasad, V.S., Dukkipati, R.V. and Osman, M.O.M. (1992). "A Group Theory for Composite Gear Trains Employing Three-Shafts." *6th International Power Transmission and Gearing Conference*, pp DE-Vol.43-1.

Rahman, M.U. et al. (1984). "An Iterative Procedure for Finite Element Stress Analysis of Frictional Contact Problems." *Computers and Structures*, **18**(6), pp 947-54.

Ramamurti, V. and Neogy, S. (1998). "Effect of Cracks on the Natural Frequency of Cantilevered Plates--A Rayleigh-Ritz Solution." *Mechanics of Structures and Machines.*, **26**(2), pp 131.

Ramamurti, V. and Rao, M.A. (1988). "Dynamic Analysis of Spur Gear Teeth." *Computers and Structures*, **29**(5), pp 831-843.

Randall, R.B. (1980). "Advances of the Application of Cepstrum Analysis to Gearbox Diagnosis." *Second International Conference: Vibration in Rotating Machinery*, pp 169-174.

Randall, R.B. (1984). "Seperating Excitation and Structural Response Effects in Gearboxes." *IMECHE, Third International Conference on Vibration in Rotating Machinery*, pp 101-108.

Randall, R.B. and Deyang, L. (1990). "Hibert Transform Techniques for Torsional Vibration Analysis." *The Institution of Engineers Australia Vibration and Noise Conference*, Australia, pp 122-126.

Randall, R.B. and Kelly, D.W. (1990). "Analytical and Experimental Vibration Analysis of a Gearbox Casing." *The Institution of Engineers Australia Vibration and Noise Conference*, Melbourn, Australia, pp 68-72.

Rao, C.R.M. and Muthuveerappan, G. (1993). "Finite Element Modelling and Stress Analysis of Helical Gear Teeth." *Computers and Structures*, **49**(6), pp 1095-1106.

Rebbechi, B. and Crisp, J.D.C. (1981). "A New formulation of Spur-Gear Vibration." *International Symposium on Gearing & Power Transmissions.*, Tokyo, pp 61-66.

Rebbechi, B. and Crisp, J.D.C. (1983). "The Kinetics of the Contact Point, and Oscillatory Mechanisms in Resilient." *The sixth world congress on theory of machines and mechanisms*, pp 802-806.

Rebbechi, B. et al. (1992). "A Comparison Between Theoretical Prediction and Experimental Measurement of the Dynamic Behaviour of Spur Gears." *6th International Power Transmission and Gearing Conference*, USA, pp 431-438.

Rebbechi, B., Oswald, F.B. and Townsend, D.P. (1996). "Measurement of Gear Tooth Dynamic Friction." *Transmission and Gearing Conference*, USA, pp 355-363.

Refaat, M.H. (1995). "Nonlinear Finite Element Analysis of Frictional Contact Problem Using Variational Inequalities," , University of Toronto, Toronto.

Refaat, M.H. and Meguid, S.A. (1994a). "A Novel Finite Element Analysis of the General Contact Problem Using Variational Inequalities." *Recent Advances in Structural Mechanics ASME*, pp 93-98.

Refaat, M.H. and Meguid, S.A. (1994b). "On the Elastic Solution of Frictional Contact Problems Using Variational Inequalities." *Inc. J. Mech. Sci.*, **36**(4), pp 329-342.

Refaat, M.H. and Meguid, S.A. (1995). "On the Contact Stress Analysis of Spur Gears Using Variational Inequalities." *Computers and Structures*, **57**(5), pp 871-882.

Refaat, M.H. and Meguid, S.A. (1996). "A Novel Finite Element Approach to Frictional Contact Problems." *International Journal for Numerical Methods in Engineering*, **39**, pp 3889-3902.

Regalado, I. and Houser, D.R. (1998). "Profile Modifications for Minimum Static Transmission Error in Cylindrical Gears." *1998 ASME Design Engineering Technical Conference*, Atlanta, GA, USA, pp DETC98/PTG-5781.

Remmers, E.P. (1978). "Gear Mesh Excitation Spectra for Arbitrary Tooth Spacing Errors, Load and Design Contact Ratio." *Journal of Mechanical Design*, **100**(October), pp 715-722.

Richard E. Dippery, J., Echempati, R. and Ellis, J. (1998). "Design and Stress Analysis of Gears Using the Boundary Element Method." *1998 ASME Design Engineering Technical Conference*, Atlanta, GA, USA, pp DETC98/PTG-5791.

Roosmalen, A.N.J.V. (1995). "Noise Generation Mechanism of Gear Transmissions." *IMechE 1995*, **2**(c492/002), pp 141-151.

Rothert, H. et al. (1985). "On Geometrically Nonlinear Contact Problems with Friction." *Computer Methods in Applied Mechanics and Engineering*, **51**, pp 139-55.

Sabot, J. and Perret-Liaudet, J. (1994). "Computation of the Noise Radiated by a Simplified Gearbox." *1994 International Gearing Conference*, University of Newcastle, UK, pp 63-68.

Sabot, J. and Perret-Liaudet, J. (1994). "Computational of the Noise Radiated by a Simplified Gearbox." *1994 International Gearing Conference*, University of Newcastle, UK, pp 63-68.

Sachdeva, T.D., Ramakrishnan, C.V. and Natarajan, R. (1981). "A Finite Element Method for the Elastic Contact Problems." *Journal of Engineering for Industry*, **103**, pp 457-61.

Sayegh, A.F. and Tso, F.K. (1986). "Treatment of Frictionless Contact Boundaries by Direct Minimization." *Computers and Structures*, **22**(6), pp 905-15.

Seol, I.H. and Litvin, F.L. (1996). "Computerized Design, Generation and Simulation of Meshing and Contact of Modified Involute, Klingelnberg and Flender Type Worm-Gear Drives." *Journal of Mechanical Design*, **118**(December), pp 551-555.

Seol, I.H. and Litvin, F.L. (1996). "Computerized Design, Generation and Simulation of Meshing and Contact of Worm-Gear Drives with Improved Geometry." *Computer Methods in Applied Mechanics and Engineering*, **138**, pp 73-103.

Sirichai, S. et al. (1997). "Finite Element Analysis of Gears in Mesh." *Fifth International Congress on Sound and Vibration*, Australia, pp 869-876.

Sirichai, S. et al. (1997). "A Synthetic Verification of 2D Contact Stiffness." *Second International Conference on the Application of Numerical Methods in Engineering*, Malaysia, pp 261-271.

Sirichai, S. et al. (1998). "A Finite Element Model of Spur Gears in Mesh with a Single Tooth Crack." *Third International Symposium on Advanced & Aerospace Science and Technology in Indonesia*, Indonesia, pp 233-241.

Sirichai, S. et al. (1998). "The Static Transmission Error of Cracked Spur Gear Teeth Using FEA." *1998 ASME Design Engineering Technical Conference*, Atlanta, GA, USA, pp DETC98/CIE-5510.

Sirichai, S. et al. (1996). "The Measurement of Static Torsional Stiffness of Gears in Mesh." *Third International Symposium on Measurement Technology and Intelligent Instruments*, Japan, pp 251-258.

Smith, J.D. (1983). *Gears and Their Vibration*, Marcel Dekker, USA.

Smith, J.D. (1987). "Gear Transmission Error Accuracy with Small Rotary Encoders." *Journal of Mechanical Engineering Science*, **201**(c2), pp 133-5.

Smith, J.D. (1987). "The Uses and Limitations Error." *American Gear Manufacturers Association*, Cicinnati, pp 87-FTM-5.

Smith, R.E. (1987). "The Relationship of Measured Gear Noise to Measured Gear Transmission Errors." *American Gear Manufacturers Association*, pp 1-10.

Stadtfeld, H.J. (1998). "Single Flank Test, Structure-Borne Noise Analysis and Digital Imaging of Tooth Contact." *1998 ASME Design Engineering Technical Conference*, Atlanta, GA, USA, pp DETC98/PTG-5783.

Su, X. and Houser, D.R. (1998). "Calculation of Wobble From Lead Inspection Data Gear Teeth with Modifications." *1998 ASME Design Engineering Technical Conference*, Atlanta, GA, USA, pp DETC98/PTG-5782.

Sundarajan, S. and Amin, S. (1991). "Finite Element Analysis of Ring Gear/Casing Spline Contact." *Journal of Propulsion and Power*, **7**(4), pp 602-604.

Sundarajan, S. and Young, B.G. (1990). "Finite Element Analysis of Large Spur and Helical Gear Systems." *Journal of Propulsion and Power*, **6**(4), pp 451-454.

Sundaresan, S., Ishii, K. and Houser, D.R. (1994). "A Parametric Study on the Effect of Geometric Gear Design Variables on Static Transmission Error." *International Gearing Conference*, UK, pp 383-388.

Sweeney, P.J. and Randall, R.B. (1996). "Gear Transmission Error Measurement Using Phase Demodulation." *Journal of Mechanical Engineering Science*, **210**(3), pp 201-213.

Talaslidis, D. and Panagiotopoulos, P.D. (1982). "A Linear Finite Element Approach to the Solution of the Variational Inequalities Arising in Contact Problems of Structural Dynamics." *International Journal for Numerical Methods in Engineering*, **18**, pp 1505-20.

Tavares, H.F. and Prodonoff, V. (1986). "A New Approach for Gearbox Modeling in Finite Element Analysis of Torsional Vibration of Gear-Branched Propulsion Systems." *Shock and Vibration Bulletin*, **56**(2), pp 117-125.

Tordian, G.V. and Geraldin, H. (1967). "Dynamic Measurement of the Transmission Error in Gears." *Proc. JSME 1967 Semi-International Symposium September 1967*, pp 279-287.

Tordion, G.V. and Gerardin, H. (1967). "Dynamic Measurement of the Transmission Error in Gears." *Proceedings of the Japanese Society of Mechanical Engineers Semi-International Gearing Symposium*, pp 279-284.

Toshinari, I. (1995). "Development of Transmission Error Apparatus for Final Drive Unit - Improvement of Torsional Vibration Characteristic." *ImechE 1995*, pp 163-170.

Townsend, D.P. (1991). *Dudley's Gear Handbook*, McGRAW-HILL, INC., New York.

Tradegard, A., Nilsson, F. and Ostlund, S. (1998). "FEM-Remeshing Technique Applied to Crack Growth Problems." *Computer Methods in Applied Mechanics and Engineering*, **160**(1/2), pp 115.

Tsai, Y.C. and Chang, H.L. (1992). "Reconsideration of the Logic Gear Using a General Mathematical Model of Composite Gear Profiles." *6th International Power Transmission and Gearing Conference*, Scotts dale, Arizona, pp 169-176.

Tseng, J. and Olsen, M.D. (1981). "The Mixed Finite Element method Applied to Two-Dimensional Elastic Contact Problems." *International Journal for Numerical Methods in Engineering*, **17**, pp 991-1014.

Tuma, J., Kubena, R. and Nykl, V. (1994). "Assessment of Gear Quality Considering the Time Domain Analysis of Noise and Vibration Signals." *International Gearing Conference*, UK, pp 463-468.

Tzou, H.S. and Schiff, A.J. (1987). "Development and Evaluation of a Pseudo-force Approximation Applied to Nonlinear Dynamic Contacts and Viscoelastic Damping." *Computers and Structures*, **26**(3), pp 481-93.

Umeyama, M. (1994). "Effect of Modified Tooth Surface of a Helical Gear Pair on the Transmission Error and Its Optimal Design." *International Gearing Conference*, UK, pp 377-382.

Umezawa, K., Ajima, T. and Houjoh, H. (1986). "Vibration of Three Axes Gear System." *Bulletin of the JSME*, **29**(249), pp 950-957.

Underhill, W.R.C., Dokainish, M.A. and Oravas, G.E. (1997). "A Method for Contact Problem Using Virtual Elements." *Computer Methods in Applied Mechanics and Engineering*, **143**, pp 229-247.

Utagawa, M. and Harada, T. (1962). "Dynamic Loads on Spur Gear Teeth Having Pitch Errors At High Speed." *Bulletin of the JSME*, **5**(18), pp 374-381.

Velex, P., Maatar, M. and Octrue, M. (1995). "Loaded Transmission Error Predictions and Measurements on Spur Gears with Profile Reliefs." *IMechE 1995*, pp 199-208.

Velinsky, S.A. (1996). "Torsional Stiffness of a Machine Drive Element with Tensile Web Structure." *Mechanism and Machine Theory*, **31**(8), pp 1043.

Vijayakar, S.M., Busby, H.R. and Houser, D.R. (1988). "Linearization of Multibody Frictional Contact Problems." *Computers and Structures*, **29**(4), pp 569-576.

Vijayakar, S.M. and Houser, D.R. (1993). "Contact Analysis of Gears Using a Combined Finite Element and Surface Integral Method." *Gear Technology*, pp 26-33.

Vijayarangan, S. and Ganesan, N. (1994). "Static Contact Stress Analysis of a Spur Gear Tooth Using the Finite Element Method, Including Frictional Effects." *Computers and Structures*, **51**(6), pp 765-770.

Vinayak, H. and Houser, D.R. (1992). "A Comparison of Analytical Predictions with Experiment Measurements of Transmission Error of Misaligned Loaded Gears." *6th International Power Transmission and Gearing Conference*, USA, pp 11-18.

Walford, T.L.H. and Stone, B.J. (1980). "Some Damping and Stiffness Characteristics of Angular Contact Bearings under Oscillating Radial Load." *Second International Conference: Vibration in Rotating Machinery*, pp 157-162.

Wallace, D.B. and Seireg, A. (1973). "Computer Simulation of Dynamic Stress, Deformation, and Fracture of Gear Teeth." *Journal of Engineering for Industry*, pp 1108-1114.

Wang, C.C. (1985). "On analytical Evaluation of Gear Dynamic Factors Based on Rigid Body Dynamics." *Journal of Mechanisms, Transmissions, and Automation in Design*, **107**, pp 301-311.

Wang, S.M. (1974). "Analysis of Non-linear Transient Motion of a Geared Torsional." *Journal of Engineering for Industry*, **96**, pp 51-59.

Wang, S.M. and Morse, I.E. (1972). "Torsional Response of a Gear Train System." *Journal of Engineering for Industry, Transactions of the ASME 94*, pp 583-594.

Wang, Y.-F. and Tong, Z.-F. (1996). "Influence of Gear Errors on Acceleration Noise From Spur Gears." *J. Accoust. Soc. Am.*, **99**(5), pp 2922-2929.

Welbourn, D.B. (1972). "Forcing Frequencies Due to Gears." *Proc., Vibr., in Rotating Syst. Conf.*, pp 25-40.

Welbourn, D.B. (1979). "Fundamental Knowledge of Gear Noise - A Survey,." *Proc., Noise & Vib. of Engineering and Transmissions*, Cranfield, UK, pp 9-14.

Wilcox, L. and Coleman, W. (1973). "Application of Finite Element to the Analysis of Gear Tooth Stresses." *Journal of Engineering for Industry, Transactions of the ASME*, pp 1139-1148.

Wilson, E.A. and Parsons, B. (1970). "Finite Element Analysis of Elastic Contact problems Using Differential Displacements." *International Journal for Numerical Methods in Engineering*, **2**, pp 387-95.

Xu, Y. and Saigal, S. (1998). "An element free Galerkin formulation for stable crack growth in an elastic solid." *Computer Methods in Applied Mechanics and Engineering*, **154**(3/4), pp 331.

Yang, F., Qian, C. and Li, J.C.M. (1996). "Finite Element Analysis of a Subsurface Crack." *International Journal of Fracture*, **77**, pp 337-350.

Yau, E., Busby, H.R. and Houser, D.R. (1994). "A Rayleigh-Ritz Approach to Modeling Bending and Shear Deflections of Gear Teeth." *Computers and Structures*, **50**(5), pp 705-713.

Young, W.C. (1985). *Roark's formular for Stress & Strain*, McGraw-Hill, New York.

Zakrajsek, J.J. and al., e. (1990). "Gear Noise, Vibration, and Diagnostic Studies at NASA Lewis Research Centre." *First International Conference, Gearbox Noise and Vibration, Proceeding of the Institute of Mechanical Engineers*, pp 27-34.

Zeman, J. (1957). "Dynamische Zusatzkrafter in Zahnbradgetrieben." *Zeitschrift des Vereines Deutscher Ingiere*(99), pp 244.

Zhang, T. and Kohler, H.K. (1994). "A Gearbox Structural Optimisation Procedure for Minimising Noise Radiation." *international gearing conference*, Uk, pp 87-92.

Zhang, T., Kohler, H.K. and lack, G.K. (1994). "Noise Optimisation of a Double Helical Parallel Shaft Gearbox." *1994 International Gearing Conference*, University of Newcastle, pp 93-98.

Zhang, Y. and Fang, Z. (1998). "Analysis of tooth contact and load distribution of helical gears with crossed axes." *Mechanism and machine theory*, **34**(1), pp 41.

Zhang, Y. et al. (1994). "Computerized Analysis of Meshing and Contact of Gear Real Tooth Surfaces." *Journal of Mechanical Design*, **116**(September), pp 667-682.

Zhong, W.X. and Sun, S.M. (1988). "A Finite Element Method for Elasto Plastic Structures and Contact Problems by Parametric Quadratic Programming." *International Journal for Numerical Methods in Engineering*, **26**, pp 2723-38.

Zhong, Z.-H. (1993). *Finite Element procedures for Contact-Impact Problems*, Oxford University Press Inc.

Zhong-Sheng, L., Su-Huan, C. and Tao, X. (1993). "Derivatives of Eigenvalues for Torsional Vibration of Geared Shaft Systems." *Journal of Vibration and Acoustics*, **115**(July), pp 277-276.

Zienkiewicz, O.C. (1967). "The Finite Element Method in Structural and Continum Mechanics." European Civil Engineering Series, London, pp 99-0388-272.

Zienkiewicz, O.C. (1971). *The Finite Element Method in Engineering Science*, McGraw-Hill, London.

Zienkiewicz, O.C. (1977). *The Finite Element Method*, McGRAW-Hill, London.

Zienkiewicz, O.C. and Taylor, R.L. (1994). *The Finite Element Method: Volume 1*, McGRAW-Hill, New York.

Zienkiewicz, O.C. and Taylor, R.L. (1994). *The Finite Element Method: Volume 2*, McGRAW-Hill, New York.

APPENDIX A

LISTING OF AN AUTOCAD PROGRAMMING LANGUAGE FOR GENERATING INVOLUTE AND FILLET PROFILES OF THE SPUR GEAR

AutoLisp File

```
; Firstly load AutoLisp files from Load Application in Tools of Main menu.
; Then type in command (t).
; Press Esc after trochoid curve (fillet curve) touch dedendum circle.
; Convert angle (degrees to radians)
    (defun dtr (a)
        (* pi (/ a 180.0))
    )
; Convert angle (radians to degrees)
    (defun rtd (a)
        (* 180 (/ a pi))
    )
```

```
; Start main program
    (defun t ()
    (expand 10)
; Input parameter
    (setq module (getreal "\tModule(mm) ? ")
        radpit (getreal "\tPitch radius(mm) ? ")
        teenum (getint "\tNumber of teeth ? ")
        angpre (getreal "\tPressure angle(degrees) ? ")
        offset (getreal "\tCutter offset for addendum modification is(usually 0) ? ")
        dist1 0.1
        angpre (dtr angpre)
        modadd (/ offset module);addendum modification factor
        alpha 1.25
        beta 1.00
        gamma 0.25
        addum (* alpha module);addendum gear rack
        radadd (+ (/ (* teenum module) 2.0) (* (+ 1 modadd) module));addendum radii
        dedum (* beta module);dedendum gear rack
        radded (- radpit (* module 1.25));dedendum radii
        rc (* module gamma);tip radius
        angset 0.0 ;increment angle
        angjoi 0.0
        angend 0.0
        angsta 0.0
        keypoint 0.0
        angcal 0.0 ;test angle
        anginc 0.01
    )
; Generates Pitch, Addendum, and Dedendum circle
    (command "circle" (list 0.0 0.0) radadd)
    (command "circle" (list 0.0 0.0) radpit)
    (command "circle" (list 0.0 0.0) (* radpit (cos angpre)))
    (command "circle" (list 0.0 0.0) radded)
; Define centre line
    (command "line" (list 0.0 0.0) (list 0.0 138.0) "")
;Calculate constant variable U and V
    (setq U
```

```
        (- 0
                (+
                        (/ pi 4.0)
                        (*
                            (- alpha gamma)
                            (/ (sin angpre) (cos angpre))
                        )
                        (/ gamma (cos angpre))
                )
        )
    )
    (setq V
        (- gamma alpha)
    )
;Calculate minimum. involute angle,(angjoi),and maximum. involute angle,(angsta)
    (setq angjoi
        (*
            (/ 2.0 teenum)
            (+ U
                (* (+ V modadd)
                    (/ (cos angpre) (sin angpre))
                )
            )
        )
    )
    (setq angsta
        (-
            (*
                (/ 1 (* teenum (cos angpre)))
                (sqrt
                    (-
                        (expt (+ 2.0 teenum (* 2.0 modadd)) 2.0)
                        (expt (* teenum (cos angpre)) 2.0)
                    )
```

```
                    )
                )
                (*
                    (+ 1 (/ (* 2.0 modadd) teenum))
                    (/ (sin angpre) (cos angpre))
                )
                (/ pi (* 2.0 teenum))
            )
        )
; Start generates loop of involute curve
(setq angset angsta)
(while (>= angset angjoi)
    (setq
        angcal angset
        xinv
        (*
            (/ (* teenum module) 2.0)
            (-
                (sin angcal)
                (*
                    (+
                        (*
                            (+ angcal (/ pi (* 2.0 teenum)))
                            (cos angpre)
                        )
                        (*
                            (/ (* 2.0 modadd) teenum)
                            (sin angpre)
                        )
                    )
                    (cos (+ angcal angpre))
                )
            )
        )
```

```
    yinv
    (*
        (/ (* teenum module) 2.0)
        (+
            (cos angcal)
            (*
                (+
                    (*
                        (+ angcal (/ pi (* 2.0 teenum)))
                        (cos angpre)
                    )
                    (*
                        (/ (* 2.0 modadd) teenum)
                        (sin angpre)
                    )
                )
                (sin (+ angcal angpre))
            )
        )
    )
    pt1
    (list xinv yinv)
)
(setq
    angcal (- angset anginc)
    xinv
    (*
        (/ (* teenum module) 2.0)
        (-
            (sin angcal)
            (*
                (+
                    (*
                        (+ angcal (/ pi (* 2.0 teenum)))
```

```
                    (cos angpre)
                )
                (*
                    (/ (* 2.0 modadd) teenum)
                    (sin angpre)
                )
            )
            (cos (+ angcal angpre))
        )
    )
)
yinv
(*
    (/ (* teenum module) 2.0)
    (+
        (cos angcal)
        (*
            (+
                (*
                    (+ angcal (/ pi (* 2.0 teenum)))
                    (cos angpre)
                )
                (*
                    (/ (* 2.0 modadd) teenum)
                    (sin angpre)
                )
            )
            (sin (+ angcal angpre))
        )
    )
)
pt2
(list xinv yinv)
dist2
```

```
        (distance pt1 pt2)
    )
        (if (> dist2 dist1)
            (setq
                anginc (* anginc 0.999)
            )
                (if (< dist2 (* dist1 0.999))
                    (setq
                        anginc (* anginc 1.001)
                    )
                        (progn
                            (setq
                                angset
                                    (- angset anginc)
                                    keypoint
                                    (1+ keypoint)
                                    dist1
                                    dist2
                            )
                             (command "point" pt1)
                        )
                )
        )
    )
;Calculate minimum trochoid angle,(angjoi),and
;maximum trochoid angle,(angend)
    (setq angset angjoi)
    (setq angend (/ (* 2.0 U) teenum))
;Start generate loop of trochoid curve
    (while (<= angset angend)
    (setq
        angcal (+ angset anginc)
        L
        (sqrt
```

```
        (+ 1
            (* 4.0
                (expt (/ (+ V modadd) (- (* 2.0 U) (* teenum angcal))) 2.0)
            )
        )
    )
)
(setq P (+ (/ gamma L) (- U (/ (* teenum angcal) 2.0))))
(setq Q
    (+
        (*
            (/ (* 2.0 gamma) L)
            (/ (+ V modadd) (- (* 2.0 U) (* teenum angcal)))
        )
        V
        (/ teenum 2.0)
        modadd
    )
)
(setq
    xtroch
    (* module (+ (* Q (sin angcal)) (* P (cos angcal))))
    ytroch
    (* module (- (* Q (cos angcal)) (* P (sin angcal))))
    pt2
    (list xtroch ytroch)
    dist2
    (distance pt1 pt2)
)
        (if (> dist2 dist1)
            (setq
                anginc (* anginc 0.99)
            )
                (if (< dist2 (* dist1 0.65))
```

```
                    (setq
                        anginc (* anginc 1.1)
                    )
                        (progn
                            (setq
                                angset
                                (+ angset anginc)
                                keypoint
                                (1+ keypoint)
                                dist1
                                dist2
                                pt1
                                pt2
                            )
                            (command "point" pt1)
                        )
                    )
                )
)
(command "")
)
```

APPENDIX B

LISTING OF AN ANSYS PARAMETRIC DESIGN LANGUAGE FOR THE NORMAL CONTACT STIFFNESS AND TORSIONAL MESH STIFFNESS OF UNDAMAGED GEARS IN MESH

```
/GST,ON                    ! Turns graphical solution tracking on
!*
*DIM,ROT, ,12,1,1,         ! ROT(),TOR(),TA(), and AA() are array
*DIM,TOR, ,12,1,1,         parameter for computing the combined
*DIM,TA, ,12,1,1,          torsional mesh stiffness.
*DIM,AA, ,12,1,1,
!*
*DIM,KMG, ,69              ! Pinion torsional mesh stiffness, KMG().
*DIM,KFG, ,69              ! Gear torsional mesh stiffness, KFG().
!*
*DIM,FGC, ,69              ! FGC( ) and MGC( ) are array parameter
*DIM,MGC, ,69              of master couple node number of gear
!*                         and pinion respectively
*DIM,KMG1, ,69             ! KMG1(), KMG2(), KFG1( ), and
```

```
*DIM,KMG2, ,69
*DIM,KFG1, ,69
*DIM,KFG2, ,69
!*
*DIM,KN, ,69
!*
*DIM,ANG, ,69
ANG(1)=0.0,1.1575,2.315,3.4725,3.6171875
ANG(6)=3.761875, 3.9065625,3.97890625
ANG(9)=4.015078125,4.033164063,4.05125
ANG(12)=4.1959375,4.340625,4.4853125,4.63
ANG(16)=4.7746875, 4.919375,5.0640625
ANG(19)=5.20875,5.226835937,5.244921875
ANG(22)=5.28109375,5.3534375,5.498125
ANG(25)=5.6428125,5.7875, 6.945,8.1025
ANG(29)=9.26,9.27,9.6595, 10.059,10.858,11.657
ANG(35)=12.456,13.255, 14.054,14.853,15.2525
ANG(40)=15.642, 15.652,16.8095,17.967,19.1245
ANG(45)=19.2691875,19.413875, 19.5585625
ANG(48)=19.63090625,19.66707813,19.68516406
ANG(51)=19.70325, 19.8479375,19.992625
ANG(54)= 20.1373125,20.282,20.4266875
ANG(57)=20.571375,20.7160625,20.86075
ANG(60)=20.87883594,20.89692188, 20.93309375
ANG(63)=21.0054375,21.150125,21.2948125
ANG(66)=21.4395,22.597,23.7545,24.912
FNAM=1
PARSAV,ALL,ANGLE_C0,,
:DOLOOP
RESUME,m1c0,db,,
PARRES, ,ANGLE_C0,, ,,
/PREP7
TYPE,1,
MAT,1,
REAL,1,
ESYS,0,
CSYS,1
PENN=1E-5
ASEL,S,LOC,X,0,.069
AGEN, ,ALL, , , ,ANG(%FNAM%), , , ,1
```

KFG2( ) are array parameter of the keypoints number at the contact point of the first pair and second pair of pinion and gear respectively.

! KN() is combined normal contact stiffness in each meshing position.

! Defines, ANG(), an array parameter and its dimensions of meshing position.

! Angle array parameter of meshing position in one complete cyclic mesh is 24.912 degrees. Actually, you can analyse any meshing position within cyclic mesh.

! Sets initial meshing position.

! Write all parameter to file

! :DOLOOP of meshing position in a cyclic. Resumes the model and database and replace current parameter set with all scalar and array parameter from file then enters the model creation preprocessor

! Sets the element type, element material, element real constant, and element coordinate system

! PENN is Lagrange multiplier.

! Select a subset areas of the pinion only then rotate FE model through particular

```
ALLSEL,ALL                                  meshing position in degrees
CSYS,11,
ASEL,S,LOC,X,0,.069                         ! Select a subset areas of the gear only
AGEN, ,ALL, , , ,-ANG(%FNAM%), , , ,1       then rotate FE model through particular
ALLSEL,ALL                                  meshing position in degrees
*IF,FNAM,EQ,1,THEN
*GO,:LOOP1                                  ! LOOP1 for initial double pair contact
*ELSEIF,FNAM,EQ,29
*GO,:LOOP3                                  ! LOOP3 for recess double pair contact
*ELSEIF,FNAM,GE,30
*GO,:LOOP4                                  ! LOOP4 for single pair contact
*ELSEIF,FNAM,GE,2
*GO,:LOOP2                                  ! LOOP2 for double pair contact zone
*ENDIF
!* Start LOOP1 for initial double pair contact
:LOOP1
CSYS,1
ACLEAR,91                                   ! Delete nodes and elements associated
ACLEAR,4                                    with selected areas of teeth in double pair
ACLEAR,90                                   contact
ACLEAR,2
NUMSTR,KP,500,                              ! Establishes starting numbers of keypoint
KMG1(%FNAM%)=500                            and line number. Specifies the divisions
NUMSTR,LINE,500,                            and spacing ratio on unmeshed lines of
LSBL,367,4, ,DELETE,KEEP                    first pair contact tooth of pinion then
LESIZE,500,0.001, , ,1,                     mesh tooth area and groups potential
LESIZE,501,0.001, , ,1,                     contact nodes of this tooth into
LCCAT,500,501                               component for further generate contact
AMESH,91                                    elements.
LSEL,S, , ,500,501,
NSLL,S,1
CM,NMG1,NODE
ALLSEL,ALL
NUMSTR,KP,600,                              ! Establishes starting numbers of keypoint
KFG1(%FNAM%)=600                            and line number. Specifies the divisions
NUMSTR,LINE,600,                            and spacing ratio on unmeshed lines of
LSBL,184,4, ,DELETE,KEEP                    first pair contact tooth of gear then mesh
LESIZE,600,0.001, , ,1,                     tooth area and groups potential contact
LESIZE,601,0.001, , ,1,                     nodes of this tooth into component for
LCCAT,600,601                               further generate contact elements
```

```
AMESH,4
LSEL,S, , ,600,601,
NSLL,S,1
CM,NFG1,NODE
ALLSEL,ALL
NUMSTR,KP,700,
KMG2(%FNAM%)=700
NUMSTR,LINE,700,
LSBL,1,4, ,DELETE,KEEP
LESIZE,700,0.001, , ,1,
LESIZE,701,0.001, , ,1,
LCCAT,700,701
AMESH,90
LSEL,S, , ,700,701,
NSLL,S,1
CM,NMG2,NODE
ALLSEL,ALL
KFG2(%FNAM%)=148
LESIZE,3,0.001, , ,1,
AMESH,2
LSEL,S, , ,3,
NSLL,S,1
CM,NFG2,NODE
ALLSEL,ALL
*GO,:MLOOP2
!* Start LOOP2 of double pair contact zone
:LOOP2
CSYS,1
ACLEAR,91
ACLEAR,4
ACLEAR,90
ACLEAR,2
NUMSTR,KP,500,
KMG1(%FNAM%)=500
NUMSTR,LINE,500,
LSBL,367,4, ,DELETE,KEEP
LESIZE,500,0.001, , ,1,
LESIZE,501,0.001, , ,1,
LCCAT,500,501
AMESH,91
```

! One of the most important criteria for each meshing position was that the first potential contact nodes of both particular contact teeth must be created exactly on the intersection point between the pressure line and the involute curve.

! Establishes starting numbers of keypoint and line number. Specifies the divisions and spacing ratio on unmeshed lines of second pair contact tooth of pinion then mesh tooth area and groups potential contact nodes of this tooth into component for further generate contact elements.

! Defines contact keypoint number of second pair of the gear. Specifies the divisions and spacing ratio on unmeshed lines of second pair contact tooth of gear then mesh tooth area and groups potential contact nodes of this tooth into component for further generate contact elements.

! Delete nodes and elements associated with selected areas of teeth in double pair contact

! Establishes starting numbers of keypoint and line number. Specifies the divisions and spacing ratio on unmeshed lines of first pair contact tooth of pinion and concatenates multiple lines into one line for mapped meshing then mesh tooth area and groups potential contact nodes of this tooth into component for further generate

```
LSEL,S, , ,500,501,
NSLL,S,1
CM,NMG1,NODE
ALLSEL,ALL
NUMSTR,KP,600,
KFG1(%FNAM%)=600
NUMSTR,LINE,600,
LSBL,184,4, ,DELETE,KEEP
LESIZE,600,0.001, , ,1,
LESIZE,601,0.001, , ,1,
LCCAT,600,601
AMESH,4
LSEL,S, , ,600,601,
NSLL,S,1
CM,NFG1,NODE
ALLSEL,ALL
NUMSTR,KP,700,
KMG2(%FNAM%)=700
NUMSTR,LINE,700,
LSBL,1,4, ,DELETE,KEEP
LESIZE,700,0.001, , ,1,
LESIZE,701,0.001, , ,1,
LCCAT,700,701
AMESH,90
LSEL,S, , ,700,701,
NSLL,S,1
CM,NMG2,NODE
ALLSEL,ALL
NUMSTR,KP,800,
KFG2(%FNAM%)=800
NUMSTR,LINE,800,
LSBL,3,4, ,DELETE,KEEP
LESIZE,800,0.001, , ,1,
LESIZE,801,0.001, , ,1,
LCCAT,800,801
AMESH,2
LSEL,S, , ,800,801,
NSLL,S,1
CM,NFG2,NODE
ALLSEL,ALL
```

contact elements.

! Establishes starting numbers of keypoint and line number. Specifies the divisions and spacing ratio on unmeshed lines of first pair contact tooth of gear and concatenates multiple lines into one line for mapped meshing then mesh tooth area and groups potential contact nodes of this tooth into component for further generate contact elements

! Establishes starting numbers of keypoint and line number. Specifies the divisions and spacing ratio on unmeshed lines of second pair contact tooth of pinion and concatenates multiple lines into one line for mapped meshing then mesh tooth area and groups potential contact nodes of this tooth into component for further generate contact elements.

! Establishes starting numbers of keypoint and line number. Specifies the divisions and spacing ratio on unmeshed lines of second pair contact tooth of gear and concatenates multiple lines into one line for mapped meshing then mesh tooth area and groups potential contact nodes of this tooth into component for further generate contact elements.

```
*GO,:MLOOP2
!* Start LOOP3 for recess double pair contact
:LOOP3
ALLSEL,ALL
CSYS,1
ACLEAR,91                    ! Delete nodes and elements associated
ACLEAR,4                     with selected areas of teeth in double pair
ACLEAR,90                    contact
ACLEAR,2
KMG1(%FNAM%)=17              ! Defines contact keypoint number of first
LESIZE,367,0.001, , ,1,      pair of the pinion. Specifies the divisions
AMESH,91                     and spacing ratio on unmeshed lines of
LSEL,S, , ,367,              first pair contact tooth of pinion then
NSLL,S,1                     mesh tooth area and groups potential
CM,NMG1,NODE                 contact nodes of this tooth into
ALLSEL,ALL                   component for further generate contact
NUMSTR,KP,600,               elements.
KFG1(%FNAM%)=600             ! Establishes starting numbers of keypoint
NUMSTR,LINE,600,             and line number. Specifies the divisions
LSBL,184,4, ,DELETE,KEEP     and spacing ratio on unmeshed lines of
LESIZE,600,0.001, , ,1,      first pair contact tooth of gear and
LESIZE,601,0.001, , ,1,      concatenates multiple lines into one line
LCCAT,600,601                for mapped meshing then mesh tooth area
AMESH,4                      and groups potential contact nodes of this
LSEL,S, , ,600,601,          tooth into component for further generate
NSLL,S,1                     contact elements
CM,NFG1,NODE
ALLSEL,ALL
NUMSTR,KP,700,               ! Establishes starting numbers of keypoint
KMG2(%FNAM%)=700             and line number. Specifies the divisions
NUMSTR,LINE,700,             and spacing ratio on unmeshed lines of
LSBL,1,4, ,DELETE,KEEP       second pair contact tooth of pinion and
LESIZE,700,0.001, , ,1,      concatenates multiple lines into one line
LESIZE,701,0.001, , ,1,      for mapped meshing then mesh tooth area
LCCAT,700,701                and groups potential contact nodes of this
AMESH,90                     tooth into component for further generate
LSEL,S, , ,700,701,          contact elements.
NSLL,S,1
CM,NMG2,NODE
ALLSEL,ALL
```

```
NUMSTR,KP,800,
KFG2(%FNAM%)=800
NUMSTR,LINE,800,
LSBL,3,4, ,DELETE,KEEP
LESIZE,800,0.001, , ,1,
LESIZE,801,0.001, , ,1,
LCCAT,800,801
AMESH,2
LSEL,S, , ,800,801,
NSLL,S,1
CM,NFG2,NODE
ALLSEL,ALL
*GO,:MLOOP2
!* Start LOOP4 of single pair contact
:LOOP4
ALLSEL,ALL
CSYS,1
ACLEAR,90
ACLEAR,2
NUMSTR,KP,700,
KMG2(%FNAM%)=700
NUMSTR,LINE,700,
LSBL,1,4, ,DELETE,KEEP
LESIZE,700,0.001, , ,1,
LESIZE,701,0.001, , ,1,
LCCAT,700,701
AMESH,90
LSEL,S, , ,700,701,
NSLL,S,1
CM,NMG2,NODE
ALLSEL,ALL
NUMSTR,KP,800,
KFG2(%FNAM%)=800
NUMSTR,LINE,800,
LSBL,3,4, ,DELETE,KEEP
LESIZE,800,0.001, , ,1,
LESIZE,801,0.001, , ,1,
LCCAT,800,801
AMESH,2
LSEL,S, , ,800,801,
```

! Establishes starting numbers of keypoint and line number. Specifies the divisions and spacing ratio on unmeshed lines of second pair contact tooth of gear and concatenates multiple lines into one line for mapped meshing then mesh tooth area and groups potential contact nodes of this tooth into component for further generate contact elements.

! Delete nodes and elements associated with selected areas of teeth in single pair contact

! Establishes starting numbers of keypoint and line number. Specifies the divisions and spacing ratio on unmeshed lines contact of pinion tooth and concatenates multiple lines into one line for mapped meshing then mesh tooth area and groups potential contact nodes of this tooth into component for further generate contact elements.

! Establishes starting numbers of keypoint and line number. Specifies the divisions and spacing ratio on unmeshed lines contact of gear tooth and concatenates multiple lines into one line for mapped meshing then mesh tooth area and groups potential contact nodes of this tooth into component for further generate contact elements.

```
NSLL,S,1
CM,NFG2,NODE
ALLSEL,ALL
TYPE,2,
MAT,1,
REAL,3,
ESYS,0,
GCGEN,NMG2,NFG2,3, ,TOP,
TYPE,2,
MAT,1,
REAL,4,
ESYS,0,
GCGEN,NFG2,NMG2,3, ,TOP,
*GO,:MLOOP1
! * Start at MLOOP2 generates contact element for double pair contact zone.
:MLOOP2
TYPE,2,
MAT,1,
REAL,1,
ESYS,0,
GCGEN,NMG1,NFG1,3, ,TOP,
TYPE,2,
MAT,1,
REAL,2,
ESYS,0,
GCGEN,NFG1,NMG1,3, ,TOP,
TYPE,2,
MAT,1,
REAL,3,
ESYS,0,
GCGEN,NMG2,NFG2,3, ,TOP,
TYPE,2,
MAT,1,
REAL,4,
ESYS,0,
GCGEN,NFG2,NMG2,3, ,TOP,
! *Start at MLOOP1 generates contact element for single pair contact zone.
:MLOOP1
```

! Sets the contact element type 2, element material, element real constant set 3, and element coordinate system then generates 2-D symmetric contact elements on pinion tooth as contact surface and on gear tooth as target surface.

! Sets the contact element type 2, element material, element real constant set 4, and element coordinate system then generates 2-D symmetric contact elements on gear tooth as contact surface and on pinion tooth as target surface.

! Sets the contact element, material, real constant, and coordinate system then generates symmetric contact elements on first pair pinion tooth as contact surface and on gear tooth as target surface.

! Sets the contact element, material, real constant, and coordinate system then generates symmetric contact elements on first pair gear tooth as contact surface and on pinion tooth as target surface.

! Sets the contact element, material, real constant, and coordinate system then generates symmetric contact elements on second pair pinion tooth as contact surface and on gear tooth as target surface.

! Sets the contact element, material, real constant, and coordinate system then generates symmetric contact elements on second pair gear tooth as contact surface and on pinion tooth as target surface.

```
CPDELE,ALL,,,ANY
CSYS,1,
NSEL,S,LOC,X,0,.013
NROTAT,ALL                          ! Generates the coupled subset of nodes at
CP,1,UY,ALL                         pinion hub and gear hub
CP,2,UX,ALL
ALLSEL,ALL
CSYS,11,
NSEL,S,LOC,X,0,.013
NROTAT,ALL
CPLIST,ALL,,,ANY
CP,3,UY,ALL
CP,4,UX,ALL
ALLSEL,ALL
NSEL,S,CP,,1
CSYS,1
NROTAT,ALL                          ! Get master node number of coupled set
*GET,MGC(%FNAM%),NODE,0,NUM,MIN,    of pinion hub.
ALLSEL,ALL
NSEL,S,CP,,3
CSYS,11
NROTAT,ALL                          ! Get master node number of coupled set
*GET,FGC(%FNAM%),NODE,0,NUM,MIN,    of gear hub.
ALLSEL,ALL
CSYS,1                              ! Defines gears material property
MP,EX,1,69E9
MP,DENS,1,2770
MP,ALPX,1,2.27E-5
MP,NUXY,1,.33
MP,MU,1,.06
MP,KXX,1,190
MP,C,1,963
MP,EMIS,1,1
FINISH
!* Start main loop, MLOOP3, for compute combine
normal contact stiffness.
:MLOOP3
/SOLU
ANTYPE,STATIC,NEW                   ! Restraints all DOF at contact keypoints.
DK,KMG1(%FNAM%), ,0, ,0,ALL
```

```
DK,KFG1(%FNAM%), ,0, ,0,ALL
DK,KMG2(%FNAM%), ,0, ,0,ALL
DK,KFG2(%FNAM%), ,0, ,0,ALL                    ! Defines DOF constraints at master
D,FGC(%FNAM%), ,0, , , ,UX                     couple nodes of pinion hub and gear hub
D,FGC(%FNAM%), ,7.3E-5, , , ,UY
D,MGC(%FNAM%), ,0, , , ,UX
D,MGC(%FNAM%), , 7.3E-5, , , ,UY
TIME,0
AUTOTS,1                                       ! Applying load to both gear hubs in a
NSUBST,1,1,1,0                                 single-iteration analysis.
KBC,0
NEQIT,1,
SOLVE
FINISH
/POST26
RFORCE,2,MGC(%FNAM%),F,Y,                      ! Specifies the total reaction tangent force
RFORCE,3,FGC(%FNAM%),F,Y,                      at pinion hub and gear hub
PROD,4,2, , ,K1, , ,.0127*.0127/7.3E-5,1,1,
PROD,5,3, , ,K2, , ,.0127*.0127/7.3E-5,1,1,
PROD,6,4,5, ,K1*K2, , ,1,1,1,                  ! Computed the input torque at pinion and
ADD,7,4,5, ,K1+K2, , ,1,1,1,                   gear hub then calculated the combine
QUOT,8,6,7, ,KN, , ,1,1,                       normal contact stiffness. The result also
*GET,KN(%FNAM%),VARI,8,RTIME,1,                redirects save to a file in specific
/OUTPUT,KN%FNAM%,txt,,                         directory.
PRVAR,4,5,8, , , ,
/OUTPUT, TERM
FINISH
!* Start main loop, MLOOP4, deletes DOF restraints
at contact keypoint, sets element key options, and
defines the element real constants with Lagrange
multiplier.
:MLOOP4
/PREP7
DKDELE,KMG1(%FNAM%),ALL                        ! Deletes DOF restraints at contact
DKDELE,KFG1(%FNAM%),ALL                        keypoint.
DKDELE,KMG2(%FNAM%),ALL
DKDELE,KFG2(%FNAM%),ALL
KEYOPT,1,1,0                                   ! Sets element key options.
KEYOPT,1,2,0
KEYOPT,1,3,2
```

```
KEYOPT,1,5,0
KEYOPT,1,6,0
KEYOPT,2,1,0
KEYOPT,2,2,1
KEYOPT,2,3,1
KEYOPT,2,7,0
R,1,KN(%FNAM%),0,PENN,0,0,0,
R,2,KN(%FNAM%),0, PENN,0,0,0,
R,3,KN(%FNAM%),0, PENN,0,0,0,
R,4,KN(%FNAM%),0, PENN,0,0,0,
FINISH
```

! Defines the element real constants with Lagrange multiplier.

```
!*Define the combined torsional mesh stiffness of the pinion.
:MLOOP5
/SOLU
ANTYPE,STATIC
NROPT,AUTO, ,
EQSLV,FRONT,1e-008,0,
TOFFST,0,
D,FGC(%FNAM%), ,0, , , ,ALL
OUTRES,BASIC,ALL,
AUTOTS,1
NSUBST,20,100,11,0
KBC,0
SOLVE
FINISH
/POST26
NSOL,2,MGC(%FNAM%),U,Y,
RFORCE,3,MGC(%FNAM%),F,Y,
QUOT,4,2, , ,angtwist, , ,1,.0127,
PROD,5,3, , ,torque, , ,.0127,.015,1,
PROD,6,5,4, ,tor*ang, , , , , ,
PROD,7,4,4, ,ang**2, , , , , ,
VGET,ROT(1),4,
VGET,TOR(1),5,
VGET,TA(1),6,
VGET,AA(1),7,
*VSCFUN,TORSUM,SUM,TOR(4)
*VSCFUN,ROTSUM,SUM,ROT(4)
*VSCFUN,TASUM,SUM,TA(4)
```

! The combined torsional mesh stiffness of pinion is defined as the ratio between the torsional load and the angular rotation of the gear body. At each particular meshing position, the angular rotation of the pinion due to tooth bending, shearing and contact displacement is calculated in the gear reference frame by restrained the gear from rotating, with the pinion having a torque input load.

! Restraints all DOF at master couple node of the gear hub. Applying load to pinion hub by defines DOF constraints to master couple node of the pinion hub. Then specifies optimized nonlinear solution and some enhanced internal solution algorithms, such as number of substeps, etc.

! Computes the angle of rotation and torque in each substeps of the gear. Then compute the combined torsional meshes stiffness of the gear by defines the gradient of relationship between torque and angle of rotation. The result also redirects save to a file in specific directory. The further analysis of gradient of the combined torsional mesh stiffness is done in Microsoft Excel.

```
*VSCFUN,AASUM,SUM,AA(4)
KMG(%FNAM%)=(((ROTSUM*TORSUM)/9)-
TASUM)/(((ROTSUM**2)/9)-AASUM)
/OUTPUT,KMG%FNAM%,txt,,
PRVAR,4,5,,,,,
/OUTPUT, TERM
FINISH
```

```
!*Define the combined torsional mesh stiffness of the gear
:MLOOP6
/SOLU
ANTYPE,STATIC
NROPT,AUTO,,
EQSLV,FRONT,1e-008,0,
TOFFST,0,
D,MGC(%FNAM%),,0,,,,ALL
D,FGC(%FNAM%),,0,,,,UX
D,FGC(%FNAM%),,7.3E-5,,,,UY
OUTRES,BASIC,ALL,
AUTOTS,1
NSUBST,20,100,11,0
KBC,0
SOLVE
/POST26
NSOL,2,FGC(%FNAM%),U,Y,
RFORCE,3,FGC(%FNAM%),F,Y,
QUOT,4,2,,,angtwist,,,1,.0127,
PROD,5,3,,,torque,,,.0127,.015,1,
PROD,6,5,4,,tor*ang,,,,,,
PROD,7,4,4,,ang**2,,,,,,
VGET,ROT(1),4,
VGET,TOR(1),5,
VGET,TA(1),6,
VGET,AA(1),7,
*VSCFUN,TORSUM,SUM,TOR(4)
*VSCFUN,ROTSUM,SUM,ROT(4)
*VSCFUN,TASUM,SUM,TA(4)
*VSCFUN,AASUM,SUM,AA(4)
KFG(%FNAM%)=(((ROTSUM*TORSUM)/9)-
TASUM)/(((ROTSUM**2)/9)-AASUM)
```

! In relation to the pinion reference frame, the combined torsional mesh stiffness of gear is generated by restrained the pinion from rotating, while the gear having the input load and the resulting angular rotation of the gear and torque is computed.

! Restraints all DOF at master couple node of the pinion hub. Applying load to gear hub by defines DOF constraints to master couple node of the gear hub. Then specifies optimized nonlinear solution and some enhanced internal solution algorithms, such as number of substeps, etc.

! Computes the angle of rotation and torque in each substeps of the gear. Then compute the combined torsional meshes stiffness of the gear by defines the gradient of relationship between torque and angle of rotation. The result also redirects save to a file in specific directory. The further analysis of gradient of the combined torsional mesh stiffness is done in Microsoft Excel.

```
/OUTPUT,KFG%FNAM%,txt,,
PRVAR,4,5, , , , ,
/OUTPUT, TERM
FINISH
FNAM=FNAM+1
*IF,FNAM,EQ,41,:ENDLOOP
PARSAV,ALL,ANGLE_C0,,                ! Write all parameter to file.
*GO,:DOLOOP                          ! Go back to: DOLOOP line action.
:ENDLOOP                             ! End a do-loop when completed a cyclic
FINISH                               mesh.
!* End of program
```

APPENDIX C

LISTING OF AN ANSYS PARAMETRIC DESIGN LANGUAGE PROGRAM FOR THE NORMAL CONTACT STIFFNESS AND TORSIONAL MESH STIFFNESS OF DAMAGED GEARS IN MESH

```
/GST,ON                    ! Turns graphical solution tracking on
!*
*DIM,ROT, ,12,1,1,         ! ROT(),TOR(),TA(), and AA() are array
*DIM,TOR, ,12,1,1,         parameter for computing the combined
*DIM,TA, ,12,1,1,          torsional mesh stiffness.
*DIM,AA, ,12,1,1,
!*
*DIM,KMG, ,69              ! Pinion torsional mesh stiffness, KMG().
*DIM,KFG, ,69              ! Gear torsional mesh stiffness, KFG().
!*
*DIM,FGC, ,69              ! FGC( ) and MGC( ) are array parameter
*DIM,MGC, ,69              of master couple node number of gear and
!*                         pinion respectively
*DIM,KMG1, ,69             ! KMG1(), KMG2(), KFG1( ), and KFG2(
```

```
*DIM,KMG2, ,69
*DIM,KFG1, ,69
*DIM,KFG2, ,69
!*
*DIM,KN, ,69
!*
*DIM,ANG, ,69
ANG(1)=0.0,1.1575,2.315,3.4725,3.6171875
ANG(6)=3.761875, 3.9065625,3.97890625
ANG(9)=4.015078125,4.033164063,4.05125
ANG(12)=4.1959375,4.340625,4.4853125,4.63
ANG(16)=4.7746875, 4.919375,5.0640625
ANG(19)=5.20875,5.226835937,5.244921875
ANG(22)=5.28109375,5.3534375,5.498125
ANG(25)=5.6428125,5.7875, 6.945,8.1025
ANG(29)=9.26,9.27,9.6595, 10.059,10.858,11.657
ANG(35)=12.456,13.255, 14.054,14.853,15.2525
ANG(40)=15.642, 15.652,16.8095,17.967,19.1245
ANG(45)=19.2691875,19.413875, 19.5585625
ANG(48)=19.63090625,19.66707813,19.68516406
ANG(51)=19.70325, 19.8479375,19.992625
ANG(54)= 20.1373125,20.282,20.4266875
ANG(57)=20.571375,20.7160625,20.86075
ANG(60)=20.87883594,20.89692188, 20.93309375
ANG(63)=21.0054375,21.150125,21.2948125
ANG(66)=21.4395,22.597,23.7545,24.912
FNAM=1
PARSAV,ALL,ANGLE_C5,,
:DOLOOP
RESUME,m1c5,db,,
PARRES, ,ANGLE_C5,, ,,
/PREP7
TYPE,1,
MAT,1,
REAL,1,
ESYS,0,
CSYS,1
PENN=1E-5
ASEL,S,LOC,X,0,.069
AGEN, ,ALL, , , ,ANG(%FNAM%), , , ,1
```

) are array parameter of the keypoints number at the contact point of the first pair and second pair of pinion and gear respectively.

! KN() is combined normal contact stiffness in each meshing position.

! Defines, ANG(), an array parameter and its dimensions of meshing position.

! Angle array parameter of meshing position in one complete cyclic mesh is 24.912 degrees. Actually, you can analyses any meshing position within cyclic mesh.

! Sets initial meshing position.

! Write all parameter to file

! :DOLOOP of meshing position in a cyclic. Resumes the model and database and replace current parameter set with all scalar and array parameter from file then enters the model creation preprocessor.

! Sets the element type, element material, element real constant, and element coordinate system

! PENN is Lagrange multipliers.

! Select a subset areas of the pinion only then rotate FE model through particular

```
ALLSEL,ALL                                  meshing position in degrees
CSYS,11,
ASEL,S,LOC,X,0,.069                         ! Select a subset areas of the gear only
AGEN, ,ALL, , , ,-ANG(%FNAM%), , , ,1       then rotate FE model through particular
ALLSEL,ALL                                  meshing position in degrees
*IF,FNAM,EQ,1,THEN
*GO,:LOOP1                                  ! LOOP1 for initial double pair contact
*ELSEIF,FNAM,EQ,41
*GO,:LOOP5                                  ! loop5 for meshing geometry as loop1.
*ELSEIF,FNAM,EQ,69
*GO,:LOOP7                                  ! loop7 for recess of cracked pinion tooth.
*ELSEIF,FNAM,EQ,29
*GO,:LOOP3                                  ! LOOP3 for recess double pair contact
*ELSEIF,FNAM,GE,42
*GO,:LOOP6                                  ! LOOP6 for double pair contact zone
*ELSEIF,FNAM,GE,30
*GO,:LOOP4                                  ! LOOP4 for single pair contact
*ELSEIF,FNAM,GE,2
*GO,:LOOP2                                  ! LOOP2 for double pair contact zone.
*ENDIF
!* Start LOOP1 for initial double pair contact
:LOOP1
.....
.....                                       ! See LOOP1 of Appendix B
.....
*GO,:MLOOP2
!* Start LOOP2 for double pair contact zone
:LOOP2
.....
.....                                       ! See LOOP2 of Appendix B
.....
*GO,:MLOOP2
!* Start LOOP3 for recess double pair contact
:LOOP3
.....
.....                                       ! See LOOP3 of Appendix B
.....
*GO,:MLOOP2
!* Start LOOP4 for single pair contact
:LOOP4
```

```
.....
.....                                   ! See LOOP4 of Appendix B
.....
*GO,:MLOOP1
!* Start LOOP5 for other pair come into double pair
contact zone like meshing position 1.
:LOOP5
CSYS,1
ACLEAR,90                               ! Delete nodes and elements associated
ACLEAR,2                                with selected areas of teeth in double pair
ACLEAR,92                               contact
ACLEAR,46
NUMSTR,KP,500,                          ! Establishes starting numbers of keypoint
KMG1(%FNAM%)=500                        and line number. Specifies the divisions
NUMSTR,LINE,500,                        and spacing ratio on unmeshed lines of
LSBL,1,4, ,DELETE,KEEP                  first pair contact tooth of pinion then mesh
LESIZE,500,0.001, , ,1,                 tooth area and groups potential contact
LESIZE,501,0.001, , ,1,                 nodes.
LCCAT,500,501                           ! One of the most important criteria for
AMESH,90                                each meshing position was that the first
LSEL,S, , ,500,501,                     potential contact nodes of both particular
NSLL,S,1                                contact tooth must be created exactly on
CM,nmg1,NODE                            the intersection point between the pressure
ALLSEL,ALL                              line and the involute curve.
NUMSTR,KP,600,                          ! Establishes starting numbers of keypoint
KFG1(%FNAM%)=600                        and line number. Specifies the divisions
NUMSTR,LINE,600,                        and spacing ratio on unmeshed lines of
LSBL,3,4, ,DELETE,KEEP                  first pair contact tooth of gear then mesh
LESIZE,600,0.001, , ,1,                 tooth area and groups potential contact
LESIZE,601,0.001, , ,1,                 nodes of this tooth into component for
LCCAT,600,601                           further generate contact elements
AMESH,2
LSEL,S, , ,600,601,
NSLL,S,1
CM,nfg1,NODE
ALLSEL,ALL
NUMSTR,KP,700,                          ! Establishes starting numbers of keypoint
KMG2(%FNAM%)=700                        and line number. Specifies the divisions
NUMSTR,LINE,700,                        and spacing ratio on unmeshed lines of
LSBL,370,4, ,DELETE,KEEP                second pair contact tooth of pinion then
```

```
LESIZE,700,0.001, , ,1,
LESIZE,701,0.001, , ,1,
LCCAT,700,701
AMESH,92
LSEL,S, , ,700,701,
NSLL,S,1
CM,nmg2,NODE
ALLSEL,ALL
KFG2(%FNAM%)=280
LESIZE,380,0.001, , ,1,
AMESH,46
LSEL,S, , ,380,
NSLL,S,1
CM,nfg2,NODE
ALLSEL,ALL
*GO,:MLOOP2
!* Start LOOP6 for double pair contact zone like meshing position 2-28.
:LOOP6
CSYS,1
ACLEAR,90
ACLEAR,2
ACLEAR,92
ACLEAR,46
NUMSTR,KP,500,
KMG1(%FNAM%)=500
NUMSTR,LINE,500,
LSBL,1,4, ,DELETE,KEEP
LESIZE,500,0.001, , ,1,
LESIZE,501,0.001, , ,1,
LCCAT,500,501
AMESH,90
LSEL,S, , ,500,501,
NSLL,S,1
CM,nmg1,NODE
ALLSEL,ALL
NUMSTR,KP,600,
KFG1(%FNAM%)=600
NUMSTR,LINE,600,
LSBL,3,4, ,DELETE,KEEP
```

mesh tooth area and groups potential contact nodes of this tooth into component for further generate contact elements.

! Defines contact keypoint number of second pair of the gear. Specifies the divisions and spacing ratio on unmeshed lines of second pair contact tooth of gear then mesh tooth area and groups potential contact nodes of this tooth into component for further generate contact elements.

! Delete nodes and elements associated with selected areas of teeth in double pair contact

! Establishes starting numbers of keypoint and line number. Specifies the divisions and spacing ratio on unmeshed lines of first pair contact tooth of pinion and concatenates multiple lines into one line for mapped meshing then mesh tooth area and groups potential contact nodes of this tooth into component for further generate contact elements.

! Establishes starting numbers of keypoint and line number. Specifies the divisions and spacing ratio on unmeshed lines of first pair contact tooth of gear and

```
LESIZE,600,0.001, , ,1,
LESIZE,601,0.001, , ,1,
LCCAT,600,601
AMESH,2
LSEL,S, , ,600,601,
NSLL,S,1
CM,nfg1,NODE
ALLSEL,ALL
NUMSTR,KP,700,
KMG2(%FNAM%)=700
NUMSTR,LINE,700,
LSBL,370,4, ,DELETE,KEEP
LESIZE,700,0.001, , ,1,
LESIZE,701,0.001, , ,1,
LCCAT,700,701
AMESH,92
LSEL,S, , ,700,701,
NSLL,S,1
CM,nmg2,NODE
ALLSEL,ALL
NUMSTR,KP,800,
KFG2(%FNAM%)=800
NUMSTR,LINE,800,
LSBL,380,4, ,DELETE,KEEP
LESIZE,800,0.001, , ,1,
LESIZE,801,0.001, , ,1,
LCCAT,800,801
AMESH,46
LSEL,S, , ,800,801,
NSLL,S,1
CM,nfg2,NODE
ALLSEL,ALL
*GO,:MLOOP2
!* Start LOOP7 for recess of damage pinion tooth
like meshing position 29.
:LOOP7
CSYS,1
ACLEAR,90
ACLEAR,2
ACLEAR,92
```

concatenates multiple lines into one line for mapped meshing then mesh tooth area and groups potential contact nodes of this tooth into component for further generate contact elements

! Establishes starting numbers of keypoint and line number. Specifies the divisions and spacing ratio on unmeshed lines of second pair contact tooth of pinion and concatenates multiple lines into one line for mapped meshing then mesh tooth area and groups potential contact nodes of this tooth into component for further generate contact elements.

! Establishes starting numbers of keypoint and line number. Specifies the divisions and spacing ratio on unmeshed lines of second pair contact tooth of gear and concatenates multiple lines into one line for mapped meshing then mesh tooth area and groups potential contact nodes of this tooth into component for further generate contact elements.

! Delete nodes and elements associated with selected areas of teeth in double pair contact

```
ACLEAR,46
KMG1(%FNAM%)=3
LESIZE,1,0.001, , ,1,
AMESH,90
LSEL,S, , ,1,
NSLL,S,1
CM,nmg1,NODE
ALLSEL,ALL
NUMSTR,KP,600,
KFG1(%FNAM%)=600
NUMSTR,LINE,600,
LSBL,3,4, ,DELETE,KEEP
LESIZE,600,0.001, , ,1,
LESIZE,601,0.001, , ,1,
LCCAT,600,601
AMESH,2
LSEL,S, , ,600,601,
NSLL,S,1
CM,nfg1,NODE
ALLSEL,ALL
NUMSTR,KP,700,
KMG2(%FNAM%)=700
NUMSTR,LINE,700,
LSBL,370,4, ,DELETE,KEEP
LESIZE,700,0.001, , ,1,
LESIZE,701,0.001, , ,1,
LCCAT,700,701
AMESH,92
LSEL,S, , ,700,701,
NSLL,S,1
CM,nmg2,NODE
ALLSEL,ALL
NUMSTR,KP,800,
KFG2(%FNAM%)=800
NUMSTR,LINE,800,
LSBL,380,4, ,DELETE,KEEP
LESIZE,800,0.001, , ,1,
LESIZE,801,0.001, , ,1,
LCCAT,800,801
AMESH,46
```

! Defines contact keypoint number of first pair of the pinion. Specifies the divisions and spacing ratio on unmeshed lines of first pair contact tooth of pinion then mesh tooth area and groups potential contact nodes of this tooth into component for further generate contact elements.

! Establishes starting numbers of keypoint and line number. Specifies the divisions and spacing ratio on unmeshed lines of first pair contact tooth of gear and concatenates multiple lines into one line for mapped meshing then mesh tooth area and groups potential contact nodes of this tooth into component for further generate contact elements

! Establishes starting numbers of keypoint and line number. Specifies the divisions and spacing ratio on unmeshed lines of second pair contact tooth of pinion and concatenates multiple lines into one line for mapped meshing then mesh tooth area and groups potential contact nodes of this tooth into component for further generate contact elements.

! Establishes starting numbers of keypoint and line number. Specifies the divisions and spacing ratio on unmeshed lines of second pair contact tooth of gear and concatenates multiple lines into one line for mapped meshing then mesh tooth area and groups potential contact nodes of this tooth into component for further generate

```
LSEL,S, , ,800,801,                    contact elements.
NSLL,S,1
CM,nfg2,NODE
ALLSEL,ALL
*GO,:MLOOP2
!*Start of MLOOP2 generates contact element for
double pair contact zone.
:MLOOP2
.....
.....                                  ! See MLOOP2 of Appendix B
.....
!*Start at MLOOP1 generates contact element for
single pair contact zone.
:MLOOP1
.....
.....                                  ! See MLOOP1 of Appendix B
.....
!*Start main loop, MLOOP3, for compute combine
normal contact stiffness.
:MLOOP3
.....
.....                                  ! See MLOOP3 of Appendix B
.....
!* Start main loop, MLOOP4, deletes DOF
restraints at contact keypoint, sets element key
options, and defines the element real constants with
Lagrange multiplier.
:MLOOP4
.....
.....                                  ! See MLOOP4 of Appendix B
.....
!*Define the combined torsional mesh stiffness of
the pinion.
:MLOOP5
.....
.....                                  ! See MLOOP5 of Appendix B
.....
!*Define the combined torsional mesh stiffness of
the gear
:MLOOP6
```

```
.....
.....                                   ! See MLOOP6 of Appendix B
.....
FINISH
FNAM=FNAM+1                             ! Sets next meshing position.
*IF,FNAM,EQ,70,:ENDLOOP
PARSAV,ALL,ANGLE_C5,,                   ! Write all parameter to file.
*GO,:DOLOOP                             ! Go back to :DOLLOP line action.
:ENDLOOP                                ! End a do-loop when completed a cyclic
FINISH                                  mesh.
!* End of program
```

APPENDIX D

LISTING OF AN ANSYS PARAMETRIC DESIGN LANGUAGE PROGRAM FOR THE STATIC TRANSMISSION ERROR AND LOAD SHARING RATIO OF UNDAMAGED GEARS IN MESH

```
/GST,ON
*DIM,ANG, ,69
ANG(1)=0.0,1.1575,2.315,3.4725,3.6171875
ANG(6)=3.761875, 3.9065625,3.97890625
ANG(9)=4.015078125,4.033164063,4.05125
ANG(12)=4.1959375,4.340625,4.4853125,4.63
ANG(16)=4.7746875, 4.919375,5.0640625
ANG(19)=5.20875,5.226835937,5.244921875
ANG(22)=5.28109375,5.3534375,5.498125
ANG(25)=5.6428125,5.7875, 6.945,8.1025
ANG(29)=9.26,9.27,9.6595, 10.059,10.858,11.657
ANG(35)=12.456,13.255, 14.054,14.853,15.2525
ANG(40)=15.642, 15.652,16.8095,17.967,19.1245
ANG(45)=19.2691875,19.413875, 19.5585625
```

! Turns graphical solution tracking on

! Defines an array parameter and its dimensions of meshing position.

! Angle array parameter of meshing position in one complete cyclic mesh is 24.912 degrees. Actually, you can analyse any meshing position within the cyclic mesh.

```
ANG(48)=19.63090625,19.66707813,19.68516406
ANG(51)=19.70325, 19.8479375,19.992625
ANG(54)= 20.1373125,20.282,20.4266875
ANG(57)=20.571375,20.7160625,20.86075
ANG(60)=20.87883594,20.89692188, 20.93309375
ANG(63)=21.0054375,21.150125,21.2948125
ANG(66)=21.4395,22.597,23.7545,24.912
*DIM,FGC, ,69                    ! FGC( ) and MGC( ) are array parameter
*DIM,MGC, ,69                    of master couple node number of gear
!*                               and pinion respectively
*DIM,KMG1, ,69                   ! KMG1( ), KMG2( ), KFG1( ), and
*DIM,KMG2, ,69                   KFG2( ) are array parameter of the
*DIM,KFG1, ,69                   keypoints number at the contact point of
*DIM,KFG2, ,69                   the first pair and second pair of pinion
!*                               and gear respectively.
*DIM,TE,,69,4,1                  ! TE( ) is the transmission error, rad.
*DIM,FXP1,,69,4,1                ! FXP1( ), FYP1( ), FXP2( ), FYP2( )
*DIM,FYP1,,69,4,1                FXG1( ), FYG1( ), FXG2( ), and FYG2( )
*DIM,FXP2,,69,4,1                are reaction force in global Cartesian
*DIM,FYP2,,69,4,1                coordinate system at contact nodes of
*DIM,FXG1,,69,4,1                pinion and gear for first and second pair
*DIM,FYG1,,69,4,1                contact respectively, N.
*DIM,FXG2,,69,4,1
*DIM,FYG2,,69,4,1
*DIM,FNP1,,69,4,1                ! FNP1() and FNP2() are normal reaction
*DIM,FNP2,,69,4,1                forces of first and second pinion pair
!*                               contact respectively, N.
*DIM,FN_T1,,69,4,1               ! FN_T1() and FN_T2() are load sharing
*DIM,FN_T2,,69,4,1               ratio of the first and second pair contact
!*                               respectively, N.
*DIM,KN, ,69                     ! KN() is combined normal contact
!*                               stiffness in each meshing position.
*DIM,MZP,,69,4,1                 ! MZP( ), MZG( ) are the total applied
*DIM,MZG,,69,4,1                 torque of the pinion and gear
!*                               respectively, N.m.
*DIM,ANGP,,69,4,1                ! ANGP( ), ANGG( ) are The transverse
*DIM,ANGG,,69,4,1                plane angular rotation of the pinion and
!*                               gear body respectively, rad.
COL=1                            ! Sets initial varying load and meshing
FNAM=1                           position.
```

```
PARSAV,ALL,TE_C0,,                          ! Write all parameter to file
:DOLOOP                                     ! :DOLOOP of meshing position.
RESUME,m1c0,db,,                            ! Resumes the model and database.
PARRES,,TE_C0,, ,,                          ! Replaces current parameter set.
UYI=1E-10                                   ! UYI is nonzero initial pre-displacement.
FYP=200000*COL                              FYP is force loads at master couple node
PENN=1E-5                                   of pinion. PENN is Lagrange multipliers.
/PREP7
TYPE,1,                                     ! Sets the element type, element material,
MAT,1,                                      element real constant, and element
REAL,1,                                     coordinate system
ESYS,0,
CSYS,1
ASEL,S,LOC,X,0,.069                         ! Select a subset areas of the pinion only
AGEN, ,ALL, , , ,ANG(%FNAM%), , , ,1        then rotate FE model through particular
ALLSEL,ALL                                  meshing position in degrees
CSYS,11,
ASEL,S,LOC,X,0,.069                         ! Select a subset areas of the gear only
AGEN, ,ALL, , , ,-ANG(%FNAM%), , , ,1       then rotate FE model through particular
ALLSEL,ALL                                  meshing position in degrees
*IF,FNAM,EQ,1,THEN
*GO,:LOOP1                                  ! LOOP1 for initial double pair contact
*ELSEIF,FNAM,EQ,29
*GO,:LOOP3                                  ! LOOP3 for recess double pair contact
*ELSEIF,FNAM,GE,30
*GO,:LOOP4                                  ! LOOP4 for single pair contact
*ELSEIF,FNAM,GE,2
*GO,:LOOP2                                  ! LOOP2 for double pair contact zone
*ENDIF
!* Start LOOP1 for initial double pair contact
:LOOP1
.....
.....                                       ! See LOOP1 of Appendix B
.....
*GO,:MLOOP2
!* Start LOOP2 of double pair contact zone
:LOOP2
.....
.....                                       ! See LOOP2 of Appendix B
.....
```

*GO,:MLOOP2

!* Start LOOP3 for recess double pair contact

:LOOP3

.....

..... **! See LOOP3 of Appendix B**

.....

*GO,:MLOOP2

!* Start LOOP4 of single pair contact

:LOOP4

.....

..... **! See LOOP4 of Appendix B**

.....

*GO,:MLOOP1

!*Start main loop 1 and 2 for generates contact element. For double pair contact zone use MLOOP2.

:MLOOP2

.....

..... **! See MLOOP2 of Appendix B**

.....

!*Start MLOOP1 generates contact element for single pair contact zone.

:MLOOP1

.....

..... **! See MLOOP1 of Appendix B**

.....

!*Start main loop, MLOOP3, for compute combine normal contact stiffness.

:MLOOP3

.....

..... **! See MLOOP3 of Appendix B**

.....

!* Start main loop, MLOOP4, deletes DOF restraints at contact keypoint, sets element key options, and defines the element real constants with Lagrange multiplier.

:MLOOP4

.....

..... **! See MLOOP4 of Appendix B**

.....

```
FINISH
!*Start main loop, MLOOP5, for compute angular rotation of the pinion hub and the load sharing ratio.
:MLOOP5
/SOLU
CSYS,1
ANTYPE,STATIC
D,FGC(%FNAM%), ,0, , , ,ALL
D,MGC(%FNAM%), ,0, , , ,UX
D,MGC(%FNAM%), ,UYI, , , ,UY
SOLCON,ON
OUTRES,ALL,ALL,
NSUBST,1,,,0
SOLVE
DDELE,MGC(%FNAM%),UY,
F,MGC(%FNAM%),FY,FYP,
NSUBST,20,,,0
SOLVE
FINISH
/POST1
SET,LAST
RSYS,1
ESLA,S
*IF,FNAM,GE,30,THEN
*IF,FNAM,LE,40,THEN
*GO,:MLOOPP2
*ENDIF
*ENDIF
CMSEL,S,NMG1
FSUM
*GET,FXP1(FNAM,COL,1),FSUM,0,ITEM,FX
*GET,FYP1(FNAM,COL,1),FSUM,0,ITEM,FY
*GET,MZP1,FSUM,0,ITEM,MZ
ALLSEL,ALL
ESLA,S
*AFUN,DEG
FNP1(FNAM,COL,1)=ABS(FXP1(FNAM,COL,1)*
COS(20))+ABS(FYP1(FNAM,COL,1)*COS(70))
*AFUN,RAD
:MLOOPP2
```

! The procedure of how to computed transmission error and load sharing ratio is, firstly, restrained the gear hub from rotating then input load to pinion hub.

! Activates a cylindrical coordinate system of the pinion.

! Restraints all DOF at FGC().

! Restraints DOF in radian-axis at MGC()

! Defines initial pre-defines DOF constraints at master couple node of the pinion hub and solve in single iteration.

! Deletes initial pre-defines DOF constraints at master couple node of the pinion hub then defines tangential force at master couple node of the pinion hub.

! Defines the last data set to be read from the results file.

! Conditionally skips commands to :MLOOPP2 for single pair contact zone.

! Selects a subset of potential nodes on the pinion tooth of first pair contact.

! Retrieves sum force values, FXP1( ) and FYP1( ), of the contact nodal force in global Cartesian coordinate system and sum moment values, MZP1, due to these nodal forces.

! Computes the normal forces to the tooth surface.

```
CMSEL,S,NMG2                                    ! Selects a subset of potential nodes on
FSUM                                            the pinion tooth of second pair contact.
*GET,FXP2(FNAM,COL,1),FSUM,0,ITEM,FX            ! Retrieves sum force values, FXP2( ) and
*GET,FYP2(FNAM,COL,1),FSUM,0,ITEM,FY            FYP2( ), of the contact nodal force in
*GET,MZP2,FSUM,0,ITEM,MZ                        global Cartesian coordinate system and
ALLSEL,ALL                                      sum moment values, MZP2, due to these
*AFUN,DEG                                       nodal forces.
FNP2(FNAM,COL,1)=ABS(FXP2(FNAM,COL,1)*          ! Computes the normal forces to the tooth
COS(20))+ABS(FYP2(FNAM,COL,1)*COS(70))          surface.
*AFUN,RAD
FN_TOTAL=FNP1(FNAM,COL,1)+FNP2(FNAM,            ! Computes total of the normal forces.
COL,1)
FN_T1(FNAM,COL,1)=FNP1(FNAM,COL,1)/FN_          ! Computes load sharing ratio on the first
TOTAL                                           pair.
FN_T2(FNAM,COL,1)=FNP2(FNAM,COL,1)/FN_          ! Computes load sharing ratio on the
TOTAL                                           second pair.
RSYS,11
ESLA,S
*IF,FNAM,GE,30,THEN                             ! Conditionally skips commands to
*IF,FNAM,LE,40,THEN                             :MLOOPG2 for single pair contact zone.
*GO,:MLOOPG2
*ENDIF
*ENDIF
CMSEL,S,NFG1                                    ! Selects a subset of potential nodes on
SPOINT, ,0,.138,0,                              the gear tooth of first pair contact.
FSUM                                            ! Retrieves sum force values, FXG1( )
*GET,FXG1(FNAM,COL,1),FSUM,0,ITEM,FX            and FYG1( ), of the contact nodal force
*GET,FYG1(FNAM,COL,1),FSUM,0,ITEM,FY            in global Cartesian coordinate system and
*GET,MZG1,FSUM,0,ITEM,MZ                        sum moment values, MZG1, due to these
ALLSEL,ALL                                      nodal forces.
ESLA,S
:MLOOPG2
CMSEL,S,NFG2                                    ! Selects a subset of potential nodes on
FSUM                                            the gear tooth of second pair contact.
*GET,FXG2(FNAM,COL,1),FSUM,0,ITEM,FX            ! Retrieves sum force values, FXG2( )
*GET,FYG2(FNAM,COL,1),FSUM,0,ITEM,FY            and FYG2( ), of the contact nodal force
*GET,MZG2,FSUM,0,ITEM,MZ                        in global Cartesian coordinate system and
ALLSEL,ALL                                      sum moment values, MZG2, due to these
RESET                                           nodal forces.
MZP(FNAM,COL,1)=MZP1+MZP2                       ! Computes total pinion torque.
```

```
MZG(FNAM,COL,1)=MZG1+MZG2                    ! Computes total gear torque.
FYG=MZG(FNAM,COL,1)/0.0127                   ! Computes equivalent tangential force at
RSYS,1                                       the gear hub.
*GET,UYP,NODE,MGC(%FNAM%),U,SUM              ! Retrieves displacement of the pinion
ANGP(FNAM,COL,1)=UYP/.0127                   hub then computes angular rotation of the
FINISH                                       pinion hub.
!*Start main loop, MLOOP6, for compute angular ! In relation to the pinion reference frame,
rotation of the gear hub and the static transmission the angular rotation of the gear hub is
error of gear mesh.                          generated by restrained the pinion from
!*                                           rotating, while the gear having the input
:MLOOP6                                      load and the resulting angular rotation of
/SOLU                                        the gear is computed.
DDELE,ALL,ALL                                ! Deletes all DOF constraints.
CSYS,11                                      ! Activates a local cylindrical coordinate
ANTYPE,STATIC                                system of the gear.
D,MGC(%FNAM%), ,0, , , ,ALL                  ! Restraints all DOF at MGC().
D,FGC(%FNAM%), ,0, , , ,UX                   ! Restraints DOF in radian-axis at FGC().
D,FGC(%FNAM%), ,UYI, , , ,UY                 ! Defines initial pre-defines DOF
OUTRES,BASIC,ALL,                            constraints at master couple node of the
SOLCON,ON                                    gear hub and solve in single iteration.
OUTRES,ALL,ALL,
NSUBST,1,,,0
SOLVE
DDELE,FGC(%FNAM%),UY,                        ! Deletes initial pre-defines DOF
F,FGC(%FNAM%),FY,FYG,                        constraints at master couple node of the
NSUBST,20,,,0                                gear hub then defines equivalent
SOLVE                                        tangential force at master couple node of
FINISH                                       the gear hub.
/POST1
SET,LAST                                     ! Defines the last data set to be read from
RSYS,11                                      the result file.
*GET,UYG,NODE,FGC(%FNAM%),U,SUM              ! Retrieves a displacement value of the
ANGG(FNAM,COL,1)=UYG/.0127                   gear hub, UYG, then computed angular
AG=ANGG(FNAM,COL,1)                          rotation of the gear hub, ANGG ().
AP=ANGP(FNAM,COL,1)
TE(FNAM,COL,1)=(AG+AP)/2                     ! Computed the transmission error at each
FINISH                                       particular meshing position, TE ().
FNAM=FNAM+1
*IF,FNAM,EQ,70,THEN                          ! Sets next meshing position.
FNAM=1                                       ! If completed cyclic mesh.
```

```
COL=COL+1
*ENDIF                          ! Sets different input value load.
*IF,COL,EQ,5,:ENDLOOP           ! If completed varying load end program.
PARSAV,ALL,TE_C0,,              ! Write all parameter to file.
*GO,:DOLOOP                     ! Go back to :DOLOOP line action.
:ENDLOOP                        ! End a do-loop when completed a cyclic
FINISH                          mesh.
!* End of program
```

APPENDIX E

LISTING OF AN ANSYS PARAMETRIC DESIGN LANGUAGE PROGRAM FOR THE STATIC TRANSMISSION ERROR AND LOAD SHARING RATIO OF A DAMAGED TOOTH IN MESH

```
/GST,ON
*DIM,ANG, ,69
ANG(1)=0.0,1.1575,2.315,3.4725,3.6171875
ANG(6)=3.761875, 3.9065625,3.97890625
ANG(9)=4.015078125,4.033164063,4.05125
ANG(12)=4.1959375,4.340625,4.4853125,4.63
ANG(16)=4.7746875, 4.919375,5.0640625
ANG(19)=5.20875,5.226835937,5.244921875
ANG(22)=5.28109375,5.3534375,5.498125
ANG(25)=5.6428125,5.7875, 6.945,8.1025
ANG(29)=9.26,9.27,9.6595, 10.059,10.858,11.657
ANG(35)=12.456,13.255, 14.054,14.853,15.2525
ANG(40)=15.642, 15.652,16.8095,17.967,19.1245
ANG(45)=19.2691875,19.413875, 19.5585625
```

! Turns graphical solution tracking on

! Defines an array parameter and its dimensions of meshing position.

! Angle array parameter of meshing position in one complete cyclic mesh is 24.912 degrees. Actually, you can analyse any meshing position within cyclic mesh.

```
ANG(48)=19.63090625,19.66707813,19.68516406
ANG(51)=19.70325, 19.8479375,19.992625
ANG(54)= 20.1373125,20.282,20.4266875
ANG(57)=20.571375,20.7160625,20.86075
ANG(60)=20.87883594,20.89692188, 20.93309375
ANG(63)=21.0054375,21.150125,21.2948125
ANG(66)=21.4395,22.597,23.7545,24.912
*DIM,FGC, ,69                    ! FGC( ) and MGC( ) are array parameter
*DIM,MGC, ,69                    of master couple node number of gear and
!*                               pinion respectively
*DIM,KMG1, ,69                   ! KMG1( ), KMG2( ), KFG1( ), and
*DIM,KMG2, ,69                   KFG2( ) are array parameter of the
*DIM,KFG1, ,69                   keypoints number at the contact point of
*DIM,KFG2, ,69                   the first pair and second pair of pinion and
!*                               gear respectively.
*DIM,TE,,69,4,1                  ! TE( ) is the transmission error, rad.
*DIM,FXP1,,69,4,1                ! FXP1( ), FYP1( ), FXP2( ), FYP2( )
*DIM,FYP1,,69,4,1                FXG1( ), FYG1( ), FXG2( ), and FYG2( )
*DIM,FXP2,,69,4,1                are reaction force in global Cartesian
*DIM,FYP2,,69,4,1                coordinate system at contact nodes of
*DIM,FXG1,,69,4,1                pinion and gear for first and second pair
*DIM,FYG1,,69,4,1                contact respectively, N.
*DIM,FXG2,,69,4,1
*DIM,FYG2,,69,4,1
*DIM,FNP1,,69,4,1                ! FNP1() and FNP2() are normal reaction
*DIM,FNP2,,69,4,1                forces of first and second pinion pair
!*                               contact respectively, N.
*DIM,FN_T1,,69,4,1               ! FN_T1() and FN_T2() are load sharing
*DIM,FN_T2,,69,4,1               ratio of the first and second pair contact
!*                               respectively, N.
*DIM,KN, ,69                     KN() is combined normal contact stiffness
!*                               in each meshing position.
*DIM,MZP,,69,4,1                 ! MZP( ), MZG( ) are the total applied
*DIM,MZG,,69,4,1                 torque of the pinion and gear respectively,
!*                               N.m.
*DIM,ANGP,,69,4,1                ! ANGP( ), ANGG( ) are The transverse
*DIM,ANGG,,69,4,1                plane angular rotation of the pinion and
!*                               gear body respectively, rad.
COL=1                            ! Sets initial varying load and meshing
FNAM=1                           position.
```

```
PARSAV,ALL,TE_C5,,                          ! Write all parameter to file
:DOLOOP                                     ! :DOLOOP of meshing position.
RESUME,m1c0,db,,                            ! Resumes the model and database.
PARRES,,TE_C5,, ,,                          ! Replaces current parameter set.
UYI=1E-10                                   ! UYI is nonzero initial pre-displacement.
FYP=200000*COL                              FYP is force loads at master couple node
PENN=1E-5                                   of pinion. PENN is Lagrange multipliers.
/PREP7
TYPE,1,                                     ! Sets the element type, element material,
MAT,1,                                      element real constant, and element
REAL,1,                                     coordinate system
ESYS,0,
CSYS,1
ASEL,S,LOC,X,0,.069                         ! Select a subset areas of the pinion only
AGEN, ,ALL, , , ,ANG(%FNAM%), , , ,1        then rotate FE model through particular
ALLSEL,ALL                                  meshing position in degrees
CSYS,11,
ASEL,S,LOC,X,0,.069                         ! Select a subset areas of the gear only
AGEN, ,ALL, , , ,-ANG(%FNAM%), , , ,1       then rotate FE model through particular
ALLSEL,ALL                                  meshing position in degrees
*IF,FNAM,EQ,1,THEN
*GO,:LOOP1                                  ! LOOP1 for initial double pair contact
*ELSEIF,FNAM,EQ,41
*GO,:LOOP5                                  ! loop5 for meshing geometry as loop1.
*ELSEIF,FNAM,EQ,69
*GO,:LOOP7                                  ! loop7 for recess of cracked pinion tooth.
*ELSEIF,FNAM,EQ,29
*GO,:LOOP3                                  ! LOOP3 for recess double pair contact
*ELSEIF,FNAM,GE,42
*GO,:LOOP6                                  ! LOOP6 for double pair contact zone
*ELSEIF,FNAM,GE,30
*GO,:LOOP4                                  ! LOOP4 for single pair contact
*ELSEIF,FNAM,GE,2
*GO,:LOOP2                                  ! LOOP2 for double pair contact zone.
*ENDIF
!* Start LOOP1 for initial double pair contact
:LOOP1
.....
.....                                       ! See LOOP1 of Appendix B
.....
```

*GO,:MLOOP2

!* Start LOOP2 for double pair contact zone

:LOOP2

.....

..... **! See LOOP2 of Appendix B**

.....

*GO,:MLOOP2

!* Start LOOP3 for recess double pair contact

:LOOP3

.....

..... **! See LOOP3 of Appendix B**

.....

*GO,:MLOOP2

!* Start LOOP4 for single pair contact

:LOOP4

.....

..... **! See LOOP4 of Appendix D**

.....

*GO,:MLOOP1

!* Start LOOP5 for other pair come into double pair contact zone like meshing position 1.

:LOOP5

.....

..... **! See LOOP5 of Appendix C**

.....

*GO,:MLOOP2

!* Start LOOP6 for double pair contact zone like meshing position 2-28.

:LOOP6

.....

..... **! See LOOP6 of Appendix C**

.....

*GO,:MLOOP2

!* Start LOOP7 for recess of damage pinion tooth like meshing position 29.

:LOOP7

.....

..... **! See LOOP7 of Appendix C**

.....

*GO,:MLOOP2

!*Start main loop 1 and 2 for generates contact element. For double pair contact zone use LOOP2.

:MLOOP2

.....

..... **! See MLOOP2 of Appendix B**

.....

!*Start MLOOP1 for single pair contact zone.

:MLOOP1

.....

..... **! See MLOOP1 of Appendix B**

.....

!*Start main loop, MLOOP3, for compute combine normal contact stiffness.

:MLOOP3

.....

..... **! See MLOOP3 of Appendix B**

.....

!* Start main loop, MLOOP4, deletes DOF restraints at contact keypoint, sets element key options, and defines the element real constants with Lagrange multiplier.

:MLOOP4

.....

..... **! See MLOOP4 of Appendix B**

.....

FINISH

!*Start main loop, MLOOP5, for compute angular rotation of the pinion and load sharing ratio.

:MLOOP5

.....

..... **! See MLOOP5 of Appendix D**

.....

!*Start main loop, MLOOP6, for compute angular rotation of the gear and the static transmission error of gear mesh.

:MLOOP6

.....

..... **! See MLOOP6 of Appendix D**

.....

FINISH

```
FNAM=FNAM+1                    ! Sets next meshing position.
*IF,FNAM,EQ,70,THEN            ! If completed cyclic mesh.
FNAM=1
COL=COL+1                      ! Sets different input value load.
*ENDIF
*IF,COL,EQ,5,:ENDLOOP          ! If completed varying load end program.
PARSAV,ALL,TE_C5,,             ! Write all parameter to file.
*GO,:DOLOOP                    ! Go back to :DOLOOP line action.
:ENDLOOP                       ! End a do-loop when completed a cyclic
FINISH                         mesh.
!* End of program
```

APPENDIX F

MEASUREMENT OF THE COMBINED TORSIONAL MESH STIFFNESS

F.1 INTRODUCTION

This appendix presents data measured from a static gear test rig, (Aguilera 1995; Sirichai et al. 1996), which was designed to create a pure torque transmitted to a spur gear pair in mesh. Once the gears were pre-loaded, the known torque load was increased while the angular deflection of the spur gears was measured by a pair of optical auto-collimators. The same procedure was followed for a variety of different loads allowing a graph of torque versus angular displacement to be obtained. The relationship between torque and angular displacement was linear within the elastic range as expected. From the measurements, the static combined torsional mesh stiffness of the gear mesh at particular positions was obtained by calculating the gradient from the corresponding torque versus angular displacement relationship. By changing the meshing positions, the combined torsional mesh stiffness of the input gear during the entire meshing cycle was obtained.

In the spur involute teeth gears being studied, the load was transmitted by one and two pairs of teeth alternatively. The combined torsional mesh stiffness of the two

spur gears in mesh varied within the meshing cycle as the number and position of teeth in mesh changed from two to one tooth in contact. In general, the combined torsional mesh stiffness decreased as the meshing of the teeth changed from two to one in contact. If the gears were absolutely rigid, devoid of all inaccuracies and changes in meshing geometry were ignored, the tooth load in the zone of the double tooth contact would be half that of the single tooth contact. However, in reality the teeth become deformed under the influence of the teeth bending and shear stresses as the mesh geometry changes, and these factors alter the load variation along the path of contact. Furthermore every gear contains surface finishing and pitching errors, which alter the load variation yet again. Since the teeth are comparatively stiff, even small errors have a notable influence. The effect of the elastic tooth deformation can be shock loading. In order to avoid shock loading as the gear teeth move into and out of mesh, the tooth flanks are tip relieved. The tip reliefs are designed so that as the tooth passes through the mesh zone, the load increases uniformly and then reduces back to zero again.

The combined torsional mesh stiffness of gears is the ratio between the torsional load and the total elastic angular deflection of the gear body. Total angular deflection is defined as the angle through which a gear body turns due to bending deflection, shearing displacement and contact deformation of the gear teeth when under load. The angular deflection depends on the contacting load vector and the transverse plane contact radius vector which both factors are vary along the path of contact. Therefore the angular deflection and hence the combined torsional mesh stiffness, varies at different positions through the meshing cycle.

It appears that the gear combined torsional mesh stiffness variation has not been experimentally investigated in great detail. The primary purpose of this appendix was to measure the cyclic combined torsional mesh stiffness of the input gear of gear teeth in mesh. The static torsional test rig is presented and initial results from a test spur gear pair are discussed. A simple analytical model of the combined torsional mesh stiffness variation is also given.

F.2 ANALYTICAL MODEL

Figure F.2.1 illustrates two gears whilst in mesh along the path of contact. Two pair of teeth are in the double contact zone AB and DE, and one pair of teeth are in the single zone contact BD. The distance AD and BE corresponds to the transverse base pitch of the gears. The pinion and gear denote the driving gear and the driven gear respectively. Point A indicates the initial contact where the addendum circle of the gear (the driven gear) intersects the line of action. For involute gears the line of action is in the common tangent line to the base circles. When the first tooth pair contacts at point A, between the tooth tip of the gear and the root of the pinion, a second tooth pair is already in contact at point D. As the gear rotates, the point of contact will move along the line of action APE. When the first tooth pair reaches point B, the second tooth pair disengages at point E leaving only the first tooth pair in the single contact zone. When this first tooth pair rotates to point D the next tooth pair begins engagement at point A and starts another mesh cycle.

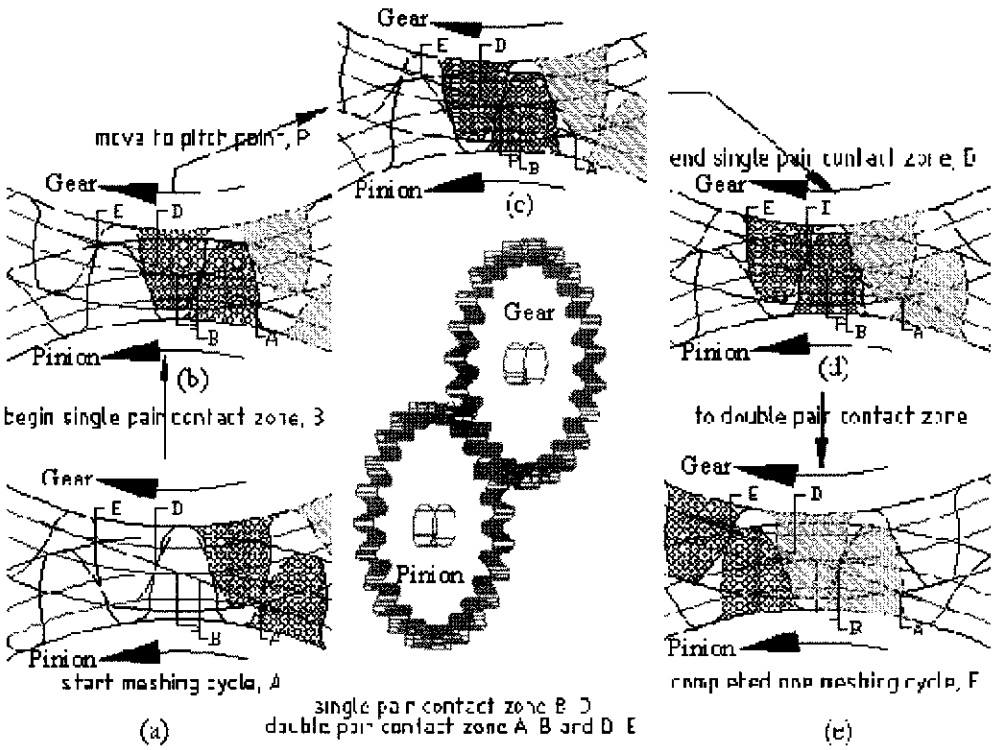

Figure F.2.1. Illustration of one complete meshing cycle.

In order to simplify the complexity of the problem, the load sharing compatibility condition is based on the fact that:

The driving and driven gear rotation caused by the angular displacement in the transverse plane of any tooth under load must be the same for all simultaneously meshing tooth pairs: This condition will lead to the following equations,

For pinion:

$$\theta_p^A = \theta_p^D \tag{F.2.1}$$

And gear:

$$\theta_g^A = \theta_g^D \tag{F.2.2}$$

Where θ_p^A and θ_p^D are the transverse plane angular rotation of the pinion body caused by bending deflection, shearing displacement and contact deformation of the single tooth pair A and D while the gear stays put. Where θ_g^A and θ_g^D are the transverse plane angular rotation of the gear body caused by bending deflection, shearing displacement and contact deformation of the single tooth pair A and D while the pinion stays put.

The sum of the torque contribution of each meshing tooth pair must equal the total applied torque. Considering the two contacts at A and D, see Figure F.2.1(a), the torque will then be given by,

For pinion:

$$\begin{aligned} T_{tot,p}^{A,D} &= T_p^A + T_p^D \\ &= \left(R_p^A * F_p^A\right) + \left(R_p^D * F_p^D\right) \end{aligned} \tag{F.2.3}$$

And gear:

$$\begin{aligned} T_{tot,g}^{A,D} &= T_g^A + T_g^D \\ &= \left(R_g^A * F_g^A\right) + \left(R_g^D * F_g^D\right) \end{aligned} \tag{F.2.4}$$

Where T_p^A, T_p^D, T_g^A, T_g^D are the torque vectorial contributions to the total applied torque of tooth pairs at A and D of the pinion and gear respectively and $T_{tot,p}^{A,D}$, and $T_{tot,g}^{A,D}$ are the total applied torque vectors of the pinion and gear respectively. The transverse plane contact radius vectors on the pinion and gear tooth pair A and D are given by R_p^A, R_p^D, R_g^A, R_g^D and the load share vectors F_p^A, F_p^D, F_g^A, F_g^D are part of the total applied force vector $F_{tot,p}^{A,D}$ and $F_{tot,g}^{A,D}$, at the contact points A and D of the pinion and gear respectively.

F.3 APPARATUS AND PROCEDURES

The static torsional test rig is shown in Figure F.3.1 which demonstrates the overall equipment set up which was used for measuring the combined torsional mesh stiffness of the gears in mesh.

Table F.3.1 shows the test gear parameters. The test gears were identical spur gears with a ratio of 1:1. One of the test gears, the output gear, was fixed and attached to the rotary table. The second gear, the input gear, was loaded with a pure torque as shown in the test rig layout of Figure F.3.2.

Table F.3.1. Test Gear Parameters

• gear type	standard involute, full-depth teeth
• material	aluminum
• modulus of elasticity, E	69 Gpa,
• Poisson's ratio, ν	0.33
• face width	0.015 m.
• module, m	6 mm.
• number of teeth	23
• pressure angle	20 degrees
• theoretical contact ratio	1.59
• theoretical angle of meshing cycle	24.912 degrees
• addendum	1.00m

- dedendum 1.25m

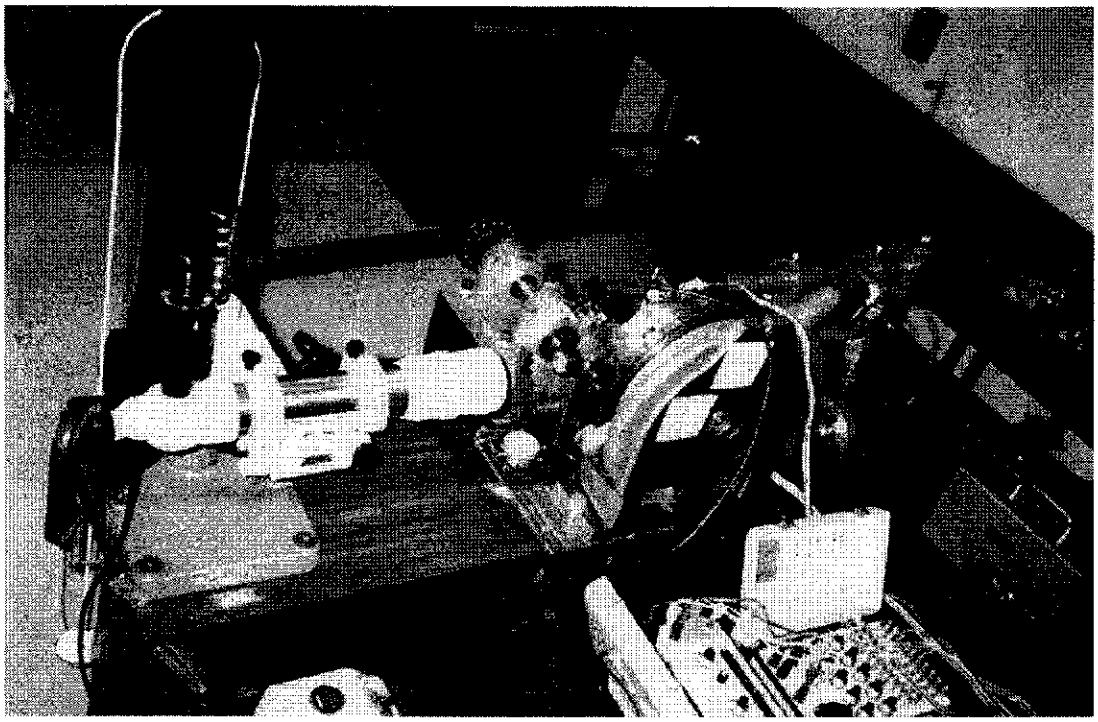

Figure F.3.1. The combined torsional mesh stiffness test rig.

The combined torsional mesh stiffness of the input gear at particular meshing positions was obtained by rotating both gears using the rotary head. The rotary head was then locked in position and pre-load masses were placed on the hook at the end of the loading bar. On the other end of the loading bar the same upward force was applied by turning the nut on the top of the stand bar and using the strain-load relationship which was found when the gauge was calibrated. Once the gears were pre-loaded, the known torque load was increased while the angular deflection of the spur gears was measured by a pair of optical auto-collimators. The same procedure was followed for a variety of different loads allowing a graph of torque versus angular displacement to be obtained as shown in Figure F.3.3.

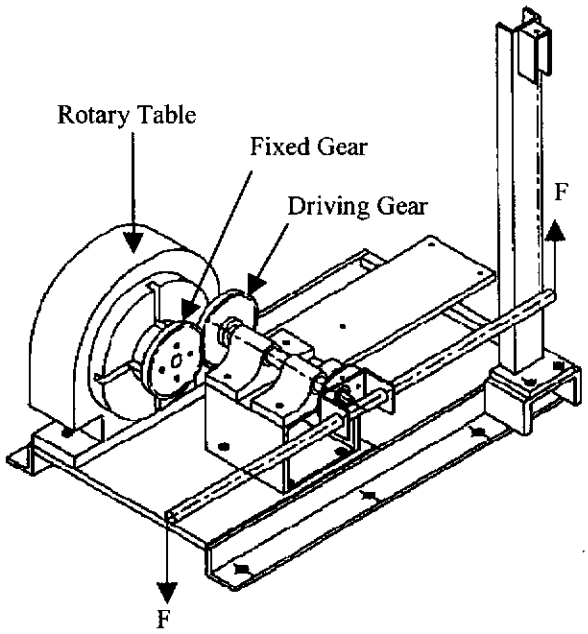

Figure F.3.2. Test rig lay out.

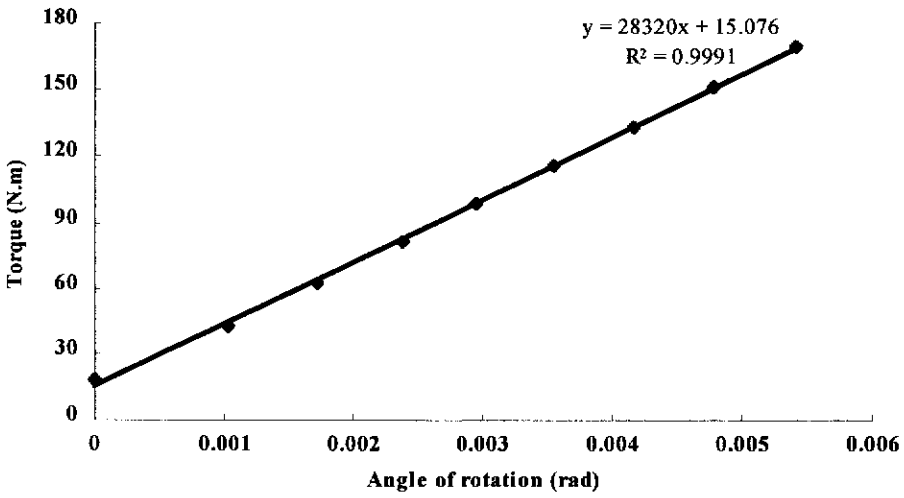

Figure F.3.3. The combined torsional mesh stiffness at one meshing position.

From the results as shown in Figure F.3.3, the combined torsional mesh stiffness of the input gear at particular meshing positions was obtained by calculating the gradient of the linear relationship between torque and angular displacement. The meshing position was then changed, by rotating the rotary head through increments of 0.5 degrees. At each position, the torsional mesh stiffness of the gear was measured and in this manner the combined torsional mesh stiffness of the input gear over the entire meshing cycle was obtained. Many different meshing positions

covering more than one completed meshing cycle were investigated as shown in Figure F.3.4.

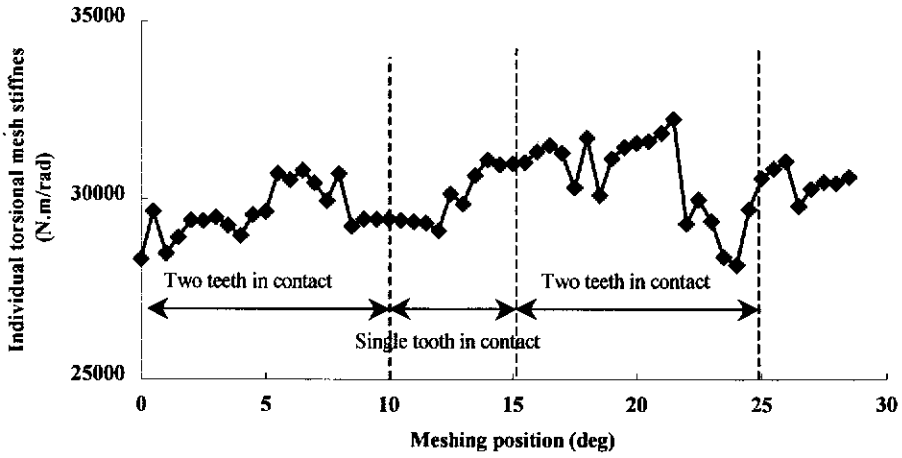

Figure F.3.4. Cycle of combined torsional mesh stiffness.

F.4 RESULT AND CONCLUSION

From each graph, such as shown in Figure F.3.4, the combined torsional mesh stiffness of the gear mesh of the input gear at particular positions was obtained by calculating the gradient from the corresponding torque versus angular displacement relationship. By changing the meshing positions, the combined torsional mesh stiffness of the gear during the entire meshing cycle was obtained. All together 58 meshing positions were investigated, each mesh position differing by 0.5 degrees. The meshing measurements started at reference 0 degree on the rotary head and finished at 28.5 degrees. However, one complete meshing cycle is 24.912 degrees. The path length contact of one complete meshing cycle, by calculation is 28.19 mm. The total length of the double contact zone (distance AB+DE of Figure F.2.1) is 20.96 mm. (18.52 degrees) and the length of single contact zone (distance BD) is 7.23 mm, (6.39 degrees). The graph of the combined torsional mesh stiffness versus meshing position indicates that the combined torsional mesh stiffness changes according to the actual meshing position of the gears. When the meshing position was subjected to double teeth pair in contact, the combined torsional mesh stiffness increased and then decreased as the meshing approached one tooth pair in contact.

When the meshing position was subjected to two teeth in contact, the torsional stiffness was higher than when a single tooth pair was in contact.

This test rig has dealt with the initial investigation of the static combined torsional mesh stiffness of gear in mesh. Many measurements have already been taken, and many more tests are still to be done and analysed, so these results can only present preliminary findings of the static cyclic combined torsional mesh stiffness. The results give an initial investigation of what is happening to the combined torsional mesh stiffness. It should be particularly useful for ongoing dynamic analysis and modelling of gearmesh vibration. Further testing and analysis will be conducted on more accurate gears, with and without artificial teeth cracks.

The main reason why the experimental results of the combined torsional mesh stiffness are very different to the FEA results is because the transverse plane angular rotation of the each spur gears was measured by a pair of optical auto-collimators where the auto-collimator mirror was clamped to the gear body. Therefore the measurement results were obtained from the angular deflection of the gear body in the particular position on the gear body where the auto-collimator mirror was clamped. On the other hand the FEA results have been obtained from the angular rotation of the gear hub. The FEA results have also shown that the actual location of the measurement point on the gear blank will affect the results.

Ongoing research using a new experimental arrangement where the auto-collimators are located on the shaft near the gear hub is under consideration. By locating the auto-collimators on the shaft near the gear hub, the angular deflection of the input and output gear hubs should be able to be measured.